RESEARCH ARTICLE

Applied Mathematics

Nonlinear Dynamics of Pulsatile Blood Flow in Viscoelastic Vessels: A Dispersive Wave Approach

Rim El Cheikh[1*] | Alexey Cheviakov[2*] | Denys Dutykh[3*] | Dimitrios Mitsotakis[4*]

[1]Univ. Grenoble Alpes, Univ. Savoie Mont Blanc, CNRS, LAMA, 73000 Chambéry, France.

[2]Department of Mathematics and Statistics, University of Saskatchewan, Saskatoon, Canada

[3]Mathematics Department, Khalifa University of Science and Technology, PO Box 127788, Abu Dhabi, United Arab Emirates

[4]Victoria University of Wellington, School of Mathematics and Statistics, PO Box 600, Wellington 6149, New Zealand

Correspondence
Mathematics Department, Khalifa University of Science and Technology, PO Box 127788, Abu Dhabi, United Arab Emirates
Email: denys.dutykh@ku.ac.ae

Funding information
This publication is based upon work supported by the Khalifa University of Science and Technology under Award No. FSU-2023-014. AC is grateful to NSERC of Canada for support through a Discovery grant RGPIN-2024-04308.

In this study, we investigate the dynamics of pulsatile flow in viscoelastic vessels, beginning with the axisymmetric full Euler equations with a free surface. Though highly accurate, this comprehensive model presents considerable analytical and computational challenges. To address these difficulties, we derive the fully nonlinear cylindrical Serre–Green–Naghdi (SGN) equations, which describe the propagation of long-crested pulses in cylindrical vessels. However, due to the complexity of these equations, we proceed by applying the weak nonlinearity assumption, leading to the derivation of the cylindrical Boussinesq equations. These equations offer a more tractable model while still capturing essential dispersive and nonlinear effects. In the final step, we derive the classical unidirectional approximations, such as the Korteweg–de Vries (KdV) and Benjamin–Bona–Mahony (BBM) equations, further simplifying the wave propagation analysis in this setting. Additionally, we investigate the modulation of periodic waves and establish the existence of Modulational Instability (MI) within this context, providing new insights into the stability of wave trains in cylindrical geometries. The results presented in this work contribute to a deeper understanding of fluid-structure interactions

[*]Equally contributing authors.

in biomedical applications, particularly in modelling blood flow in large arteries.

KEYWORDS
blood flows; axisymmetric flows; compliant vessels; long wave model; nonlinear dispersive systems

Contents

1 | INTRODUCTION

All models are approximations. Essentially, all models are wrong, but some are useful. However, the approximate nature of the model must always be borne in mind.

George E.P. Box

The study of pulsatile flow in viscoelastic vessels is a fundamental topic in fluid dynamics with significant applications in biomedical science, particularly in the modelling of blood flow in large arteries Fung (1997). Accurately describing fluid-structure interactions within vessels is critical to understanding hemodynamic processes, such as the propagation of pressure pulses generated by the heart. Large arteries exhibit both elastic and viscoelastic properties, storing elastic energy during the systolic phase and releasing it during diastole, which makes their modelling mathematically challenging Chandran et al. (2012); Quarteroni and Formaggia (2004); van de Vosse and Stergiopulos (2011). The present manuscript builds upon the PhD thesis of the first author, Rim El Cheikh, and aims to develop a systematic framework to describe the dynamics of such flows using asymptotic modelling techniques.

The Euler equations, which describe the motion of an inviscid fluid, provide a starting point for analyzing blood flow, but they neglect the viscous effects that are present in real blood vessels. Although blood is not a perfect inviscid fluid, these effects can be assumed to be small in large arteries, where the flow is fast, and the diameter is large, as compared to smaller vessels where viscous effects become more significant. Furthermore, the assumption of axisymmetry simplifies the problem by reducing the number of spatial dimensions to two, which is a common approach in fluid mechanics. However, it is important to note that real blood vessels may have complex geometries, especially at bifurcations and bends. The choice of a cylindrical geometry allows for a more manageable mathematical treatment, and it is a common approximation for long, straight vessels.

Previous research has proposed several models to tackle the complexities of fluid flow in elastic and viscoelastic vessels. In Mitsotakis et al. (2018), the authors derived new asymptotic one-dimensional equations of Boussinesq type, which are weakly nonlinear and weakly dispersive, for the study of inviscid and irrotational fluid flow in elastic vessels. These models serve as an alternative to the Euler equations and offer significant computational advantages while maintaining accuracy in simulating blood flow in arteries. Additionally, the work extended these models to

incorporate dissipative effects arising from fluid viscosity, providing a more comprehensive framework for arterial blood flow.

Building on the framework developed in Mitsotakis et al. (2018), the subsequent study Mitsotakis et al. (2019) considered the inclusion of viscoelastic effects in the vessel walls, further refining the model to account for the realistic biomechanical behaviour of arteries. This study introduced asymptotic models describing the propagation of solitary and periodic waves in viscoelastic vessels, providing valuable insights into the wave dynamics in such systems. These two contributions laid the groundwork for investigating more complex interactions between the fluid and the vessel walls, including both dispersive and nonlinear effects.

In this manuscript, we advance this line of research by investigating the dynamics of pulsatile flow in viscoelastic vessels, beginning with the axisymmetric full Euler equations with a free surface. While this comprehensive model offers a high degree of accuracy, it also presents significant analytical and computational challenges. To mitigate these complexities, we derive the fully nonlinear cylindrical Serre–Green–Naghdi (SGN) equations, which provide a more tractable model for the propagation of long-crested pulses in cylindrical geometries. Subsequently, we simplify the system further by applying the weak nonlinearity assumption, leading to the derivation of the cylindrical Boussinesq equations, which capture essential dispersive and nonlinear effects while being more amenable to analysis and computation.

The SGN equations, despite being one-dimensional (1D) models, still retain the fully nonlinear character of the Euler equations, which can be important for capturing certain types of wave propagation effects. By retaining the nonlinear terms, the Serre equations allow for the modelling of phenomena such as wave steepening and the formation of shocks, which may arise in pulsatile blood flow. However, unlike the full Euler equations, the Serre equations do not require solving a system of partial differential equations in two spatial dimensions, but rather, they reduce the dimensionality of the problem, leading to a more efficient computational approach. It is important to note that the Serre equations are derived under the assumption of long waves, which means that they are most accurate when the wavelength of the disturbances is significantly larger than the vessel radius. They provide a framework for studying the propagation of pressure pulses in arteries, but their limitations are clear: the one-dimensional representation is a significant simplification of the actual complex geometry of the circulatory system, and they are less accurate when the wavelength of the pressure and flow disturbances becomes comparable to or smaller than the vessel radius.

The cylindrical Boussinesq equations are derived from the SGN equations under a weak nonlinearity assumption, and they maintain some dispersive effects that are essential for capturing certain aspects of wave propagation in blood vessels. The balance between nonlinear and dispersive effects is known to be important for understanding the formation of stable pulses, and these equations allow the study of this balance through various analytical and numerical techniques. The Boussinesq equations, like the Serre equations, are also 1D models. However, by applying this assumption, they will generally lose their capacity to model the steepening of waves or shocks as they are derived under the assumption that nonlinear terms are small. While they are mathematically simpler than the Serre equations, they may still require significant computational resources for numerical wave propagation and stability studies.

Finally, we derive classical unidirectional approximations, including the Korteweg–de Vries (KdV) and Benjamin–Bona–Mahony (BBM) equations, to further simplify the wave propagation analysis. These unidirectional models are particularly useful in studying wave modulation and stability. Notably, we explore the modulation of periodic waves and establish the existence of Modulational Instability (MI), which provides new insights into the stability of wave trains in cylindrical vessels. Our findings contribute to a deeper understanding of fluid-structure interactions in biomedical applications and offer new perspectives on the modelling of blood flow in large arteries. The results presented in this paper contribute to a deeper understanding of fluid-structure interactions in biomedical applications, particularly in the modelling of blood flow in large arteries. By providing a hierarchy of models ranging from the full

Euler equations to simplified unidirectional approximations, this work offers a comprehensive framework for analyzing pulsatile flow in viscoelastic vessels across various scales and levels of complexity.

The Korteweg–de Vries (KdV) and Benjamin–Bona–Mahony (BBM) equations are classical unidirectional models which describe wave propagation, and they are widely used in various fields of physics and engineering to study long-wave phenomena. Both of these equations are further simplifications of the Boussinesq system. While the KdV and BBM equations are both unidirectional models, they differ in their treatment of dispersive effects. The KdV equation captures the balance between nonlinearity and dispersion in a certain way, which leads to solitary wave solutions. On the other hand, the BBM equation is a valid alternative model when one is interested in modelling phenomena in which dispersion is dominated by a different type of balance than that provided by the KdV. They can also both be more amenable to wave modulation and stability studies due to their relatively simple form. The KdV and BBM equations are derived under strong assumptions, including that the wave propagation is primarily unidirectional and that nonlinear and dispersive effects are weak, so their applicability is limited to specific regimes of the flow. While these models may not fully capture the complexity of blood flow, they offer valuable insight into the basic mechanisms of wave propagation and can be useful for studying wave modulation and stability.

In the context of blood flow in large arteries, these models can help to explain the relationship between the pulsatile nature of blood flow, the elastic and viscoelastic properties of the vessel wall, and the propagation of pressure waves. By considering a range of models of different levels of complexity, we will be able to evaluate the importance of different physical effects and parameters, such as the viscosity of blood, the stiffness of the vessel walls, and the presence of geometric features such as bifurcations and bends, and assess their influence on wave propagation and energy transport. The MI analysis offers insights into the long-term stability of wave trains in arteries, which is important for understanding phenomena such as pulse wave reflections, the interaction of waves, and wave energy dissipation. This can contribute to a more complete understanding of blood flow dynamics in the cardiovascular system and the effects of factors such as ageing and disease on the mechanical properties of blood vessels.

This manuscript is organized as follows. First, in Section 2, we present the parent-level mathematical model and the underlying physical assumptions, including both dimensional and dimensionless formulations. We then derive a new fully nonlinear weakly dispersive model, detailing the asymptotic expansion of the velocity field, mass conservation, and intermediate results. This is followed by the classical cylindrical Boussinesq equations and unidirectional reductions, such as the Korteweg–de Vries (KdV) and Benjamin–Bona–Mahony (BBM) models. We proceed with an in-depth analysis of the dispersion relations of these models (Section 3), shedding light on their wave propagation characteristics. The manuscript then explores numerical simulations (Section 4), Stokes expansions (Section 5), and the conservation laws and symmetries inherent in the models (Section 6). A dedicated section addresses the MI analysis (Section 7). The paper concludes with a discussion of the main findings (Section 8) and perspectives for future research (Section 9). Several supporting sections address acknowledgements, conflict of interest, data availability, and supplementary information. Finally, Appendix A presents a Windkessel model for pulsatile flow in viscoelastic vessels based on Serre-type approximations, connecting our continuum models to classical hemodynamic analogies.

2 | MATHEMATICAL MODELLING

Roughly speaking, the mathematical models in this field range from the complex three-dimensional CFD-type models Roe (2005) to very simplified zero-dimensional lumped models Milišić and Quarteroni (2004); Alastruey et al. (2008) (see also Appendix A for our Windkessel model approach). In the present study, we take an intermediate point of view,

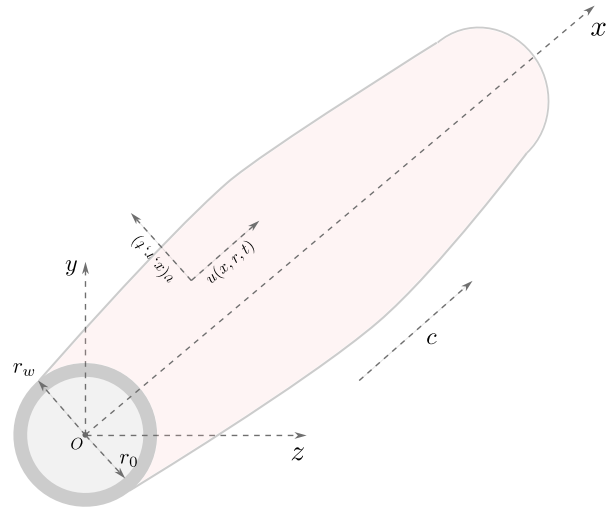

FIGURE 1 Sketch of a cylindrical elastic vessel subject to an axi-symmetric deformation filled with an ideal fluid.

where we follow the system's evolution in time and along the longitudinal direction[1] Sherwin et al. (2003); Alastruey et al. (2011) while the processes taking place in the transversal direction are being modelled based on the long wave assumption Lavrentiev (1947); Serre (1956); Bona et al. (2005); Khakimzyanov et al. (2020). This point of view has already been adopted in our previous studies Mitsotakis et al. (2018, 2019) in the weakly nonlinear regime. In the present study, we relieve this assumption in our developments as far as it will be possible.

We assume that we have an incompressible flow[2] of an ideal and homogeneous[3] fluid. This flow takes place in an elastic cylindrical vessel as schematically depicted in Figure 1. Moreover, the blood flow in large arteries is mostly laminar[4]. In order to simplify the problem and reduce its physical dimensionality, we assume the flow and, consequently, the deformation of the vessel's walls to be axi-symmetric[5]. The difference between an axi-symmetric and general deformation is schematically depicted in Figure 2.

Finally, we apply the long wave approximation Dutykh and Dias (2007a); Khakimzyanov et al. (2020). This simplifying assumption can be justified in the following way. Indeed, the Moens–Korteweg celerity $c_{MK} = O\left(10^2\right)$ cm/s Tijsseling and Anderson (2012); Lagrée (2000) and the hear pulsation period is $t_h = O\left(1\right)$ s. Consequently, the pulse wavelength can be estimated to be $\lambda = c_{MK} \cdot t_h = O\left(10^2\right)$ cm, which is much larger than a typical diameter or arteries approximately equal to $O\left(1\right)$ cm. Henceforth, the long wave assumption can be justified in this way. It is also well-known that long waves are much less affected by the viscosity Boussinesq (1895); Lamb (1932); Dutykh and Dias (2007a), which allows us to adopt the ideal fluid assumption. If necessary, the dissipative effects can be added

[1] The so-called unsteady one-dimensional models.

[2] Rough estimates show that the Mach number for blood flows is of the order of $O\left(10^{-3}\right)$ which justifies the compressibility assumption.

[3] The fluid homogeneity assumption is justified by comparing the typical pressure variations with the bulk modulus of the blood. A simple computation shows that the relative variation of the density is of the order of $O\left(5 \times 10^{-6}\right)$, which justifies our homogeneity assumption.

[4] The laminarity assumption can be discussed further. Despite the relatively high velocities in large arteries, the blood viscosity and the vessels' small diameter keep the Reynolds number in a range where laminar flow predominates. Moreover, the blood flow in arteries is pulsatile due to the rhythmic pumping of the heart. This pulsatility can actually stabilize the flow and delay the transition to turbulence.

[5] This approximate symmetry applies particularly to major arteries, such as the aorta and carotid arteries, which are approximately cylindrical with a nearly circular cross-section under normal physiological conditions. The lack of curvature minimizes asymmetrical flow disturbances in straight sections of arteries, supporting the axisymmetric assumption.

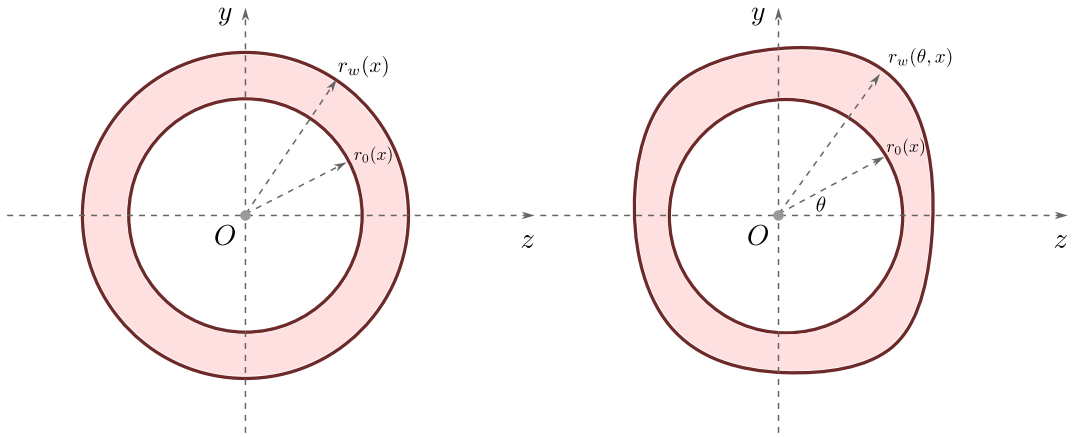

(a) An axi-symmetric deformation.

(b) A generic deformation.

FIGURE 2 A schematic illustration of an axi-symmetric (left panel) and a generic (right panel) deformations of initially cylindrical vessel cross-section. In the sequel, we are going to employ the polar coordinates in the Oyz plane.

later along the lines of our previous works on this topic Dutykh and Dias (2007b); Dutykh (2009b,a); Mitsotakis et al. (2019). We would like to mention that the long wave approximation is not new *per se*. However, historically, it has been employed to derive hydrostatic models, *cf.* Lambert (1958); Formaggia et al. (2003); Quarteroni and Formaggia (2004); Delestre and Lagrée (2013). The models resulting from this approach are usually of the hyperbolic type similar to Saint-Venant equations stemming from hydraulics and water pipe flows modelling Bourdarias and Gerbi (2007, 2008); Bourdarias et al. (2012). The peculiarity of our approach is that we go one step further in the hierarchy of models, and we include frequency dispersion effects Khakimzyanov et al. (2018).

2.1 | Base model: dimensional formulation

Taking into account the simplifying assumptions stated above, we can finally formulate our base model in scaled (physical and dimensional) variables by following Mitsotakis et al. (2018, 2019):

$$u_t + u u_x + v u_r + \frac{1}{\rho} p_x = 0, \tag{1}$$

$$v_t + u v_x + v v_r + \frac{1}{\rho} p_r = 0, \tag{2}$$

$$r u_x + (r v)_r = 0, \tag{3}$$

where ρ is the constant fluid density, u and v are horizontal and radial particle velocity vector components, respectively, and p is the fluid pressure. The subscripts with independent variables denote the partial derivatives with respect to those variables. We denote by $r^w(x,t)$ the distance between the cylinder axis and the elastic vessel's wall at a distance x and at time instance $t \geqslant 0$. The static equilibrium position of the elastic wall is denoted by $r_0(x)$. See the sketch of the fluid/solid domain in Figure 1. The elastic wall radial excursion will be denoted by $\eta(x,t)$ and the

following relation holds:

$$r^w(x,t) = r_0(x) + \eta(x,t).$$

Equations (1) to (3) should be supplemented with appropriate initial and boundary conditions to obtain a well-posed[6] IBVP. In order to avoid some obvious singularities, we impose the following condition:

$$v(x,0,t) = 0.$$

The elastic wall kinematic impermeability condition reads:

$$\eta_t + r_x^w \cdot u = v \quad \text{at} \quad r = r^w.$$

The dynamic boundary condition is nothing else but the expression of the forces balance written on vessel walls:

$$\rho^w h \eta_{tt} = p^w - \frac{E h}{r_0^2 (1-\nu^2)} \eta \quad \text{at} \quad r = r^w,$$

where ρ^w is the wall density, p^w is the pressure exerted by the fluid on the elastic wall, h is the wall thickness, E and ν characterize the elastic properties (Young modulus and Poisson ratio correspondingly) of the vessel. In this study, we assume for simplicity that E, ν, ρ^w, and h are constants.

2.2 | Potential model: dimensional formulation

We next recast the governing equations in terms of a velocity potential. Assuming the flow to be incompressible, irrotational, and axisymmetric, we introduce a smooth potential

$$\phi = \phi(x,r,t), \qquad (u,v)^\top = \nabla\phi = (\phi_x, \phi_r)^\top,$$

so that the Euler equations reduce to the Cauchy–Lagrange integral on the moving wall Mitsotakis et al. (2019):

$$\phi_t + \tfrac{1}{2}\phi_x^2 + \tfrac{1}{2}\phi_r^2 + \frac{1}{\rho} p + \kappa\phi = 0, \qquad r = r^w. \tag{4}$$

Here the instantaneous wall position is $r^w = r_0(x) + \eta(x,t)$, with r_0 the unperturbed radius and η the wall displacement. Under the potential-flow assumption the continuity equation becomes

$$r\phi_{xx} + (r\phi_r)_r = 0, \qquad 0 < r < r^w, \tag{5}$$

while the kinematic boundary conditions read

$$\phi_r = 0, \qquad r = 0, \tag{6}$$

$$\phi_r = \eta_t + r_x^w \phi_x, \qquad r = r^w(x,t). \tag{7}$$

[6]The well-posedness proof for this Initial Boundary Value Problem (IBVP) is left to future works on this subject.

Equations (4)–(7) furnish the starting point for the long-wave asymptotics carried out in the sequel of this study.

2.2.1 | Variational principles

Two complementary variational frameworks are commonly employed for irrotational surface-wave problems: Luke's Lagrangian formulation Luke (1967) and the Hamiltonian formulation of Petrov and Zakharov Petrov (1964); Zakharov (1968). Surveys by Radder (1999) and Zakharov and Kuznetsov (1997) provide extensive historical background. Luke's principle incorporates the velocity potential directly and imposes irrotationality *a priori*, whereas Zakharov's Hamiltonian requires both incompressibility and bottom impermeability to be satisfied identically, thereby rendering it more restrictive. In either case the free-surface conditions arise from the stationarity of an action functional in which part of the bulk dynamics is built in exactly and the remainder is obtained by variation. The earliest use of a pressure-based Lagrangian is due to Clebsch (1859) and Hargreaves (1908), although the concomitant free-surface boundary conditions were not explicitly recognised at the time. The following derivation highlights this connection. Recently, the variational techniques have been successfully applied to model water waves in various asymptotic regimes Clamond and Dutykh (2012); Clamond et al. (2024).

Lagrangian formulation.

First, for the irrotational case, let $\phi(x, r, t)$ be the velocity potential of a fluid lying between $r = 0$ and $r = r^w(x, t)$. The variational principle (Luke (1967)) is given by

$$\delta J = \delta \int_{t_1}^{t_2} \int_{x_1}^{x_2} \mathcal{L}\, \mathrm{d}x\, \mathrm{d}t = 0, \quad \text{with} \quad \mathcal{L} = \int_0^{r^w} \left(\phi_t + \frac{1}{2}\phi_x^2 + \frac{1}{2}\phi_r^2\right) r\, \mathrm{d}r - \frac{1}{2}\alpha\eta_t^2 - \frac{1}{2}\beta\eta^2 + p^w\eta, \tag{8}$$

where $\phi(x, r, t)$ and $r^w(x, t)$ are allowed to vary subject to the restrictions $\delta\phi = 0$ and $\delta r^w = 0$ at x_1, x_2, t_1 and t_2. The only difference from classical formulations using pressure expressions is that $r^w(x, t)$ variations are permitted here. Following standard procedures from the calculus of variations, equation (8) becomes

$$\begin{aligned}\delta J = \int_{t_1}^{t_2} \int_{x_1}^{x_2} \Bigg[\left(\phi_t + \frac{1}{2}\phi_x^2 + \frac{1}{2}\phi_r^2\right) r \Bigg|_{r=r^w} \delta r^w \\ + \int_0^{r^w} \left(\phi_x\, \delta\phi_x + \phi_r\, \delta\phi_r + \delta\phi_t\right) r\, \mathrm{d}r \Bigg] \mathrm{d}x\, \mathrm{d}t \\ + \delta \int_{t_1}^{t_2} \int_{x_1}^{x_2} \left(\frac{1}{2}\alpha\eta_t^2 - \frac{1}{2}\beta\eta^2 - p^w\eta\right) \mathrm{d}x\, \mathrm{d}t = 0. \end{aligned} \tag{9}$$

Natural boundary conditions at $r = 0$ and $r = r^w$ follow from the careful integration of (8). We consider the decomposition:

1. $\int_0^{r^w} r\phi_x\, \delta\phi_x\, \mathrm{d}r = \int_0^{r^w} \left[r\phi_x\, \delta\phi\right]_x \mathrm{d}r - \int_0^{r^w} r\phi_{xx}\, \delta\phi\, \mathrm{d}r = -r_x^w r^w \phi_x\, \delta\phi \Big|_{r=r^w} + \partial_x \int_0^{r^w} r\phi_x\, \delta\phi\, \mathrm{d}r,$
2. $\int_0^{r^w} r\phi_r\, \delta\phi_r\, \mathrm{d}r = \left[r\phi_r\, \delta\phi\right]_{r=0}^{r=r^w} - \int_0^{r^w} \left(\phi_r + r\phi_{rr}\right) \delta\phi\, \mathrm{d}r,$
3. $\int_0^{r^w} r\, \delta\phi_t\, \mathrm{d}r = \int_0^{r^w} \partial_t\left(r\, \delta\phi\right) \mathrm{d}r = -r^w r_t\, \delta\phi \Big|_{r=r^w} + \partial_t \int_0^{r^w} r\, \delta\phi\, \mathrm{d}r.$

Additionally, we compute

$$\delta \int_{t_1}^{t_2} \int_{x_1}^{x_2} \left(-\frac{1}{2}\,\alpha\,\eta_t^2 - \frac{1}{2}\,\beta\,\eta^2 + p^w\,\eta \right) \mathrm{d}x\,\mathrm{d}t = \int_{t_1}^{t_2} \int_{x_1}^{x_2} \left(-\alpha\,\eta_t\,\delta\eta_t - \beta\,\eta\,\delta\eta + p^w\,\delta\eta \right) \mathrm{d}x\,\mathrm{d}t\,.$$

Substituting all these contributions into (8), we obtain

$$\begin{aligned}\delta J = \int_{t_1}^{t_2} \int_{x_1}^{x_2} \Bigg[\left(\phi_t + \frac{1}{2}\,\phi_x^2 + \frac{1}{2}\,\phi_r^2 \right) r \Bigg|_{r=r^w} \delta r^w \\ - \left[r\,\phi_r\,\delta\phi \right]_{r=0} - \int_0^{r^w} \left(r\,\phi_{xx} + \phi_r + r\,\phi_{rr} \right) \delta\phi\,\mathrm{d}r \Bigg] \mathrm{d}x\,\mathrm{d}t \\ + \int_{t_1}^{t_2} \int_{x_1}^{x_2} \left(-\alpha\,\eta_{tt} - \beta\,\eta + p^w \right) \delta\eta\,\mathrm{d}x\,\mathrm{d}t = 0\,.\end{aligned}$$

Taking $\delta r^w = 0$ and assuming $\delta\phi\big|_{r=r^w} = \delta\phi\big|_{r=0} = 0$, and noting that $\delta\phi$ is otherwise arbitrary, we deduce the following system:

$$\phi_t + \frac{1}{2}\,\phi_x^2 + \frac{1}{2}\,\phi_r^2 - \alpha\,\eta_{tt} - \beta\,\eta + p^w = 0\,, \qquad r = r^w(x,t)\,, \tag{10}$$

$$r\,\phi_{xx} + (r\,\phi_r)_r = 0\,, \qquad 0 < r < r^w(x,t)\,, \tag{11}$$

$$\phi_r = 0\,, \qquad r = 0\,, \tag{12}$$

$$\phi_r = \eta_t + r_x^w\,\phi_x\,, \qquad r = r^w(x,t)\,, \tag{13}$$

$$p^w = \alpha\,\eta_{tt} + \beta\,\eta\,, \qquad r = r^w(x,t)\,. \tag{14}$$

Thus, we observe that the variational principle (8) elegantly recovers the complete potential flow formulation for our problem. Equation (11) represents the Laplace equation in cylindrical coordinates, which governs the irrotational flow in the fluid domain. The boundary conditions are given by the impermeability condition at the axis of symmetry (12) and the kinematic condition at the vessel wall (13). The dynamic condition (10) corresponds to the Cauchy–Lagrange integral at the vessel wall, while (14) describes the pressure law for the viscoelastic wall. This demonstrates the power of variational methods in deriving the governing equations for fluid-structure interaction problems in a systematic and physically consistent manner.

Hamiltonian formulation.

This section belongs to the relatively recent trend of applying concepts from Hamiltonian mechanics to problems in fluid dynamics. By 'Hamiltonian mechanics', we refer to the entirety of classical mechanics in the spirit of foundational texts such as Lanczos (1970); Goldstein et al. (2001); Arnold (1997), encompassing both particle mechanics and field theory. Hamiltonian approaches have proven indispensable in classical and quantum theories of particles and fields. If their only contribution were a reformulation of known results, they would be of limited value. However, substantial evidence indicates that classical mechanics methods offer a powerful and unifying framework in fluid dynamics as well. Several factors account for the effectiveness of Hamiltonian approaches. Firstly, Hamilton's formalism provides an elegant and economical representation of dynamics. Secondly, the well-established connection between symmetries of the Hamiltonian and conservation laws facilitates the construction of approximate models that preserve analogues

of exact invariants. Thirdly, Hamiltonian formulations are coordinate-invariant and thus adaptable to diverse geometrical settings. In Hamiltonian perturbation theory, for instance, dynamical approximations are naturally associated with transformations of the dependent variables. This flexibility enables one to simultaneously adjust the physical description and its mathematical representation to obtain models in their simplest possible form.

We now consider the motion governed by equations (10)–(14). The total energy of the system comprises the kinetic energy, potential energy, and surface energy, and is normalised such that the total energy vanishes in the quiescent state. The evolution equations take the abstract Hamiltonian form

$$\begin{pmatrix} \eta_t \\ \psi_t \end{pmatrix} = \mathcal{J} \begin{pmatrix} \dfrac{\delta \mathcal{H}}{\delta \eta} \\ \dfrac{\delta \mathcal{H}}{\delta \psi} \end{pmatrix}, \qquad \mathcal{J} = \begin{pmatrix} 0 & \mathbb{I} \\ -\mathbb{I} & 0 \end{pmatrix}, \tag{15}$$

where $\delta \mathcal{H}$ denotes the Gâteaux (variational) derivative, $\psi \equiv \phi(x, r, t)|_{r = r^w(x,t)}$ is the surface potential, and the Hamiltonian density and total energy are given by

$$H = \frac{1}{2} \int_0^{\eta} |\nabla \phi|^2 \, \mathrm{d}r + \left(-\frac{1}{2} \alpha \eta_t^2 - \frac{1}{2} \beta \eta^2 + p^w \eta \right), \qquad \mathcal{H} = \int_{\mathbb{R}} H \, \mathrm{d}x \,. \tag{16}$$

We now compute the variation of the Hamiltonian functional under the perturbation $\eta \mapsto \eta + \delta\eta$:

$$\begin{aligned} \mathcal{H}[\eta + \delta\eta, \phi] - \mathcal{H}[\eta, \phi] = {} & \frac{1}{2} \int_{\mathbb{R}} \int_0^{\eta + \delta\eta} |\nabla \phi|^2 \, \mathrm{d}r \, \mathrm{d}x \\ & - \frac{1}{2} \alpha \int_{\mathbb{R}} (\eta + \delta\eta)_t^2 \, \mathrm{d}x - \frac{1}{2} \beta \int_{\mathbb{R}} (\eta + \delta\eta)^2 \, \mathrm{d}x + \int_{\mathbb{R}} p^w (\eta + \delta\eta) \, \mathrm{d}x \\ & - \frac{1}{2} \int_{\mathbb{R}} \int_0^{\eta} |\nabla \phi|^2 \, \mathrm{d}r \, \mathrm{d}x + \frac{1}{2} \alpha \int_{\mathbb{R}} \eta_t^2 \, \mathrm{d}x + \frac{1}{2} \beta \int_{\mathbb{R}} \eta^2 \, \mathrm{d}x - \int_{\mathbb{R}} p^w \eta \, \mathrm{d}x \,. \end{aligned}$$

After simplification, we obtain

$$\mathcal{H}[\eta + \delta\eta, \phi] - \mathcal{H}[\eta, \phi] = \frac{1}{2} \int_{\mathbb{R}} \int_{\eta}^{\eta + \delta\eta} |\nabla \phi|^2 \, \mathrm{d}r \, \mathrm{d}x - \alpha \int_{\mathbb{R}} \eta_t \, \delta\eta_t \, \mathrm{d}x - \beta \int_{\mathbb{R}} \eta \, \delta\eta \, \mathrm{d}x + \int_{\mathbb{R}} p^w \, \delta\eta \, \mathrm{d}x \,.$$

Applying the mean value theorem to the integral over the interval $[\eta, \eta + \delta\eta]$, we finally obtain

$$\mathcal{H}[\eta + \delta\eta, \phi] - \mathcal{H}[\eta, \phi] = \frac{1}{2} \int_{\mathbb{R}} \left[|\nabla \phi|^2 \right]_{r = r^w} \delta\eta \, \mathrm{d}x - \alpha \int_{\mathbb{R}} \eta_{tt} \, \delta\eta \, \mathrm{d}x - \beta \int_{\mathbb{R}} \eta \, \delta\eta \, \mathrm{d}x + \int_{\mathbb{R}} p^w \, \delta\eta \, \mathrm{d}x \,.$$

Therefore, the non-canonical Hamiltonian evolution equations take the form

$$\begin{pmatrix} \eta_t \\ \psi_t \end{pmatrix} = \begin{pmatrix} \phi_r - r_x^w \phi_x \\ -\frac{1}{2} |\nabla \phi|^2 + \alpha \eta_{tt} + \beta \eta - p^w \end{pmatrix}, \tag{17}$$

which recover the dynamic and kinematic boundary conditions (10) and (13), respectively. It is important to emphasise that the operator $\mathcal{J}$ is skew-symmetric and satisfies the Jacobi identity (cf. Nutku (1987)), thus qualifying as a legitimate Hamiltonian operator.

In conclusion, the derivation and analysis of the non-canonical Hamiltonian structure provide a robust and system-

atic framework for investigating complex dynamical systems governed by nonlinear wave equations. The geometric properties of the Hamiltonian operator, including skew-symmetry and the Jacobi identity, ensure consistency with the underlying physics. This insight not only strengthens the theoretical foundations but also enhances the practical modelling of nonlinear dispersive systems in mathematical physics.

2.3 | Potential model: dimensionless formulation and the first derivation of the long wave model

To model blood flow in a vessel, we derive simplified equations from the Euler equations using non-dimensional variables and asymptotic techniques. This approach, relevant to arterial pulse propagation, accounts for nonlinearity and dispersion while simplifying the complex fluid-structure interaction at the vessel wall Fung (1993).

We introduce non-dimensional and scaled variables to normalize the Euler equations:

$$\eta^* = \frac{\eta}{a}, \quad x^* = \frac{x}{\lambda}, \quad r^* = \frac{r}{R}, \quad t^* = \frac{t}{T}, \quad \phi^* = \frac{\phi}{\lambda\varepsilon\tilde{c}}, \quad p^* = \frac{p}{\varepsilon\rho\tilde{c}^2}, \tag{18}$$

where η is the vessel wall displacement, a is the typical wall deviation, λ is the typical wavelength, R is the vessel radius, $T = \lambda/\tilde{c}$ is the time scale, $\tilde{c} = \sqrt{Eh/2\rho R}$ is the Moens-Korteweg speed, ϕ is the velocity potential, p is the pressure, ρ is the fluid density, E is the Young's modulus, and h is the wall thickness Fung (1993). The non-dimensional parameters are:

$$\varepsilon = \frac{a}{R}, \qquad \delta = \frac{R}{\lambda}, \tag{19}$$

where $\varepsilon = O(1)$ characterizes nonlinearity, and $\delta^2 \ll 1$ indicates weak dispersion. The external pressure is assumed zero, typical for blood flow models.

In non-dimensional form (dropping asterisks for simplicity), the governing equations and boundary conditions are:

$$\partial_t\phi + \frac{\varepsilon}{2}(\partial_x\phi)^2 + \frac{\varepsilon}{2\delta^2}(\partial_r\phi)^2 + p + \varepsilon\kappa\phi = 0, \quad \text{at } r = r^w, \tag{20}$$

$$\delta^2 r\partial_x^2\phi + \partial_r(r\partial_r\phi) = 0, \quad 0 < r < r^w, \tag{21}$$

$$\partial_r\phi = 0, \quad \text{at } r = 0, \tag{22}$$

$$\partial_r\phi = \delta^2\partial_t\eta + \delta^2[r_0(x) + \varepsilon\eta]\partial_x\phi, \quad \text{at } r = r^w, \tag{23}$$

$$p = \alpha\delta^2\partial_t^2\eta + \beta(\eta + \delta^2\gamma\partial_t\eta), \quad \text{at } r = r^w, \tag{24}$$

where $r^w = r_0(x) + \varepsilon\eta$ is the non-dimensional vessel radius, $\kappa = \kappa^*\tilde{c}\varepsilon/\lambda$ is a damping coefficient, $\alpha = \rho_w h/\rho R$, $\beta = 2R^2/r_0^2(x)$, $\gamma = \gamma^*\delta^2 T$, and ρ_w is the wall density (*cf.* Mitsotakis et al. (2019)). Following standard asymptotic techniques Bona et al. (2002), we expand the velocity potential ϕ as:

$$\phi(x, r, t) = \sum_{m=0}^{\infty} r^m\phi_m(x, t). \tag{25}$$

Substituting into (21), we obtain the recurrence relation:

$$\delta^2\partial_x^2\phi_{2m} + (2m+2)^2\phi_{2m+2} = 0, \quad \phi_{2m+1} = 0, \tag{26}$$

for $m = 0, 1, 2, \ldots$. This yields:

$$\phi_2 = -\frac{\delta^2}{4}\partial_x^2\phi_0, \tag{27}$$

and for $m = 1, 2, \ldots$:

$$\phi_{2m+2} = \frac{\delta^4}{(2m+2)^2(2m)^2}\partial_x^4\phi_{2m-2} = O(\delta^4). \tag{28}$$

Thus, the velocity potential up to $O(\delta^6)$ is:

$$\phi(x, r, t) = \phi_0(x, t) - \delta^2\frac{r^2}{4}\partial_x^2\phi_0(x, t) + \delta^4\frac{r^4}{64}\partial_x^4\phi_0(x, t) + O(\delta^6). \tag{29}$$

Using (29) in the boundary condition (23) at $r = r^w$, we approximate the mass conservation equation:

$$\partial_t\eta + r_x^w\,\partial_x\phi_0 + \frac{r^w}{2}\partial_x^2\phi_0 - \delta^2\frac{(r^w)^2 r_x^w}{4}\partial_x^3\phi_0 - \delta^2\frac{(r^w)^3}{16}\partial_x^4\phi_0 = O(\delta^4). \tag{30}$$

Substituting (29) and (24) into the Bernoulli equation (20) at $r = r^w$, we eliminate pressure to obtain the momentum equation:

$$\begin{aligned}\partial_t\phi_0 - \delta^2\frac{(r^w)^2}{4}\partial_x^2\partial_t\phi_0 + \frac{\varepsilon}{2}\left[(\partial_x\phi_0)^2 - \delta^2\frac{(r^w)^2}{2}\partial_x\phi_0\partial_x^3\phi_0\right] + \frac{\varepsilon\delta^2}{8}(r^w)^2(\partial_x^2\phi_0)^2 \\ + \varepsilon\kappa\left[\phi_0 - \delta^2\frac{(r^w)^2}{4}\partial_x^2\phi_0\right] + \alpha\delta^2\partial_t^2\eta + \beta(\eta + \delta^2\gamma\,\partial_t\eta) = O(\delta^4).\end{aligned} \tag{31}$$

Defining the horizontal velocity at the vessel center as $w(x, t) = \partial_x\phi_0(x, t)$, we rewrite (30) and (31) as:

$$\partial_t\eta + r_x^w w + \frac{r^w}{2}\partial_x w - \delta^2\frac{(r^w)^2 r_x^w}{4}\partial_x^2 w - \delta^2\frac{(r^w)^3}{16}\partial_x^3 w = O(\delta^4), \tag{32}$$

$$\partial_t w + \partial_x(\beta\eta) + \varepsilon w\,\partial_x w - \frac{\delta^2}{4}\partial_x\left[(r^w)^2\Gamma\right] + \varepsilon\kappa\left[w - \frac{\delta^2}{4}\partial_x\left((r^w)^2\partial_x w\right)\right] + \alpha\delta^2\partial_x\partial_t^2\eta + \delta^2\gamma\,\partial_x(\beta\,\partial_t\eta) = O(\delta^4), \tag{33}$$

where:

$$\Gamma = \partial_x\partial_t w + \varepsilon w\,\partial_x^2 w - \frac{\varepsilon}{2}(\partial_x w)^2. \tag{34}$$

The system (32)–(33) resembles a Serre-type system, capturing the leading-order dynamics of blood flow in a compliant vessel. The equations account for nonlinearity (ε), dispersion (δ^2), and vessel wall effects (α, β, γ). Higher-order approximations of the velocity potential could further refine this model, enhancing its accuracy for physiological applications Mitsotakis et al. (2019).

2.3.1 | Enhanced Serre-type system

In this section, we refine the Serre-type system derived in (32)–(33) by evaluating the horizontal velocity at any radius within the vessel, improving the model's applicability to blood flow dynamics. We also briefly introduce a second approach using incompressible Euler equations, which will be explored further in subsequent analyses.

To enhance the system (32)–(33), we consider the horizontal velocity at any radius $r = \theta r^w$, where $0 \leqslant \theta \leqslant 1$ and $r^w = r_0(x) + \varepsilon\eta$ is the non-dimensional vessel radius. From the velocity potential expansion (29), the horizontal velocity is:

$$u(x,r,t) = \partial_x\phi = \partial_x\phi_0 - \delta^2\frac{r^2}{4}\partial_x^3\phi_0 + O(\delta^4).$$

Defining $w(x,t) = \partial_x\phi_0(x,t)$ and evaluating at $r = \theta r^w$, we obtain:

$$u^\theta(x,t) \doteq u(x,\theta r^w,t) = w(x,t) - \delta^2\frac{\theta^2(r^w)^2}{4}\partial_x^2 w(x,t) + O(\delta^4). \tag{35}$$

Inverting this, we express w in terms of u^θ:

$$w(x,t) = u^\theta(x,t) + \delta^2\frac{\theta^2(r^w)^2}{4}\partial_x^2 u^\theta(x,t) + O(\delta^4). \tag{36}$$

Substituting (36) into the mass equation (32), we obtain:

$$\partial_t\eta + r_x^w u^\theta + \frac{r^w}{2}\partial_x u^\theta + \delta^2\frac{(2\theta^2-1)(r^w)^2 r_x^w}{4}\partial_x^2 u^\theta + \delta^2\frac{(2\theta^2-1)(r^w)^3}{16}\partial_x^3 u^\theta = O(\delta^4). \tag{37}$$

Using the vessel wall velocity $r_t^w = \varepsilon\partial_t\eta$ and approximating from (37):

$$r_t^w = \varepsilon\partial_t\eta = -\varepsilon r_x^w u^\theta - \varepsilon\frac{r^w}{2}\partial_x u^\theta + O(\varepsilon\delta^2), \tag{38}$$

we substitute (36) into the momentum equation (33) to obtain:

$$\partial_t u^\theta + \partial_x(\beta\eta) + \varepsilon u^\theta\partial_x u^\theta + \frac{\delta^2}{4}\left\{\theta^2(r^w)^2\partial_x\Gamma - \partial_x[(r^w)^2\Gamma]\right\} + \varepsilon\kappa Q + R = O(\delta^4), \tag{39}$$

where:

$$\begin{aligned}
\Gamma &= \partial_x\partial_t u^\theta + \varepsilon u^\theta\partial_x^2 u^\theta - \frac{\varepsilon}{2}(\partial_x u^\theta)^2,\\
Q &= u^\theta + \frac{\delta^2}{4}(\theta^2-1)(r^w)^2\partial_x^2 u^\theta - \delta^2 r^w r_x^w\partial_x u^\theta,\\
R &= \alpha\delta^2\partial_x\partial_t^2\eta + \delta^2\gamma\partial_x(\beta\partial_t\eta).
\end{aligned} \tag{40}$$

Choosing $\theta^2 = \frac{1}{2}$ simplifies (37) and (39), yielding a familiar Serre-type formulation that balances dispersion and nonlinearity effectively for blood flow modeling. The refined system (37)–(39) generalizes the velocity to any radial position, enhancing the model's flexibility for capturing blood flow variations across the vessel cross-section. The parameter θ allows tuning to specific radial locations, with $\theta^2 = \frac{1}{2}$ recovering a standard Serre-type system. The terms involving Γ, Q, and R account for higher-order dispersive, nonlinear, and wall interaction effects, critical for

accurate modeling of arterial waves Mitsotakis et al. (2019).

As an alternative approach, the mathematical modeling of blood flow suggests using the incompressible, ideal, and radially symmetric Euler equations. This framework, which assumes inviscid flow, will be developed further to complement the asymptotic system derived above, offering additional insights into arterial pulse dynamics.

2.4 | Base model: dimensionless formulation

In this Section, we elaborate on the scaled formulation for the Euler equations in cylindrical coordinates presented above. The first step consists of introducing non-dimensional independent variables, which are defined as follows:

$$\eta^\star = \frac{\eta}{a}, \quad x^\star = \frac{x}{\lambda}, \quad r^\star = \frac{r}{R}, \quad t^\star = \frac{t}{T}, \quad u^\star = \frac{1}{\varepsilon\,\tilde{c}}\,u, \quad v^\star = \frac{1}{\varepsilon\,\delta\,\tilde{c}}\,v, \quad p^\star = \frac{1}{\varepsilon\,\rho\,\tilde{c}^2}\,p,$$

where a is a typical amplitude of the vessel wall displacement, λ a typical wavelength of a pulse, R is a vessel's typical radius, $t = \lambda / \tilde{c}$ the characteristic timescale, while $\tilde{c} = \sqrt{E\,h / 2\rho\,R}$ is the Moens-Korteweg characteristic speed Fung (1997). The parameters ε and δ characterize the non-linearity and the non-hydrostatic effects in the system:

$$\varepsilon \coloneqq \frac{a}{R}, \quad \delta \coloneqq \frac{R}{\lambda}.$$

In the present work, we aim to keep $\varepsilon = O(1)$ as long as possible while assuming from the outset that $\delta^2 \ll 1$ is a small parameter.

Omitting the $\star$ symbol from the notation below for the sake of simplicity, the non-dimensional form of the Euler takes the form (holding for $0 < r < r^w \coloneqq r_0 + \varepsilon\,\eta$) Mitsotakis et al. (2018):

$$u_t + \varepsilon\,u\,u_x + \varepsilon\,v\,u_r + p_x = 0, \tag{41}$$

$$\delta^2\,(v_t + \varepsilon\,u\,v_x + \varepsilon\,v\,v_r) + p_r = 0, \tag{42}$$

$$r\,u_x + (r\,v)_r = 0. \tag{43}$$

We also add the dimensionless flow irrotationality condition that will be needed in our developments below Landau and Lifshitz (1987):

$$\delta^2\,v_x = u_r. \tag{44}$$

The scaled version of the kinematic boundary condition reads

$$v(x, r^w, t) = \eta_t(x, t) + r^w_x\,u(x, r^w, t), \tag{45}$$

while the dynamic boundary condition reads

$$p^w(x, t) = p(x, r^w, t) = \alpha\,\delta^2\,\eta_{tt}(x, t) + \beta(x)\,\eta(x, t) + \delta^2\beta\,\gamma\,\eta_t. \tag{46}$$

The non-singularity condition along the symmetry axis reads:

$$v(x, 0, t) = 0. \tag{47}$$

Above, we introduced the following notations:

$$\tilde{\alpha} := \frac{\rho^w h}{\rho} \quad \text{and} \quad \tilde{\beta}(x) := \frac{E h}{\rho r_0^2(x)}.$$

Then,

$$\alpha := \frac{\tilde{\alpha}}{R}, \qquad \beta(x) := \frac{2R^2\rho}{E h}\tilde{\beta}(x) \quad \text{and} \quad \gamma := \frac{\tilde{\gamma}}{\delta^2 T},$$

where ρ^w is the wall density, h is the thickness of the vessel wall, E is the young modulus of elasticity, R is a vessel's radius, $T := \frac{\lambda}{c}$ is the characteristic timescale. Below, we use the scaled governing equations in order to propose a simplified model.

2.5 | Derivation of a new fully nonlinear weakly dispersive model

In this Section, we perform the dimensionality reduction of the axi-symmetric Euler system presented above. In order to achieve this goal, we use essentially two mathematical tools: depth averaging and asymptotic expansions. In the derivation below, we follow the footsteps of our previous works on this topic Dutykh et al. (2013b); Clamond et al. (2017); Khakimzyanov et al. (2020); Clamond et al. (2024).

The horizontal velocity is approximated by its depth-averaged value:

$$\bar{u}(x,t) := \frac{1}{r_0 + \varepsilon\eta}\int_0^{r^w} u(x, r, t)\,\mathrm{d}r. \tag{48}$$

We start the derivation by integrating the continuity Equation (43):

$$\int_0^{r^w} r u_x\,\mathrm{d}r + \int_0^{r^w} (r v)_r\,\mathrm{d}r = 0,$$

where the second term can be readily integrated:

$$\int_0^{r^w} r u_x\,\mathrm{d}r + r^w v(x, r^w, t) - r^w v(x, 0, t) = 0.$$

After taking into account boundary conditions given in Equations (45) and (47), we obtain

$$\int_0^{r^w} r u_x\,\mathrm{d}r + r^w \eta_t(x, t) + r^w r_x^w u(x, r^w, t) = 0. \tag{49}$$

In a similar way, we integrate the axial momentum balance Equation (41):

$$\int_0^{r^w} u_t\,\mathrm{d}r + \varepsilon\int_0^{r^w} u u_x\,\mathrm{d}r + \varepsilon\int_0^{r^w} v u_r\,\mathrm{d}r = -\int_0^{r^w} p_x\,\mathrm{d}r. \tag{50}$$

The integral of the pressure on the right-hand side can be transformed using the classical Leibniz rule and the dynamic boundary condition expressed in Equation (46) to yield

$$\int_0^{r^w} p_x \, \mathrm{d}r = \frac{\partial}{\partial x} \int_0^{r^w} p \, \mathrm{d}r - p(x, r^w, t) r_x^w = \left[r^w \bar{p} \right]_x - \left(\alpha \delta^2 \eta_{tt} + \eta\beta + \delta^2 \beta\gamma \eta_t \right) r_x^w, \tag{51}$$

where $\bar{p}$ denotes the depth-averaged value of the pressure defined similarly to Equation (48). In order to calculate $\bar{p}$, we use the radial momentum balance Equation (42) recast as

$$p_r(x, r, t) = -\delta^2 \Gamma(x, r, t), \qquad \text{with} \qquad \Gamma \coloneqq v_t + \varepsilon u v_x + \varepsilon v v_r.$$

Integrating the derivative p_r from r to r^w, we obtain:

$$p(x, r^w, t) - p(x, r, t) = -\delta^2 \int_r^{r^w} \Gamma(x, z, t) \, \mathrm{d}z$$

and after a slight rewrite

$$-p(x, r, t) = -p(x, r^w, t) - \delta^2 \int_r^{r^w} \Gamma(x, z, t) \, \mathrm{d}z.$$

Integrating the last equation one more time over r from 0 to r^w and by substituting the dynamic boundary condition (46) for $p(x, r^w, t)$, we obtain:

$$-\int_0^{r^w} p(x, r, t) \, \mathrm{d}r = -\int_0^{r^w} \left(\alpha \delta^2 \eta_{tt} + \beta\eta + \delta^2 \beta\gamma \eta_t \right) \mathrm{d}r - \delta^2 \int_0^{r^w} \int_r^{r^w} \Gamma(x, z, t) \, \mathrm{d}z \, \mathrm{d}r.$$

After introducing the depth-averaged pressure $\bar{p}$ and computing the first integral on the right-hand side, we obtain:

$$r^w \bar{p} = \left(\alpha \delta^2 \eta_{tt} + \beta\eta + \delta^2 \beta\gamma \eta_t \right) r^w + \delta^2 \int_0^{r^w} \int_r^{r^w} \Gamma(x, z, t) \, \mathrm{d}z \, \mathrm{d}r.$$

With this result in hands, we can return to Equation (51) to substitute $r^w \bar{p}$ there to find:

$$\left(\alpha \delta^2 \eta_{tt} + \beta\eta + \delta^2 \beta\gamma \eta_t \right) r_x^w + \left(\alpha \delta^2 \eta_{tt} + \beta\eta + \delta^2 \beta\gamma \eta_t \right)_x r^w + \delta^2 \frac{\partial}{\partial x} \int_0^{r^w} \int_r^{r^w} \Gamma(x, z, t) \, \mathrm{d}z \, \mathrm{d}r - \left(\alpha \delta^2 \eta_{tt} + \beta\eta + \delta^2 \beta\gamma \eta_t \right) r_x^w.$$

Finally, we can now determine the integral of p_x:

$$\int_0^{r^w} p_x \, \mathrm{d}r = \left(\alpha \delta^2 \eta_{tt} + \beta\eta + \delta^2 \beta\gamma \eta_t \right)_x r^w + \delta^2 \frac{\partial}{\partial x} \int_0^{r^w} \int_r^{r^w} \Gamma(x, z, t) \, \mathrm{d}z \, \mathrm{d}r.$$

After substituting the last equation into Equation (50), we obtain

$$\int_0^{r^w} u_t \,\mathrm{d}r + \varepsilon \int_0^{r^w} u u_x \,\mathrm{d}r + \left(\alpha\delta^2\eta_{tt} + \beta\eta + \delta^2\beta\gamma\eta_t\right)_x r^w + \delta^2 \frac{\partial}{\partial x}\int_0^{r^w}\int_r^{r^w} \Gamma(x,z,t)\,\mathrm{d}z\,\mathrm{d}r = -\varepsilon\int_0^{r^w} v u_r \,\mathrm{d}r.$$

Further progress can be made after we approximate the horizontal velocity variable dependence on the flow depth.

2.5.1 | Velocity field asymptotic expansion

The horizontal velocity variable will be approximated with its second-order Taylor expansion around the cylinder axis $r = 0$:

$$u(x,r,t) = u_0(x,t) - \frac{1}{4}\delta^2 r^2 \frac{\partial^2 u_0}{\partial x^2} + O(\delta^4), \tag{52}$$

Notice that the incompressibility condition (43) on the velocity fields implies the following approximation of the second (vertical) velocity component:

$$v(x,r,t) = -\frac{r}{2}\frac{\partial u_0}{\partial x} + O(\delta^2). \tag{53}$$

Averaging of Equation (52) yields the following relation:

$$u_0 = \bar{u} + \frac{1}{12}\delta^2 (r^w)^2 \frac{\partial^2 \bar{u}}{\partial x^2} + O(\delta^4).$$

Thus, the variable u_0 can be eliminated from Equation (52) for the profit of the depth-averaged horizontal velocity variable:

$$u(x,r,t) = \bar{u} + \frac{1}{12}\delta^2 (r^w)^2 \frac{\partial^2 \bar{u}}{\partial x^2} - \frac{1}{4}\delta^2 r^2 \frac{\partial^2 \bar{u}}{\partial x^2} + O(\delta^4). \tag{54}$$

The same substitution can be made in Equation (53) as well:

$$v(x,r,t) = -\frac{r}{2}\frac{\partial \bar{u}}{\partial x} + O(\delta^2). \tag{55}$$

Equation (54) allows us also to approximate the derivative u_x:

$$u_x = \bar{u}_x + \frac{1}{12}\delta^2 2 r_x^w r^w \bar{u}_{xx} + \frac{1}{12}\delta^2 (r^w)^2 \bar{u}_{xxx} - \frac{1}{4}\delta^2 r^2 \bar{u}_{xxx} + O(\delta^4)$$

along with the nonlinear product $u u_x$:

$$u u_x = \bar{u}\bar{u}_x + \frac{1}{6}\delta^2 r_x^w r^w \bar{u}\bar{u}_{xx} + \frac{1}{12}\delta^2 (r^w)^2 \bar{u}\bar{u}_{xxx} - \frac{1}{4}\delta^2 r^2 \bar{u}\bar{u}_{xxx} + \frac{1}{12}\delta^2 (r^w)^2 \bar{u}_{xx}\bar{u}_x - \frac{1}{4}\delta^2 r^2 \bar{u}_{xx}\bar{u}_x + O(\delta^4).$$

These asymptotic representations allow us to evaluate also the integrals over fluid depth of $u\,u_x$:

$$\int_0^{r^w} u\,u_x\,\mathrm{d}r = r^w\,\bar{u}\,\bar{u}_x + \frac{1}{6}\,\delta^2\,r_x^w\,(r^w)^2\,\bar{u}\,\bar{u}_{xx} + O(\delta^4)$$

and of u_t :

$$\int_0^{r^w} u_t\,\mathrm{d}r = r^w\,\bar{u}_t + \frac{1}{6}\,\delta^2\,r_t^w\,(r^w)^2\,\bar{u}_{xx} + O(\delta^4)\,.$$

The asymptotic evaluation of the following integral requires the representation (55) along with the irrotationality condition (44):

$$\int_0^{r^w} v\,u_r\,\mathrm{d}r = \delta^2\int_0^{r^w} v\,v_x\,\mathrm{d}r = \delta^2\int_0^{r^w}\left(\frac{-r}{2}\,\frac{\partial\,\bar{u}}{\partial\,x}\right)\left(\frac{-r}{2}\,\frac{\partial^2\,\bar{u}}{\partial\,x^2}\right)\mathrm{d}r + O(\delta^4)$$
$$\equiv \delta^2\int_0^{r^w}\frac{r^2}{4}\,\bar{u}_x\,\bar{u}_{xx}\,\mathrm{d}r + O(\delta^4) = \frac{1}{12}\,\delta^2\,\bar{u}_x\,\bar{u}_{xx}\,(r^w)^3 + O(\delta^4)\,.$$

Equation (55) can be substituted into the fluid particle vertical acceleration $\Gamma(x,\,r,\,t)$ to obtain the following asymptotic approximation:

$$\Gamma(x,\,r,\,t) = v_t + \varepsilon\,u\,v_x + \varepsilon\,v\,v_r = -\frac{r}{2}\,\bar{u}_{xt} - \frac{r}{2}\,\varepsilon\,\bar{u}\,\bar{u}_{xx} + \varepsilon\,\frac{r}{4}\,(\bar{u}_x)^2 + O(\delta^2) =$$
$$-\frac{r}{2}\left[\bar{u}_{xt} + \varepsilon\,\bar{u}\,\bar{u}_{xx} - \frac{\varepsilon}{2}\,(\bar{u}_x)^2\right] + O(\delta^2)\,.$$

Combining the previous developments, we can state asymptotically one of the governing equations of the cylindrical Serre–Green–Naghdi (SGN) system:

$$r^w\,\bar{u}_t + \frac{\delta^2}{6}\,r_t^w\,(r^w)^2\,\bar{u}_{xx} + \varepsilon\,r^w\,\bar{u}\,\bar{u}_x + \frac{\varepsilon\,\delta^2}{6}\,r_x^w\,(r^w)^2\,\bar{u}\,\bar{u}_{xx} + \left(\alpha\,\delta^2\,\eta_{tt} + \beta\,\eta + \delta^2\,\beta\,\gamma\,\eta_t\right)_x r^w +$$
$$\frac{\varepsilon\,\delta^2}{12}\,(r^w)^3\,\bar{u}_x\,\bar{u}_{xx} - \frac{\delta^2}{6}\,\frac{\partial}{\partial\,x}\left[(r^w)^3\,(\bar{u}_{xt} + \varepsilon\,\bar{u}\,\bar{u}_{xx} - \frac{\varepsilon}{2}\,(\bar{u}_x)^2\right] = O(\delta^4)\,.$$

2.5.2 | The mass conservation

In this Section, we are going to derive the second equation of what will become the cylindrical SGN system. Namely, this equation will play the rôle of the mass conservation equation in more classical shallow water-type systems Dutykh and Clamond (2016, 2011); Dutykh et al. (2015); Dutykh and Goubet (2016); Clamond et al. (2019). For this, we return to the integrated version of the continuity Equation (49), and we substitute the approximation (54) for the horizontal velocity:

$$\int_0^{r^w} r\,u_x\,\mathrm{d}r = \int_0^{r^w} r\left(\bar{u} + \left(\frac{1}{12}\,\delta^2\,(r^w)^2 - \frac{1}{4}\,\delta^2 r^2\right)\bar{u}_{xx}\right)_x\mathrm{d}r + O(\delta^4) =$$
$$\bar{u}_x\int_0^{r^w} r\,\mathrm{d}r + \frac{\delta^2}{6}\,r_x^w\,r^w\,\bar{u}_{xx}\int_0^{r^w} r\,\mathrm{d}r + \frac{\delta^2}{12}\,\bar{u}_{xxx}\int_0^{r^w} r\,(r^w)^2\,\mathrm{d}r - \frac{\delta^2}{4}\,\bar{u}_{xxx}\int_0^{r^w} r^3\,\mathrm{d}r =$$
$$\bar{u}_x\,\frac{(r^w)^2}{2} + \frac{1}{12}\,\delta^2\,(r^w)^3\,r_x^w\,\bar{u}_{xx} + \frac{1}{12}\,\delta^2\,\bar{u}_{xxx}\,\frac{(r^w)^4}{2} - \frac{1}{4}\,\delta^2\,\bar{u}_{xxx}\,\frac{(r^w)^4}{4} + O(\delta^4)\,.$$

After a slight rewriting of the last integral, Equation (49) can be represented asymptotically as

$$\frac{(r^w)^2}{2}\bar{u}_x + \frac{\delta^2}{12} r_x^w (r^w)^3 \bar{u}_{xx} - \frac{\delta^2}{48}(r^w)^4 \bar{u}_{xxx} + r^w \eta_t + r^w r_x^w u^w(x,t) = O(\delta^4).$$

The last equation after division by r^w constitutes the desired mass conservation equation that will be explicitly written in the following Section.

2.5.3 | Intermediate conclusions

In this Section, we would like to summarize the developments made so far. We also remind that no assumption on the nonlinearity parameter has been made so far, *i.e.* $\varepsilon = O(1)$. On the other hand, all this progress has been made thanks to the long wave assumption that can be expressed as $\delta \ll 1$. We summarize below the two governing equations, which will be the prototype of the future cylindrical SGN system to be presented below after some little additional efforts[7]:

$$\frac{r^w}{2}\bar{u}_x + \frac{\delta^2}{12} r_x^w (r^w)^2 \bar{u}_{xx} - \frac{\delta^2}{48}(r^w)^3 \bar{u}_{xxx} + \eta_t + r_x^w u^w(x,t) = O(\delta^4), \tag{56}$$

$$\bar{u}_t + \frac{\delta^2}{6} r_t^w r^w \bar{u}_{xx} + \varepsilon r^w \bar{u}\bar{u}_x + \frac{\varepsilon\delta^2}{6} r_x^w r^w \bar{u}\bar{u}_{xx} + \left(\alpha\delta^2\eta_{tt} + \beta\eta + \delta^2\beta\gamma\eta_t\right)_x + \frac{\varepsilon\delta^2}{12}(r^w)^2\bar{u}_x\bar{u}_{xx} - \frac{\delta^2}{6r^w}\frac{\partial}{\partial x}\left[(r^w)^3\left(\bar{u}_{xt} + \varepsilon\bar{u}\bar{u}_{xx} - \frac{\varepsilon}{2}(\bar{u}_x)^2\right)\right] = O(\delta^4). \tag{57}$$

In order to achieve our goals, we have to determine the trace of the horizontal velocity u^w at the vessel wall. The following Section is entirely devoted to this task.

2.5.4 | Horizontal velocity trace at the vessel wall

The integration of the irrotationality condition (44) over r from r to r^w yields

$$u(x,r,t) = u(x,r^w,t) - \delta^2 \int_r^{r^w} v_x(x,s,t)\,\mathrm{d}s. \tag{58}$$

We introduce the following function[8] by following the steps of Mitsotakis et al. (2019):

$$Q(x,r,t) = \frac{1}{r}\int_0^r s\,u(x,s,t)\,\mathrm{d}s.$$

An asymptotic expression of this function Q can be readily obtained by using the just obtained horizontal velocity exact representation (58):

$$Q(x,r,t) = \frac{1}{r}\int_0^r s\,u^w(x,t)\,\mathrm{d}s + O(\delta^2) = \frac{r}{2}u^w(x,t) + O(\delta^2). \tag{59}$$

[7] In reality, we just divided both equations by $r^w > 0$ which does not vanish in normal (healthy) conditions.

[8] In the literature this quantity is usually referred to as the average volume flux.

The integration of the continuity Equation (43) this time from $r = 0$ to $r = r^w$, we obtain:

$$\int_0^r (s\,v)_s \,\mathrm{d}s = -\int_0^r s\,u_x \,\mathrm{d}s,$$

and after an elementary evaluation of the integral on the left-hand side by using the condition (47), we come to the following *exact* representation of the vertical velocity variable:

$$v(x, r, t) = -\frac{1}{r}\int_0^r s\,u_x \,\mathrm{d}s \equiv -Q_x(x, r, t).$$

Combining the last identity with the asymptotic formula (59), we obtain:

$$v(x, r, t) = -\frac{r}{2}\,u^w_x(x, t) + O(\delta^2). \tag{60}$$

The last asymptotic formula can be used to eliminate the vertical velocity from the Equation (58):

$$u(x, r, t) = u^w(x, t) + \delta^2 \int_r^{r^w} \frac{s}{2}\,u^w_{xx}(x, t)\,\mathrm{d}s + O(\delta^4).$$

After evaluating the integral and flipping the equality sides of variables u and u^w, we obtain:

$$u^w(x, t) = u(x, r, t) - \delta^2 u^w_{xx}(x, t)\,\frac{(r^w)^2 - r^2}{4} + O(\delta^4).$$

Using the last asymptotic formula recursively, one obtains:

$$u^w(x, t) = u - \delta^2\Big(u(x, r, t) - \delta^2 u^w_{xx}\,\frac{(r^w)^2 - r^2}{4}\Big)_{xx}\cdot\frac{(r^w)^2 - r^2}{4} + O(\delta^4)$$

and after some simplification, we get the following simple formula:

$$u^w(x, t) = u - \delta^2 u_{xx}(x, r, t)\,\frac{(r^w)^2 - r^2}{4} + O(\delta^4).$$

In the last equation, we may use the asymptotic representation (54) for $u(x, r, t)$ in terms of $\bar{u}(x, t)$:

$$\begin{aligned} u^w(x, t) = {} & \bar{u}(x, t) + \delta^2\Big[\frac{1}{12}(r^w)^2 - \frac{1}{4}r^2\Big]\bar{u}_{xx}(x, t) \\ & - \delta^2\Big(\bar{u}(x, t) + \frac{1}{12}\delta^2(r^w)^2\bar{u}_{xx}(x, t) - \frac{1}{4}\delta^2 r^2\bar{u}_{xx}(x, t)\Big)_{xx}\cdot\frac{(r^w)^2 - r^2}{4} + O(\delta^4) \end{aligned}$$

and after a series of asymptotic simplifications, we obtain the final result of this Section:

$$u^w(x, t) = \bar{u} - \frac{1}{6}\delta^2(r^w)^2\bar{u}_{xx} + O(\delta^4).$$

2.5.5 | Fully nonlinear weakly dispersive equations

The asymptotic formula obtained in the previous Section allows us to rewrite the intermediate system (56), (57) in terms of the depth-averaged velocity variable:

$$\frac{(r^w)^2}{2}\bar{u}_x - \frac{\delta^2}{12} r_x^w (r^w)^3 \bar{u}_{xx} - \frac{\delta^2}{48}(r^w)^4 \bar{u}_{xxx} + r^w \eta_t + r^w r_x^w \bar{u} = O(\delta^4),$$

$$r^w \bar{u}_t + \frac{\delta^2}{6} r_t^w (r^w)^2 \bar{u}_{xx} + \varepsilon r^w \bar{u}\bar{u}_x + \frac{\varepsilon\delta^2}{6} r_x^w (r^w)^2 \bar{u}\bar{u}_{xx} + \left(\alpha\delta^2\eta_{tt} + \beta\eta + \delta^2\beta\gamma\eta_t\right)_x r^w + \frac{\varepsilon\delta^2}{12}(r^w)^3 \bar{u}_x\bar{u}_{xx} - \frac{\delta^2}{6}\frac{\partial}{\partial x}\left[(r^w)^3\left(\bar{u}_{xt} + \varepsilon\bar{u}\bar{u}_{xx} - \frac{\varepsilon}{2}(\bar{u}_x)^2\right)\right] = O(\delta^4).$$

In order to close the system above, we can remember that r^w can be expressed through a known function and the unknown η as $r^w \equiv r_0(x) + \varepsilon\eta(x,t)$. Then, we obtain the following system of PDEs with variable coefficients, which constitute the celebrated fully nonlinear weakly dispersive Serre–Green–Naghdi (SGN) equations in the cylindrical axi-symmetric setting:

$$\frac{r_0}{2}\bar{u}_x + \varepsilon\frac{\eta}{2}\bar{u}_x - \frac{\varepsilon\delta^2}{12}\eta_x(r_0+\varepsilon\eta)^2\bar{u}_{xx} - \frac{\delta^2}{48}(r_0+\varepsilon\eta)^3\bar{u}_{xxx} + \eta_t + \varepsilon\eta_x\bar{u} = 0, \tag{61}$$

$$\bar{u}_t + \varepsilon\bar{u}\bar{u}_x + \frac{\varepsilon\delta^2}{6}\eta_t(r_0+\varepsilon\eta)\bar{u}_{xx} + \frac{\varepsilon^2\delta^2}{6}\eta_x(r_0+\varepsilon\eta)\bar{u}\bar{u}_{xx} + \left(\alpha\delta^2\eta_{tt} + \beta\eta + \delta^2\beta\gamma\eta_t\right)_x + \frac{\varepsilon\delta^2}{12}(r_0+\varepsilon\eta)^2\bar{u}_x\bar{u}_{xx} - \frac{\delta^2}{6(r_0+\varepsilon\eta)}\frac{\partial}{\partial x}\left[(r_0+\varepsilon\eta)^3\left(\bar{u}_{xt} + \varepsilon\bar{u}\bar{u}_{xx} - \frac{\varepsilon}{2}(\bar{u}_x)^2\right)\right] = 0. \tag{62}$$

2.6 | Classical cylindrical Boussinesq equations

The cylindrical SGN system (61), (62) presented above currently seems to be intractable to our analytical and numerical techniques. In order to be able to continue our investigation, we would like to adopt the simplifying assumption of weak nonlinearity while staying in the so-called Boussinesq regime Dougalis and Mitsotakis (2008); Dutykh and Goubet (2016); Dutykh and Dias (2007a); Dougalis et al. (2007), *i.e.* $\varepsilon \ll 1$ while $\frac{\varepsilon}{\delta^2} = O(1)$. For the sake of simplicity, we shall also assume that the vessel radius $r_0 = \text{const}$. Under these assumptions, the SGN system (61), (62) can be simplified to the following classical Boussinesq-type equations:

$$\frac{r^w}{2}\bar{u}_x - \frac{\delta^2}{48}(r_0)^3\bar{u}_{xxx} + \eta_t + r_x^w\bar{u} = O(\delta^4 + \varepsilon\delta^2), \tag{63}$$

$$\bar{u}_t + \varepsilon\bar{u}\bar{u}_x + \left(\alpha\delta^2\eta_{tt} + \beta\eta + \delta^2\beta\gamma\eta_t\right)_x - \frac{\delta^2}{6}r_0^2\bar{u}_{xxt} = O(\delta^4 + \varepsilon\delta^2). \tag{64}$$

Substituting $r^w \equiv r_0 + \varepsilon\eta(x,t)$ in the last Boussinesq system, we obtain

$$\frac{r_0}{2}\bar{u}_x + \frac{\varepsilon}{2}\eta\bar{u}_x - \frac{\delta^2}{48}r_0^3\bar{u}_{xxx} + \eta_t + \varepsilon\eta_x\bar{u} = O(\delta^4 + \varepsilon + \delta^2),$$

$$\bar{u}_t + \varepsilon\,\bar{u}\,\bar{u}_x + \alpha\,\delta^2\,\eta_{xtt} + \beta\,\eta_x + \delta^2\,\beta\,\gamma\,\eta_{xt} - \frac{\delta^2}{6}\,r_0^2\,\bar{u}_{xxt} = O\left(\delta^4 + \varepsilon + \delta^2\right).$$

The last system can be easily recast in physical variables after neglecting the asymptotically small terms on the right-hand side:

$$\frac{r_0}{2}\,\bar{u}_x + \frac{\eta}{2}\,\bar{u}_x + \eta_t - \frac{r_0^3}{48}\,\bar{u}_{xxx} + \eta_x\,\bar{u} = 0, \tag{65}$$

$$\bar{u}_t + \bar{u}\,\bar{u}_x + \tilde{\alpha}\,\eta_{xtt} + \tilde{\beta}\,\eta_x + \tilde{\beta}\,\tilde{\gamma}\,\eta_{xt} - \frac{r_0^2}{6}\,\bar{u}_{xxt} = 0, \tag{66}$$

where $r_0 > 0$ is the vessel constant radius.

To compare the present model with that proposed in Mitsotakis et al. (2019), one observes that the latter employed the potential flow formulation, whereas the current study utilises a velocity-pressure formulation. Furthermore, their model incorporates a viscous frequency parameter associated with Rayleigh damping, which is set to zero in our analysis. Accordingly, these distinctions underscore that the two systems are not equivalent representations of the Boussinesq model.

2.7 | Unidirectional model equations

In this Section, we continue the derivation of simplified weakly dispersive models for axi-symmetric flows. Namely, we are about to apply the unidirectional[9] wave propagation approximation. For this, we introduce the following non-dimensional variables:

$$\eta^\star = \frac{\eta}{a}, \qquad x^\star = \frac{x}{\lambda}, \qquad r^\star = \frac{r}{r_0}, \qquad t^\star = \frac{t}{T}, \qquad u^\star = \frac{u}{c_0},$$

where here $c_0 = \dfrac{a}{r_0}\sqrt{\dfrac{2\,E\,h}{\rho\,r_0}}$ is a modified Moens-Korteweg characteristic speed and and $T = 2\,\dfrac{a\,\lambda}{r_0\,c_0}$. System (65), (66) in these dimensionless variables reads

$$\eta^\star_{t^\star} + u^\star_{x^\star} + \varepsilon\,\eta^\star\,u^\star_{x^\star} + 2\,\varepsilon\,\eta^\star_{x^\star}\,u^\star - \frac{\delta^2}{24}\,u^\star_{x^\star x^\star x^\star} = 0, \tag{67}$$

$$u^\star_{t^\star} + \eta^\star_{x^\star} + 2\,\varepsilon\,u^\star\,u^\star_{x^\star} + \frac{1}{2}\,\delta^2\,\alpha\,\eta^\star_{x^\star t^\star t^\star} + \gamma^\star\,\delta^2\,\eta^\star_{x^\star t^\star} - \frac{1}{6}\,\delta^2\,u^\star_{x^\star x^\star t^\star} = 0, \tag{68}$$

where $\gamma^\star := \dfrac{1}{2}\,\dfrac{\sigma}{\varepsilon\,\delta^2}\,\gamma$, $\sigma := \frac{c_0}{\lambda}$, and $\varepsilon := \frac{a}{r_0}$, $\delta := \frac{r_0}{\lambda}$. As it is well known, all previous systems of equations describe the two-way propagation of nonlinear waves. In this Section, we will derive equations that describe nonlinear waves travelling essentially in one chosen direction. The two most celebrated models of this class are the KdV and BBM equations Korteweg and de Vries (1895); Benjamin et al. (1972); Bona and Smith (1975); Zabusky and Galvin (1971); Dutykh et al. (2013a); Dutykh and Pelinovsky (2014); Dutykh and Tobisch (2015). The BBM equation, in particular, serves as the foundation for our zero-dimensional Windkessel model presented in Appendix A.

[9] In some works, mostly in the field of optics, *e.g.* Agrawal and Pattanayak (1979), it is also referred to as the paraxial approximation.

In order to derive such models, we observe first that Equation (67) can be read to the first order as

$$\eta^\star_{t^\star} = -u^\star_{x^\star} + O(\varepsilon + \delta^2)$$

and thus

$$\eta^\star_{x^\star t^\star} = -u^\star_{x^\star x^\star} + O(\varepsilon + \delta^2)$$

and also

$$\eta^\star_{x^\star t^\star t^\star} = -u^\star_{x^\star x^\star t^\star} + O(\varepsilon + \delta^2).$$

Following Whitham's low-order approximation for predominantly right-running waves Whitham (1999); Dutykh and Dias (2007a), we postulate the leading-order kinematic relation between the dimensionless horizontal velocity and the free-surface elevation,

$$u^\star = \eta^\star + \varepsilon A + \delta^2 B + O(\varepsilon^2, \delta^4, \varepsilon\delta^2), \tag{69}$$

where the yet-unknown corrections $A(x^\star, t^\star)$ and $B(x^\star, t^\star)$ are smooth functions to be determined. Substituting this relation into Equations (67) and (68) we obtain

$$\eta^\star_{x^\star} + \eta^\star_{t^\star} + \varepsilon\left(A_{x^\star} + 3\eta^\star \eta^\star_{x^\star}\right) + \delta^2\left(B_{x^\star} - \frac{1}{24}\eta^\star_{x^\star x^\star x^\star}\right) = O(\varepsilon^2, \delta^4, \varepsilon\delta^2), \tag{70}$$

$$\eta^\star_{x^\star} + \eta^\star_{t^\star} + \varepsilon\left(A_{t^\star} + 2\eta^\star \eta^\star_{x^\star}\right) + \delta^2\left(B_{t^\star} - \frac{\alpha}{2}\eta^\star_{x^\star x^\star t^\star} - \gamma^\star \eta^\star_{x^\star x^\star} - \frac{1}{6}\eta^\star_{x^\star x^\star t^\star}\right) = O(\varepsilon^2, \delta^4, \varepsilon\delta^2). \tag{71}$$

Adding Equation (70) and Equation (71) and equating the coefficients of ε and δ^2 to zero yields

$$\varepsilon: \quad A_{x^\star} + 3\eta^\star \eta^\star_{x^\star} - A_{t^\star} - 2\eta^\star \eta^\star_{x^\star} = 0, \tag{72}$$

$$\delta^2: \quad B_{x^\star} - B_{t^\star} - \frac{1}{24}\eta^\star_{x^\star x^\star x^\star} + \frac{\alpha}{2}\eta^\star_{x^\star x^\star t^\star} + \gamma^\star \eta^\star_{x^\star x^\star} + \frac{1}{6}\eta^\star_{x^\star x^\star t^\star} = 0. \tag{73}$$

Assuming $\partial_{x^\star} = -\partial_{t^\star} + O(\varepsilon^2, \delta^4, \varepsilon\delta^2)$, Equations (72) and (73) give

$$A_{x^\star} = -\frac{1}{2}\eta^\star \eta^\star_{x^\star}, \qquad B_{x^\star} = \left(\frac{5 + 12\alpha}{48}\right)\eta^\star_{x^\star x^\star x^\star} - \frac{1}{2}\gamma^\star \eta^\star_{x^\star x^\star}.$$

Integrating the last relations in $x^\star$ we obtain

$$A = -\frac{1}{4}\eta^{\star 2}, \qquad B = \left(\frac{5 + 12\alpha}{48}\right)\eta^\star_{x^\star x^\star} - \frac{1}{2}\gamma^\star \eta^\star_{x^\star},$$

and the resulting KdV–Burgers equation reads

$$\eta^{\star}_{t^\star} + \eta^{\star}_{x^\star} + \frac{5}{2}\,\varepsilon\,\eta^{\star}\,\eta^{\star}_{x^\star} + \delta^2\Big(\frac{12\,\alpha+3}{48}\Big)\,\eta^{\star}_{x^\star x^\star x^\star} - \frac{1}{2}\,\delta^2\,\gamma^{\star}\,\eta^{\star}_{x^\star x^\star} = 0\,. \tag{74}$$

Dimensional form.

Restoring physical variables as in Section 2.7, Equation (74) becomes

$$\eta_t + \tilde{c}\,\eta_x + \frac{5}{2\,r_0}\,\tilde{c}\,\eta\,\eta_x + \frac{\tilde{c}\,r_0(12\,\tilde{\alpha}+3\,r_0)}{48}\,\eta_{xxx} - \frac{r_0}{4}\,\tilde{\beta}\,\gamma\,\eta_{xx} = 0\,, \tag{75}$$

where $\tilde{c} = \sqrt{E\,h/(2\,\rho\,r_0)}$ is the classical Moens–Korteweg velocity Fung (1997). The associated dispersion relation is

$$\omega = \tilde{c}\,k - \frac{r_0\,\tilde{c}(12\,\tilde{\alpha}+3\,r_0)}{48}\,k^3 - \frac{\mathrm{i}}{4}\,r_0\,\gamma\,\tilde{\beta}\,k^2\,.$$

BBM–Burgers limit.

Replacing the third-order spatial derivative by its BBM proxy yields (this regularization approach is also employed in our Windkessel model derivation in Appendix A)

$$\eta^{\star}_{t^\star} + \eta^{\star}_{x^\star} + \frac{5}{2}\,\varepsilon\,\eta^{\star}\,\eta^{\star}_{x^\star} - \delta^2\Big(\frac{12\,\alpha+3}{48}\Big)\,\eta^{\star}_{x^\star x^\star t^\star} - \frac{1}{2}\,\delta^2\,\gamma^{\star}\,\eta^{\star}_{x^\star x^\star} = 0\,. \tag{76}$$

In dimensional variables, the last equation becomes

$$\eta_t + \tilde{c}\,\eta_x + \frac{5}{2\,r_0}\,\tilde{c}\,\eta\,\eta_x - \frac{r_0(12\,\tilde{\alpha}+3\,r_0)}{48}\,\eta_{xxt} - \frac{r_0}{4}\,\gamma\,\tilde{\beta}\,\eta_{xx} = 0\,. \tag{77}$$

The linear dispersion relation of this model can be easily computed:

$$\omega = \frac{48\,\tilde{c}\,k}{48 + r_0(12\,\tilde{\alpha}+3\,r_0)k^2} - \mathrm{i}\,\frac{12\,\gamma\,r_0\,\tilde{\beta}\,k^2}{48 + r_0(12\,\tilde{\alpha}+3\,r_0)k^2}\,. \tag{78}$$

Classical solitary waves (dissipation-free).

If $\gamma = 0$, Equation (75) supports solitary waves propagating with $c_s = \tilde{c}(1 + 5A/(6\,r_0))$:

$$\eta(x,t) = \frac{6(c_s-\tilde{c})r_0}{5\tilde{c}}\ \operatorname{sech}^2\left(\sqrt{\frac{12(c_s-\tilde{c})}{\tilde{c}(12\,\tilde{\alpha}+3\,r_0)r_0}}\,(x-c_s t)\right).$$

A parallel computation for Equation (77) furnishes

$$\eta(x,t) = \frac{6(c_s-\tilde{c})r_0}{5\tilde{c}}\ \operatorname{sech}^2\left(\sqrt{\frac{12(c_s-\tilde{c})}{c_s(12\,\tilde{\alpha}+3\,r_0)r_0}}\,(x-c_s t)\right).$$

Indeed, setting $\eta = \eta(\zeta)$ with $\zeta = x - c_s t$, substituting into Equation (75), integrating twice delivers

$$\frac{\tilde{c}(12\,\tilde{\alpha}+3\,r_0)r_0}{96}\,(\eta')^2 + \frac{(-c_s+\tilde{c})}{2}\,\eta^2 + \frac{5}{12}\,\frac{\tilde{c}}{r_0}\,\eta^3 = 0,$$

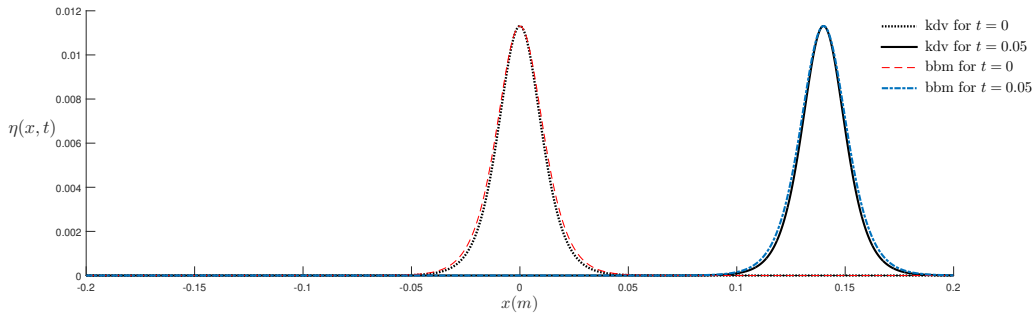

FIGURE 3 *Comparison of travelling-wave profiles generated by the KdV and BBM equations at several successive instants t.*

whose closed-form solution matches the profiles given above.

The initial disturbance is a solitary wave of amplitude $A = 0.0035$. The near-perfect overlap of the two families of curves at all reported times confirms that the BBM regularisation reproduces, to leading order, the dispersive and nonlinear balance captured by the KdV equation, thereby validating the asymptotic model for the haemodynamic parameters considered here. Figure 3 juxtaposes the solitary-wave solutions obtained from the KdV and BBM models for a vessel of undisturbed radius $r_0 = 0.01$ m, wall thickness $h = 3\times10^{-4}$ m, Young's modulus $E = 4.1\times10^5$ kg m^{-1} s^{-2}, wall density $\rho^{\omega} = 10^3$ kg m^{-3}, and computational length $L = 0.4$ m.

2.7.1 | Travelling-wave reduction of the cylindrical model

In this Section, we derive exact solitary-wave solutions for the variable-coefficient cylindrical Boussinesq-type model (65), (66). The derivation follows the computer-algebra strategy of Dutykh and Dias (2007a), implemented symbolically in Maple. We look for solutions that depend on a single travelling coordinate

$$\zeta := x - c\,t,$$

so that

$$\bar{u}(x,t) = \bar{u}(\zeta), \qquad \eta(x,t) = \eta(\zeta), \qquad r^{w} = r_0 + \eta, \qquad r_0 = \text{const}.$$

Reduction of the governing equations.

Using the low-order approximation of the continuity Equation (60) together with the boundary condition (45), one finds[10]

$$\eta_{xtt} = -\left(\frac{1}{2}\,r^{w}\,\bar{u}_x + r^{w}_x\,\bar{u}\right)_{xt} + O(\delta^2).$$

[10]Terms of order $O(\delta^4)$ and higher are consistently neglected throughout.

Substituting this expression into Equation (64) yields the cylindrical Boussinesq system

$$\eta_t + \frac{r_0}{2}\bar{u}_x + \frac{\varepsilon}{2}\eta\bar{u}_x + \varepsilon\eta_x\bar{u} - \frac{\delta^2}{48}r_0^3\bar{u}_{xxx} = O\left(\delta^4, \varepsilon\delta^2\right), \tag{79}$$

$$\bar{u}_t + \varepsilon\bar{u}\bar{u}_x - \frac{\alpha r_0}{2}\delta^2\bar{u}_{xxt} + \beta\eta_x + \delta^2\beta\gamma\eta_{xt} - \frac{\delta^2}{6}r_0^2\bar{u}_{xxt} = O\left(\delta^4, \varepsilon\delta^2\right). \tag{80}$$

Henceforth, we set $\gamma = 0$ (the purely elastic wall case). Introducing the convenience coefficients

$$a = \frac{r_0}{2}, \qquad b = \frac{r_0^3}{48}, \qquad d = \frac{\alpha r_0}{2}, \qquad e = \beta, \qquad f = \frac{r_0^2}{6},$$

and rewriting Equations (79) and (80) in the travelling frame leads, after one integration with respect to ζ, to the coupled third-order ODE system

$$c\eta' + a\bar{u}' + \frac{\varepsilon}{2}\eta\bar{u}' + \varepsilon\eta'\bar{u} - \delta^2 b\bar{u}''' = 0, \tag{81}$$

$$c\bar{u}' + \varepsilon\bar{u}\bar{u}' - \delta^2 dc\bar{u}''' + e\eta' - \delta^2 fc\bar{u}''' = 0, \tag{82}$$

where primes denote differentiation with respect to ζ. Because solitary waves are spatially localised, all dependent variables and their derivatives vanish as $\zeta \to \pm\infty$.

Proportional flow ansatz.
Guided by extensive numerical experimentation, we set

$$\bar{u}(\zeta) = A\eta(\zeta), \tag{83}$$

where the proportionality constant A will be determined self-consistently. Substituting Equation (83) into Equations (81) and (82), integrating once under the zero-boundary conditions, and collecting like terms gives the pair

$$(c + aA)\eta - \delta^2 bA\eta'' = -\frac{3}{4}\varepsilon A\eta^2, \tag{84}$$

$$(cA + e)\eta - \delta^2 cA(d + f)\eta'' = -\frac{1}{2}\varepsilon A^2\eta^2. \tag{85}$$

Demanding that the algebraic factors multiplying η and η'' coincide in Equations (84) and (85) (otherwise only the trivial solution $\eta \equiv 0$ would be admissible) yields the linear system

$$2Ac + 2aA^2 = 3Ac + 3e, \qquad -Ac + 2aA^2 = 3e, \tag{86}$$

whose unique positive solution is[11]

$$A^2 = \frac{9e(d + f)}{6a(d + f) - 2b}, \qquad c = \frac{2b}{3(d + f)}A.$$

[11] The positive root is selected to guarantee a right-propagating pulse ($c > 0$).

Restoring the original parameters,

$$A = 6\sqrt{\frac{\beta\,(3\alpha+1)}{r_0\,(36\alpha+11)}}, \qquad c = \frac{r_0}{6\alpha+2}\sqrt{\frac{\beta\,(3\alpha+1)}{r_0\,(36\alpha+11)}}\,.$$

Scalar solitary wave equation.

With the compatibility conditions (86) enforced, either of the relations (84), (85) becomes

$$A_1\,\eta' - B_1\,\eta''' = \eta\,\eta', \qquad A_1 := \frac{4be+6ae(d+f)}{9e(d+f)\,\varepsilon}, \quad B_1 := \frac{2b\,\delta^2}{3\,\varepsilon}, \tag{87}$$

which is a well-known integrable third-order ODE of the KdV type Newell (1977). Provided $A_1 B_1 > 0$, equation (87) admits the classical sech^2 solitary-wave solution:

$$\eta(\zeta) = 3\,A_1\,\operatorname{sech}^2\Big[\frac{1}{2}\sqrt{A_1/B_1}\,(\zeta-\zeta_0)\Big], \qquad \zeta_0 \in \mathbb{R}.$$

Re-expressed through the physical parameters,

$$\eta(\zeta) = -\frac{3\,r_0\,(7+18\alpha)}{54\alpha+18}\,\operatorname{sech}^2\Big[\frac{\zeta}{2\delta}\sqrt{\frac{28+72\alpha}{r_0^2(3\alpha+1)}}\Big], \tag{88}$$

and, by virtue of (76),

$$\bar{u}(\zeta) = \frac{r_0\,(7+18\alpha)}{3\alpha+1}\sqrt{\frac{\beta\,(3\alpha+1)}{r_0\,(36\alpha+11)}}\,\operatorname{sech}^2\Big[\frac{\zeta}{2\delta}\sqrt{\frac{28+72\alpha}{r_0^2(3\alpha+1)}}\Big]. \tag{89}$$

The entire derivation has been cross-checked symbolically in Maple; the annotated worksheet is provided in the accompanying codes repository.

3 | DISPERSION RELATIONS

We first examine the linear dispersion characteristics of the full three-dimensional model and compare them with those obtained from the linearised Euler equations by following Mitsotakis et al. (2018):

$$u_t + \frac{1}{\rho}\,p_x = 0, \tag{90}$$

$$v_t + \frac{1}{\rho}\,p_r = 0, \tag{91}$$

$$u_x + v_r + \frac{1}{r}\,v = 0, \tag{92}$$

subject to the boundary conditions

$$v\left(x, r^{w}, t\right) = \eta_{t}\left(x, t\right), \tag{93}$$

$$p^{w}\left(x, t\right) = \rho^{w} h \eta_{tt}\left(x, t\right) + \frac{E h}{\rho_{0}^{2}} \eta\left(x, t\right), \tag{94}$$

$$v\left(x, 0, t\right) = 0. \tag{95}$$

Normal-mode ansatz.

We consider normal modes of the form

$$u\left(x, r, t\right) = u_{0}\left(r\right) \exp\left(\mathrm{i}\left(k x - \omega t\right)\right), \qquad v\left(x, r, t\right) = v_{0}\left(r\right) \exp\left(\mathrm{i}\left(k x - \omega t\right)\right),$$

$$\eta\left(x, t\right) = \eta_{0} \exp\left(\mathrm{i}\left(k x - \omega t\right)\right), \qquad p\left(x, r, t\right) = p_{0}\left(r\right) \exp\left(\mathrm{i}\left(k x - \omega t\right)\right),$$

and substitute these expressions into the linearised Euler system. The axial velocity amplitude $u_{0}\left(r\right)$ then satisfies the modified Bessel equation

$$r u_{0}''\left(r\right) + u_{0}'\left(r\right) - r k^{2} u_{0}\left(r\right) = 0, \tag{96}$$

together with the regularity condition

$$u_{0}'\left(0\right) = 0 \tag{97}$$

and the wall conditions

$$u_{0}'\left(r_{0}\right) = \omega k \eta_{0}, \tag{98}$$

$$\rho^{w} h \omega^{2} \eta_{0} + \frac{\rho \omega}{k} u_{0}\left(r_{0}\right) - \frac{E h}{r_{0}^{2}} \eta_{0} = 0. \tag{99}$$

The Bessel problem (96)–(98) admits the solution

$$u_{0}\left(r\right) = \eta_{0} \omega \frac{I_{0}\left(k r\right)}{I_{1}\left(k r_{0}\right)},$$

where I_{0} and I_{1} are the modified Bessel functions of the first kind. Inserting this expression into (99) yields the *exact* linear dispersion relation

$$\omega_{\varepsilon}^{2}\left(k\right) = \frac{E h}{\rho r_{0}^{3}} \frac{r_{0} k I_{1}\left(k r_{0}\right)}{\frac{\rho^{w} h}{\rho r_{0}} r_{0} k I_{1}\left(k r_{0}\right) + I_{0}\left(k r_{0}\right)}. \tag{100}$$

Reduced Boussinesq system.

We next linearise the depth-averaged system (63)–(64) and again insert the normal-mode ansatz. This procedure leads to

$$\frac{r_0}{2}\,\mathrm{i}k\,\bar{u}_0 \;-\; \mathrm{i}\omega\,\eta_0 \;-\; \frac{\delta^2}{48}\,r_0^3\,(\mathrm{i}k)^3\bar{u}_0 \;=\; 0, \tag{101}$$

$$-\mathrm{i}\omega\,\bar{u}_0 \;-\; \alpha\delta^2\,k\omega^2\eta_0 \;+\; \mathrm{i}k\,\beta\,\eta_0 \;+\; \delta^2\,\beta\gamma\,(\mathrm{i}k)\omega\,\eta_0 \;+\; \frac{\delta^2}{6}\,r_0^2\,k^2\omega\,\bar{u}_0 \;=\; 0. \tag{102}$$

Elimination of $\bar{u}_0$ gives the quadratic dispersion relation

$$\Big(24\,r_0k \;+\; r_0^3k^3\Big)\Big(\alpha k \;+\; \frac{48 \;+\; 8\,\delta^2r_0^2k^2}{24\,r_0k \;+\; r_0^3k^3}\Big)\omega^2 \;+\; \mathrm{i}\,\delta^2\,\beta\gamma\,k\,\omega \;-\; \beta\,k \;=\; 0. \tag{103}$$

Modified Boussinesq system.

For the refined system (79)–(80) we proceed analogously and obtain the alternate quadratic

$$\Big(24\,r_0k \;+\; \delta^2r_0^3k^3\Big)(-48 \;-\; 24\,\alpha\delta^2r_0^2k^2 \;-\; 8\,\delta^2r_0^2k^2)\omega^2 \;-\; \mathrm{i}\,\delta^2\,\beta\gamma\,k\,\omega \;+\; \beta\,k \;=\; 0. \tag{104}$$

Comparison of phase speeds.

The phase speeds furnished by (100), (103) and (104), together with those of the classical KdV and BBM reductions, are depicted in Figure 4 for

$$r_0 = 0.01\ \mathrm{m}, \qquad h = 3\times10^{-4}\ \mathrm{m}, \qquad E = 4.1\times10^{5}\ \mathrm{kg\,m^{-1}\,s^{-2}}, \qquad \rho^{\omega} = 10^{3}\ \mathrm{kg\,m^{-3}}, \qquad \rho = 1060\ \mathrm{kg\,m^{-3}}.$$

Remarks.

The algebraic relations (103) and (104) demonstrate that both the classical and the modified depth-averaged models reproduce the low-frequency branch of the exact dispersion curve with the correct slope. The modified formulation retains this agreement while reducing the high-frequency error introduced by the classical Boussinesq truncation, thereby reinforcing its suitability for simulating arterial pulse waves over physiologically relevant wavelengths.

4 | NUMERICAL SIMULATIONS

To study solitary wave dynamics in the Boussinesq system, we implement a pseudo-spectral solver with a filtering method (Chen and Bona (2002)). This approach leverages spectral methods for high-precision solutions and incorporates filtering techniques to stabilize solitary wave simulations, ensuring accurate capture of their propagation characteristics Trefethen (2000); Boyd (2000).

The Boussinesq system, modeling nonlinear dispersive waves, is given by:

$$\partial_t\eta + \frac{r_0}{2}\,\partial_x\bar{u} + \frac{\varepsilon}{2}\eta\,\partial_x\bar{u} + \varepsilon\,\partial_x\eta\bar{u} - \frac{\delta^2r_0^3}{48}\,\partial_x^3\bar{u} = 0, \tag{105}$$

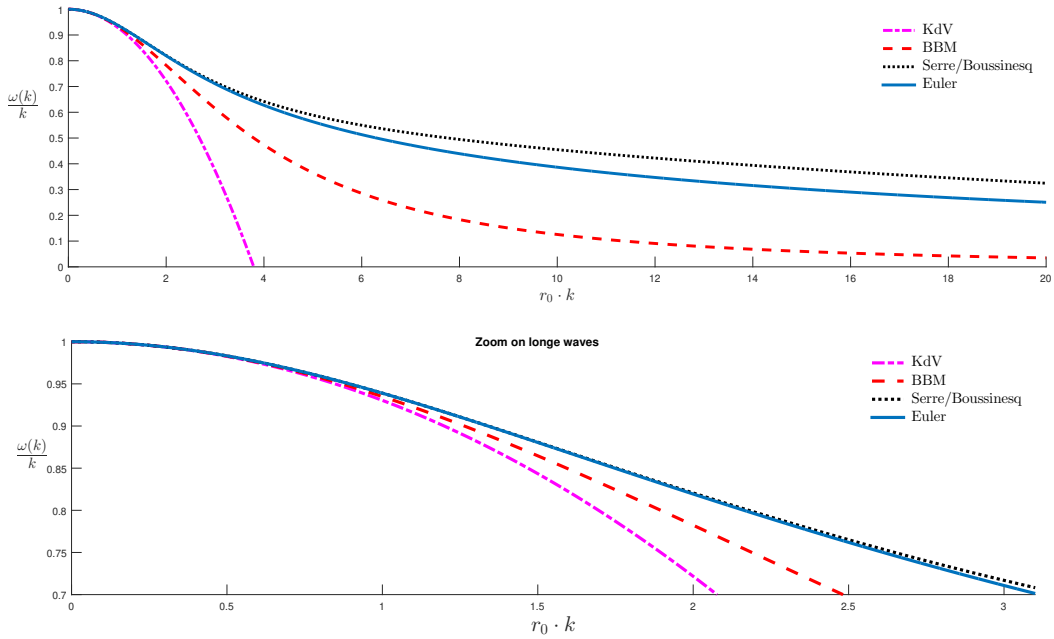

FIGURE 4 *Comparison of linear phase speeds predicted by various Boussinesq-type approximations with the reference Euler result.*

$$\partial_t \bar{u} + \varepsilon \bar{u} \partial_x \bar{u} - \frac{\alpha r_0 \delta^2}{2} \partial_x^2 \partial_t \bar{u} + \beta \partial_x \eta + \delta^2 \beta \gamma \partial_x \partial_t \eta - \frac{\delta^2 r_0^2}{6} \partial_x^2 \partial_t \bar{u} = 0, \tag{106}$$

where $\eta(x,t)$ is the free surface elevation, $\bar{u}(x,t)$ is the velocity, r_0 is a reference radius, ε and δ are nonlinearity and dispersion parameters, and α, β, γ are system parameters. For this study, we set $\gamma = 0$.

The pseudo-spectral solver transforms the variables $\eta(x,t)$ and $\bar{u}(x,t)$ into Fourier space using the Fourier transform, where $\hat{\eta}(k,t) = \mathcal{F}\{\eta\}$ and $\hat{u}(k,t) = \mathcal{F}\{\bar{u}\}$. The Fourier transform relationships are:

$$\mathcal{F}\{\partial_x \eta\} = \mathrm{i}k\hat{\eta}, \quad \mathcal{F}\{\partial_x^2 \bar{u}\} = -k^2 \hat{u}, \quad \mathcal{F}\{\partial_x^3 \bar{u}\} = -\mathrm{i}k^3 \hat{u}.$$

Applying the Fourier transform to (105) and (106), we obtain:

$$\partial_t \hat{\eta} = -\frac{r_0}{2}(\mathrm{i}k\hat{u}) - \frac{\varepsilon}{2}\mathcal{F}\{\eta \partial_x \bar{u}\} - \varepsilon \mathcal{F}\{(\partial_x \eta)\bar{u}\} + \frac{\delta^2 r_0^3}{48}(-\mathrm{i}k^3 \hat{u}), \tag{107}$$

$$\partial_t \hat{u} = -\frac{\varepsilon \mathrm{i}k \mathcal{F}\{\bar{u}\bar{u}\} + \beta \mathrm{i}k \hat{\eta}}{1 + \frac{r_0 \delta^2 k^2 (3\alpha + r_0)}{6}}, \tag{108}$$

where the denominator in (108) accounts for the dispersive terms involving $\partial_x^2 \partial_t \bar{u}$.

4.1 | Filtering Method and Time Integration

To stabilize solitary wave solutions and reduce numerical noise, we employ a filtering method, which effectively dampens high-frequency oscillations while preserving the solitary wave's key features Chen and Bona (2002); Trefethen (2000). The computational grid is defined with a refined spatial discretization to capture the wave profile accurately, and the time-stepping is adjusted to ensure stability. The solver initializes $\eta(x,0)$ and $\bar{u}(x,0)$ with given solitary wave profiles, transforming them into Fourier space to obtain $\hat{\eta}(k,0)$ and $\hat{u}(k,0)$. Temporal integration is performed using MATLAB's ODE113 solver, a variable-step, variable-order (VSVO) Adams–Bashforth–Moulton PECE solver with orders 1 to 13 (typically using order 12 with a 13th-order error estimate for extrapolation). This solver is well-suited for both stiff and non-stiff systems, providing efficient and accurate time evolution Boyd (2000). Initial tests of the pseudo-spectral solver with filtering demonstrate reliable convergence and stable solitary wave propagation, consistent with the expected behavior of the Boussinesq system. The filtering method effectively mitigates numerical instabilities, yielding precise solutions. Future work will involve thorough validation against analytical solutions and experimental data to ensure accuracy and robustness Chen and Bona (2002); Trefethen (2000).

To simulate solitary wave dynamics in the Boussinesq system, accurate numerical approximations of solitary waves are essential. While generating clean solitary waves in a laboratory is challenging, we demonstrate that numerical generation is straightforward using a filtering procedure, even without exact solutions Bona et al. (2008). This method produces reliable initial conditions for studying wave collisions and interactions.

The filtering procedure generates clean solitary waves by evolving an approximate wave profile and isolating the leading solitary wave from dispersive tails. The process is as follows:

Initial Wave Approximation: Start with an initial wave profile $\eta(x,0)$ and $\bar{u}(x,0)$ resembling a solitary wave, such as a low-order approximation. The profile need not be exact but should approximate the expected shape and amplitude.
Numerical Evolution: Evolve the initial profile in a long computational domain using the Boussinesq system (105)–(106), allowing the solitary wave to separate from dispersive tails and smaller waves over time.
Isolation of Solitary Wave: Once the leading solitary wave is distinct, isolate it by setting the remaining disturbances (dispersive tails) to zero. Shift the solitary wave to the left of the spatial domain for further refinement.
Iterative Refinement: Repeat the evolution and isolation process as needed. Typically, one iteration suffices to produce a clean solitary wave.

This filtering method effectively removes numerical noise and dispersive components, yielding high-precision solitary wave solutions Bona et al. (2008).

The Boussinesq system is solved using the pseudo-spectral solver described previously, with spatial derivatives computed in Fourier space and temporal integration performed using MATLAB's ODE113 solver. The computational domain has a length $L = 400$ and grid spacing $\Delta X = \frac{2}{N}$ with $N = 32\,768$. Parameters are set as $\alpha = \beta = r_0 = 1$, and the characteristic speed is derived as:

$$\tilde{c} = \sqrt{\frac{\beta r_0}{2}}.$$

This value is obtained by analyzing the linearized Boussinesq system up to $O(\varepsilon + \delta^2)$, as shown in the following proof:

Proof Consider the linearized Boussinesq system:

$$\begin{cases} \partial_t \eta + \frac{r_0}{2} \partial_x \bar{u} = 0, \\ \partial_t \bar{u} + \beta \partial_x \eta = 0. \end{cases} \tag{109}$$

Assume solutions of the form:

$$\eta(x,t) = \eta_0 \exp(\mathrm{i}k(x - \tilde{c}t)), \quad \bar{u}(x,t) = \bar{u}_0 \exp(\mathrm{i}k(x - \tilde{c}t)).$$

Substituting into (109), we obtain:

$$\begin{cases} -\mathrm{i}k\tilde{c}\eta_0 + \frac{r_0}{2}\mathrm{i}k\bar{u}_0 = 0, \\ -\mathrm{i}k\tilde{c}\bar{u}_0 + \beta\mathrm{i}k\eta_0 = 0. \end{cases}$$

For non-trivial solutions, the determinant of the coefficient matrix must vanish, yielding:

$$\tilde{c}^2 = \frac{\beta r_0}{2} \implies \tilde{c} = \sqrt{\frac{\beta r_0}{2}}.$$

4.1.1 | Initial Conditions and Solitary Wave Solutions

To generate initial conditions, we use solitary wave solutions of the Korteweg–de Vries (KdV) equation with $\gamma = 0$:

$$\partial_t \eta + \tilde{c}\partial_x \eta + \frac{5}{2}\frac{1}{r_0}\tilde{c}\eta\partial_x \eta + \frac{\tilde{c}(12\tilde{\alpha} + 3r_0)r_0}{48}\partial_x^3 \eta = 0. \tag{110}$$

The first-order solitary wave solution is:

$$\eta(x,t) = A\,\mathrm{sech}^2\left(\frac{1}{2}\kappa(x - ct)\right), \tag{111}$$

$$\bar{u}(x,t) = \frac{c_0}{a}A\,\mathrm{sech}^2\left(\frac{1}{2}\kappa(x - ct)\right) - \frac{c_0}{4ar_0}\left[A\,\mathrm{sech}^2\left(\frac{1}{2}\kappa(x - ct)\right)\right]^2 + \frac{c_0 r_0(5 + 12\alpha)}{48a}\partial_x^2\left[A\,\mathrm{sech}^2\left(\frac{1}{2}\kappa(x - ct)\right)\right], \tag{112}$$

where $c_0 = \frac{a}{r_0}\sqrt{\frac{2Eh}{\rho r_0}}$ is a modified Moens-Korteweg speed, and the wave parameters are:

$$\kappa = \sqrt{\frac{40\tilde{c}A}{3r_0^2(4\tilde{\alpha}\tilde{c} + r_0)}}, \quad c = \tilde{c}\left(1 + \frac{5A}{6r_0}\right).$$

These solutions are used as initial conditions, evolved, and filtered to produce clean solitary waves.

TABLE 1 Estimated solitary wave speed and amplitude for the cylindrical Boussinesq system (79)–(80).

A	A_s	c_s	c	A	A_s	c_s	c
0.05	0.0431	0.7324	0.7325	0.55	0.5460	0.9521	1.0288
0.1	0.0853	0.7551	0.7573	0.6	0.6066	0.9736	1.0645
0.15	0.1297	0.7785	0.7835	0.65	0.6693	0.9938	1.1015
0.2	0.1757	0.8015	0.8106	0.7	0.7338	1.0130	1.1395
0.25	0.2231	0.8242	0.8385	0.75	0.8003	1.0317	1.1787
0.3	0.2723	0.8466	0.8675	0.8	0.8687	1.0498	1.2190
0.35	0.3232	0.8687	0.8975	0.85	0.9389	1.0679	1.2603
0.4	0.3760	0.8910	1.2321	0.9	1.0109	1.0853	1.13028
0.45	0.4307	0.9116	0.9609	0.95	1.0847	1.1022	1.3462
0.5	0.4874	0.9327	0.9943	1	1.1603	1.1189	1.3908

4.1.2 | Numerical Results

Solitary waves of varying amplitudes A from 0.05 to 1.0 were generated, producing heights A_s from 0.0431 to 1.1603, as detailed in Table 1. The table compares simulated speeds c_s with theoretical speeds c.

Figure 5 illustrates the space-time evolution of a solitary wave with initial amplitude $A = 0.1$ from $t = 0$ to $t = 1050$, showing stable propagation. Figure 6 depicts the time evolution for $A = 0.4$ (height $A_s = 0.3760$) at times $t = 1, 80, 100, 150$, demonstrating the development of a solitary wave followed by a dispersive tail. At $t = 150$, the solitary wave is isolated by shifting it left by 130.4 units and setting the tail to zero, yielding a clean solution. Figure 7 compares the amplitude-speed relationship of the Boussinesq system with the KdV model, showing good agreement for small amplitudes.

The filtering procedure generates clean solitary wave solutions by iteratively refining approximate profiles, effectively isolating the solitary wave from dispersive tails. This method is robust for the Boussinesq system, where exact solutions may not exist due to nonlinear term complexities Bona et al. (2008). The numerical results, validated through Table 1 and Figures 5–7, confirm stable solitary wave propagation and good agreement with KdV predictions for small amplitudes. Large-amplitude solutions, while less physically relevant due to model assumptions, test the algorithm's robustness. This approach provides reliable initial conditions for studying wave interactions, enhancing our understanding of nonlinear wave dynamics in shallow water systems.

5 | STOKES EXPANSIONS

In this section, we employ Stokes expansion techniques to analyze the nonlinear wave solutions of our derived models. Stokes expansions provide a systematic approach to construct periodic wave solutions in weakly nonlinear regimes, revealing how nonlinearity affects the dispersion relation and wave profiles. We will focus particularly on applying this methodology to the KdV and BBM reductions of our cylindrical Boussinesq system, demonstrating how the interplay

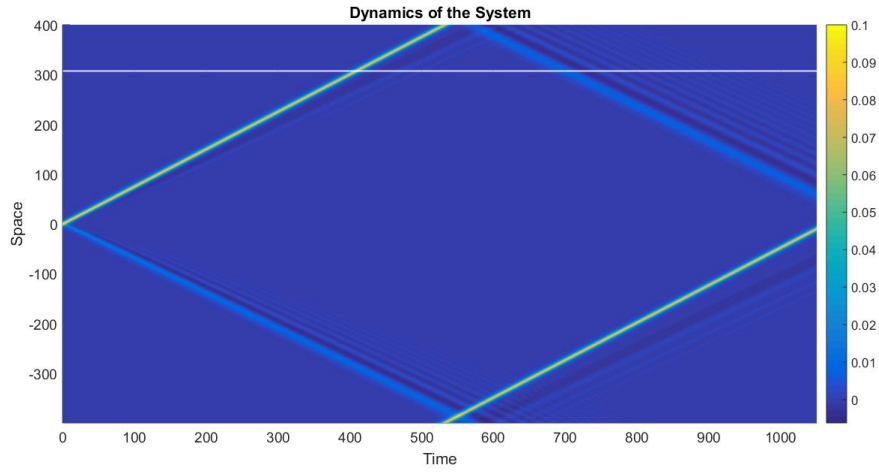

FIGURE 5 Space-time plot of the KdV soliton (110) evolution under the Boussinesq system (105)–(106) dynamics for initial amplitude $A = 0.1$ from $t = 0$ to $t = 1050$. Parameters are reported in Table 1.

between nonlinearity and dispersion shapes the propagation characteristics of arterial pulse waves. This analysis will further elucidate the amplitude-dependent modifications to wave speed and structure that are essential for accurately modeling blood flow dynamics in elastic vessels.

5.1 | Weakly nonlinear Stokes expansion for the KdV reduction

Stokes' pioneering investigations of periodic gravity waves, first published in 1847, revealed two fundamental facts that remain central to non-linear dispersive-wave theory: *(i)* coherent periodic wave-trains are admissible even when the governing equations are non-linear, and *(ii)* the dispersion relation acquires an explicit dependence on the wave amplitude. The latter feature gives rise to qualitatively new phenomena rather than mere numerical corrections.

We apply Stokes' method to the KdV reduction

$$\eta_t + \tilde{c}\,\eta_x + \frac{5}{2}\frac{\tilde{c}}{r_0}\,\eta\,\eta_x + \frac{\tilde{c}\,(12\tilde{\alpha} + 3r_0)\,r_0}{48}\,\eta_{xxx} = 0, \tag{113}$$

obtained by setting $\gamma = 0$ in (75). Introducing the small parameter ε and the travelling phase $\theta = kx - \omega t$, we seek an expansion

$$\frac{\eta}{r_0} = \varepsilon\,\xi_1(\theta) + \varepsilon^2\,\xi_2(\theta) + \varepsilon^3\,\xi_3(\theta) + \dots. \tag{114}$$

With the abbreviations

$$a = \tilde{c}, \qquad b = \frac{5\tilde{c}}{2r_0}, \qquad c = \frac{\tilde{c}\,(12\tilde{\alpha} + 3r_0)\,r_0}{48},$$

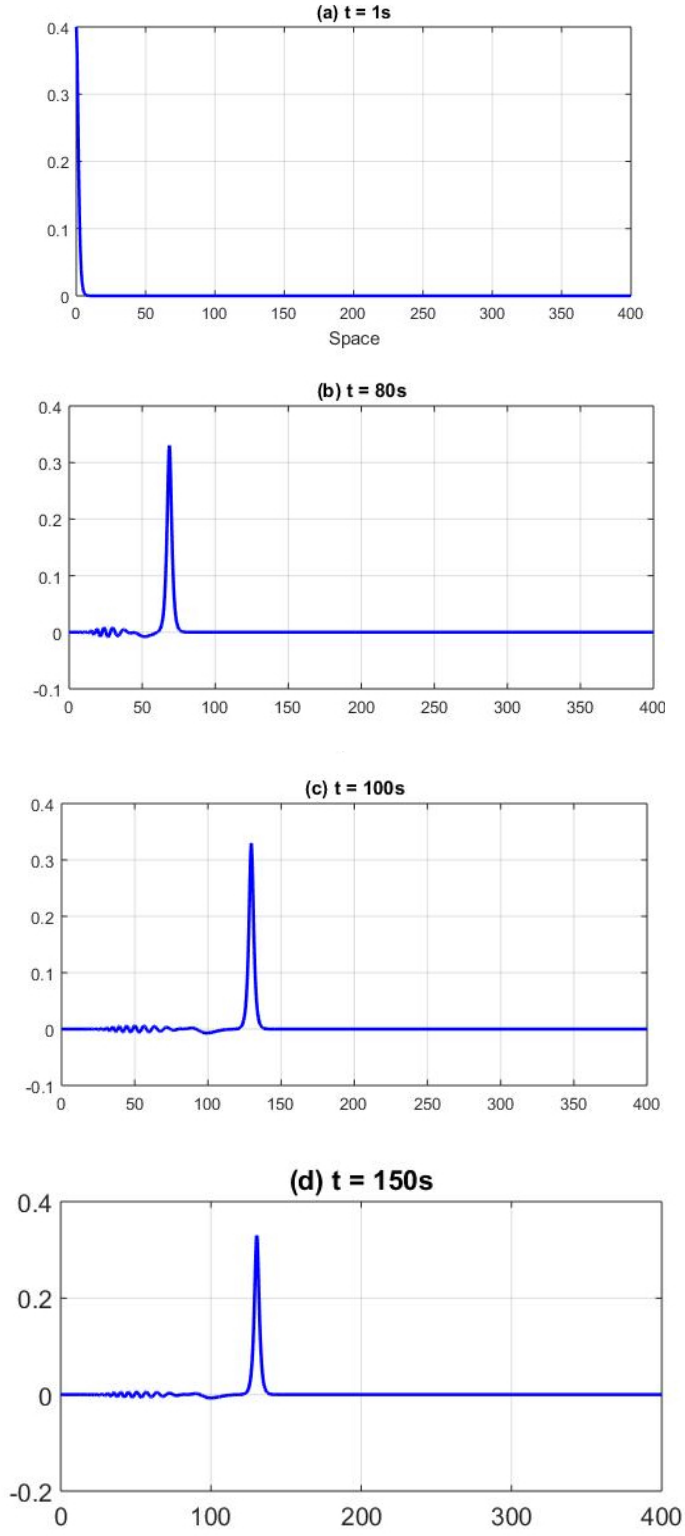

FIGURE 6 Time evolution of a solitary wave with initial amplitude $A = 0.4$ at $t = 1, 80, 100, 150$, showing the solitary wave followed by a dispersive tail.

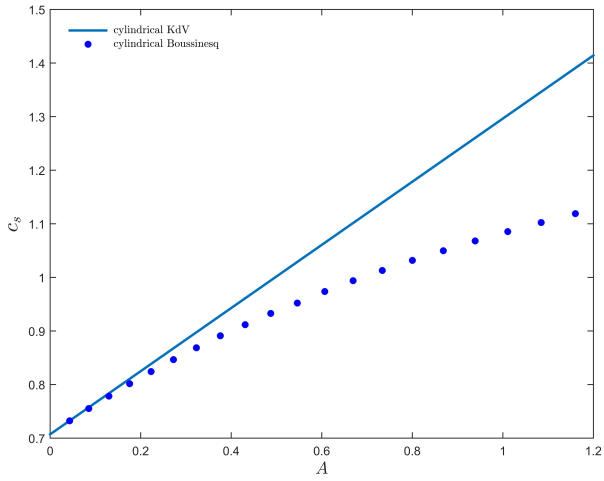

FIGURE 7 Comparison of amplitude-speed relationship between the Boussinesq system and the KdV model.

equation (113) yields the hierarchy

$$(\omega - ak)\,\xi_1' - c\,k^3\,\xi_1''' = 0, \tag{115}$$

$$(\omega - ak)\,\xi_2' - c\,k^3\,\xi_2''' = -b\,k\,\xi_1\,\xi_1', \tag{116}$$

$$(\omega - ak)\,\xi_3' - c\,k^3\,\xi_3''' = -b\,k(\xi_1^2)' - \omega_2\,\xi_1', \tag{117}$$

where $\omega = \omega_0(k) + \varepsilon^2\omega_2(k) + \ldots$ and $\omega_0(k) = ak - ck^3$. Equation (115) admits the normalised solution $\xi_1(\theta) = \cos\theta$. Solving (116) with this choice gives

$$\xi_2(\theta) = \frac{b}{12\,c\,k^2}\cos(2\theta).$$

The right-hand side of (117) contains a resonant term proportional to $\sin\theta$; eliminating it fixes $\omega_2(k) = \dfrac{b^2}{24\,c\,k}$. A particular solution of (117) is then $\xi_3(\theta) = \dfrac{b^2}{192\,c^2\,k^4}\cos(3\theta)$. The above sequence of calculations can be summarized in the form of the following theorem, which provides a closed-form expression for the periodic wave solution and the corresponding nonlinear dispersion relation up to third order in the perturbation parameter.

Theorem 1 *Let $\varepsilon \ll 1$ and let $k > 0$ be fixed. To third order in ε the KdV equation (113) possesses a $2\pi/k$-periodic Stokes wave of the form*

$$\frac{\eta}{r_0} = \varepsilon\cos\theta + \varepsilon^2\frac{b}{12\,c\,k}\cos(2\theta) + \varepsilon^3\frac{b^2}{192\,c^2\,k^4}\cos(3\theta) + O(\varepsilon^4), \qquad \theta = kx - \omega t, \tag{118}$$

where the non-linear dispersion relation is

$$\omega(k,\varepsilon) = ak - ck^3 + \varepsilon^2 \frac{b^2}{24\,c\,k} + O(\varepsilon^4). \tag{119}$$

The phase speed thus increases quadratically with amplitude, demonstrating the amplitude-dependent dispersion characteristic of Stokes waves.

Theorem 1 recovers the classical Stokes expansion for the KdV equation, with coefficients determined by the underlying physical parameters $\tilde{c}$, $\tilde{\alpha}$, and r_0. The result confirms that even weak non-linearity modifies the linear dispersion relation by an $O(\varepsilon^2)$ term proportional to the square of the wave amplitude.

5.2 | Weakly nonlinear Stokes expansion for the BBM reduction

Consider the Benjamin–Bona–Mahony (BBM) reduction obtained from the long-wave model,

$$\eta_t + \tilde{c}\,\eta_x + \frac{5\tilde{c}}{2r_0}\,\eta\,\eta_x - \frac{(12\tilde{\alpha} + 3r_0)\,r_0}{48}\,\eta_{xxt} = 0, \tag{120}$$

where, for simplicity, $\gamma = 0$ has been set. Denoting

$$a^* = \tilde{c}, \qquad b^* = \frac{5\tilde{c}}{2r_0}, \qquad c^* = \frac{\tilde{c}(12\tilde{\alpha} + 3r_0)\,r_0}{48},$$

we expand the solution in a Stokes series,

$$\frac{\eta}{r_0} = \varepsilon\,\xi_1(\theta) + \varepsilon^2\,\xi_2(\theta) + \varepsilon^3\,\xi_3(\theta) + \ldots, \qquad \theta = kx - \omega t, \tag{121}$$

with $\varepsilon \ll 1$.

Hierarchy of amplitude equations.

Insertion of (121) into (120) gives, at successive orders in ε,

$$(\omega - a^*k)\,\xi_1' - c^*\omega\,k^2\,\xi_1''' = 0, \tag{122}$$

$$(\omega - a^*k)\,\xi_2' - c^*\omega\,k^2\,\xi_2''' = b^*k\,\xi_1\xi_1', \tag{123}$$

$$(\omega - a^*k)\,\xi_3' - c^*\omega\,k^2\,\xi_3''' = b^*k\,(\xi_1^2)' - \omega_2\,\xi_1' + c^*\omega_2 k^2\,\xi_1'''. \tag{124}$$

The dispersion relation is again expanded as

$$\omega(k,\varepsilon) = \omega_0(k) + \varepsilon^2\,\omega_2(k) + \ldots, \qquad \omega_0(k) = \frac{a^*k}{1 + c^*k^2}.$$

Taking $\omega_1 = 0$ eliminates secular terms at $O(\varepsilon)$.

First- and second-order solutions.
Equation (122) admits the normalised solution

$$\xi_1(\theta) = \cos\theta.$$

Solving (123) for ξ_2 gives

$$\xi_2(\theta) = \frac{b^*(1+c^*k^2)}{12\,a^*c^*k^2}\cos(2\theta). \tag{125}$$

Elimination of resonances at third order.
The right-hand side of (124) contains the resonant term $\propto \sin\theta$. Choosing

$$\omega_2(k) = \frac{b^{*2}}{24\,c^*k}, \tag{126}$$

cancels this term. Integrating once then yields

$$\xi_3(\theta) = \frac{b^{*2}(1+c^*k^2)}{192\,c^{*2}k^4}\cos(3\theta). \tag{127}$$

The above sequence of calculations can be summarized in the form of the following theorem, which provides a closed-form expression for the periodic wave solution and the corresponding nonlinear dispersion relation up to third order in the perturbation parameter.

Theorem 2 *Let $\varepsilon \ll 1$ and $k > 0$. The BBM equation (120) possesses a $2\pi/k$-periodic Stokes wave of the form*

$$\frac{\eta}{r_0} = \varepsilon\cos\theta + \varepsilon^2\frac{b^*(1+c^*k^2)}{12\,a^*c^*k^2}\cos(2\theta) + \varepsilon^3\frac{b^{*2}(1+c^*k^2)}{192\,c^{*2}k^4}\cos(3\theta) + O(\varepsilon^4), \qquad \theta = kx - \omega t, \tag{128}$$

where the non-linear dispersion relation is

$$\omega(k,\varepsilon) = \frac{a^*k}{1+c^*k^2} + \varepsilon^2\frac{b^{*2}}{24\,c^*k} + O(\varepsilon^4). \tag{129}$$

Consequently, the phase speed obeys $c_{\text{ph}} = \omega/k$ and increases quadratically with the wave amplitude, reflecting the weakly non-linear character of the BBM model.

Theorem 2 mirrors the result obtained earlier for the KdV equation, but with the BBM-specific linear dispersion $\omega_0(k) = a^*k/(1+c^*k^2)$ and modified amplitude coefficients. Together with Theorem 1, it emphasises that both the KdV and BBM reductions support periodic Stokes waves whose speeds are augmented by non-linearity, thereby enriching the spectrum of observable dynamics in pulsatile blood-flow models.

6 | CONSERVATION LAWS AND SYMMETRIES

Every transformation that maps the solution manifold of a system of differential equations (DEs) into itself is termed a *symmetry*. The classical Lie method furnishes a systematic procedure for constructing single- and multi-parameter Lie

groups of point symmetries and has been successfully employed for algebraic, ordinary, and partial differential equations Cheviakov (2007). Analogous computational frameworks exist for the determination of contact and higher-order symmetries, as well as for non-local symmetries. Closely related methodologies have been developed for approximate symmetries, symmetries of difference schemes, and those of integro-differential equations; see, for instance, the extensive compendium in Ibragimov (1995).

Information about a PDE system's conservation laws is indispensable for a profound understanding of its symmetry structure. Conservation laws encode the fundamental physical invariants of the underlying process and underpin analytical results on existence, uniqueness, and stability Olver (1993); Evans (2010). They likewise play a pivotal rôle in geometric analyses of solution manifolds Bluman and Kumei (1987) and in the design of robust numerical schemes that preserve key physical quantities LeVeque (2002).

In this section we introduce the recently developed Maple package `GeM` Cheviakov (2007). The package provides fully automated routines for the local symmetry analysis of ODEs and PDEs and for the systematic search of conservation laws. All determining equations are generated symbolically in a form amenable to efficient automatic reduction and solution.

6.1 | Conservation laws

Divergence expressions that vanish on the solution set of a PDE system represent its *local conservation laws*. Such laws arise ubiquitously: classical examples include the conservation of mass, momentum, charge, and energy. For time-dependent systems on bounded domains they yield first integrals, while for ODEs they provide conserved quantities Cheviakov (2010). Conservation laws play a decisive rôle in the analytical theory of nonlinear PDEs, notably in the study of stability and in the construction of numerical schemes Lax (1968); Knops and Stuart (1984). Moreover, a local conservation law often serves to introduce non-local (potential) variables, thereby generating auxiliary PDE systems with identical solution sets Bluman and Kumei (1987); Sjöberg and Mahomed (2004).

The four standard flux-construction techniques, together with the direct method for conservation-law derivation, have all been implemented symbolically in `GeM` Cheviakov (2007). Package routines return the determining equations in a form suitable for automatic reduction and solution. They are capable of treating high-order systems with numerous dependent and independent variables and can typically be executed on a standard desktop computer.

Consider an N-equation PDE system of order K for

$$x = (x^1, \dots, x^n), \qquad u(x) = (u^1(x), \dots, u^m(x)),$$

written compactly as

$$L^\sigma[u] \;=\; L^\sigma\big(x, u, \partial u, \dots, \partial^K u\big) \;=\; 0, \qquad \sigma \in \{1, \dots, N\}. \tag{130}$$

We denote first-order derivatives by

$$u^\nu_i \;=\; \frac{\partial u^\nu}{\partial x^i},$$

and collect all derivatives of order p in

$$\partial^p u \;=\; \Big\{ \partial_{x^{i_1} \dots x^{i_p}} u^\nu \;\Big|\; \nu \in \{1, \dots, m\},\; i_1, \dots, i_p \in \{1, \dots, n\} \Big\}. \tag{131}$$

A *solved form* of (130) is obtained when

$$L^\sigma[u] \;=\; u^{j_\sigma}_{i_{\sigma,1}\dots i_{\sigma,s}} \;-\; M^\sigma\big(x,u,\partial u,\dots,\partial^K u\big) \;=\; 0, \qquad \sigma=1,\dots,N, \tag{132}$$

where $1\leqslant j_\sigma\leqslant m$, $s\leqslant K$, and $1\leqslant i_{\sigma,k}\leqslant n$. The set $\{u^{j_\sigma}_{i_{\sigma,1}\dots i_{\sigma,s}}\}_{\sigma=1}^N$ contains N linearly independent leading derivatives that do not appear in the right-hand sides M^σ.

Total and Euler operators.

The total derivative with respect to x^i is

$$D_i \;=\; \frac{\partial}{\partial x^i} \;+\; u^\nu_i\frac{\partial}{\partial u^\nu} \;+\; u^\nu_{ii_1}\frac{\partial}{\partial u^\nu_{i_1}} \;+\; u^\nu_{ii_1i_2}\frac{\partial}{\partial u^\nu_{i_1i_2}} \;+\; \dots, \qquad i\in\{1,\dots,n\}.$$

The Euler operator acting on a differential function $U(x)$ is

$$E_U \;=\; \frac{\partial}{\partial U} \;-\; D_i\frac{\partial}{\partial U_i} \;+\; \dots \;+\; (-1)^s D_{i_1}\dots D_{i_s}\frac{\partial}{\partial U_{i_1\dots i_s}} \;+\; \dots \tag{133}$$

Local conservation laws.

A divergence expression

$$\operatorname{div}\Phi \;\equiv\; D_i\,\phi^i[u] \;=\; D_1\phi^1 \;+\; \dots \;+\; D_n\phi^n \;=\; 0 \tag{134}$$

valid on the solution set of (130) is called a local conservation law. The fluxes ϕ^i may depend on x, u, and finitely many derivatives of u.

A conservation law (134) is *trivial* if

$$\phi^i \;=\; A^i[u] \;+\; D_j H^{ij}[u],$$

where A^i vanishes on solutions of (130) and $\operatorname{div} H\equiv 0$ identically.

Direct construction by multipliers.

Non-trivial conservation laws arise from multipliers $\{\Lambda_\sigma(x,U,\partial U,\dots,\partial^\ell U)\}_{\sigma=1}^N$ that satisfy

$$\Lambda_\sigma[U]\,L^\sigma[U] \;\equiv\; D_i\,\phi^i[U], \tag{135}$$

identically in the jet space. On any solution $U=u$ of (130) the right-hand side of (135) vanishes, yielding a local conservation law. Completeness of the direct method has been established for broad classes of systems, including those in (generalised) Kovalevskaya form Olver (1993):

Theorem 3 *For every local conservation law $D_i\phi^i[u]=0$ of a system in solved form (132) there exists an equivalent conservation law whose fluxes contain no leading derivatives, viz.*

$$D_i\,\tilde\phi^i[U] \;=\; \widetilde\Lambda_\sigma[U]\,\big(U^{j_\sigma}_{i_{\sigma,1}\dots i_{\sigma,s}} - M^\sigma[U]\big),$$

for some non-singular multipliers $\{\widetilde{\Lambda}_\sigma\}_{\sigma=1}^{N}$. *The correspondence between conservation laws and multiplier sets is, however, not always one-to-one.*

The `GeM` workflow.

A typical sequence for conservation-law computation in `GeM` proceeds as follows:

(i) Initialisation:
```
restart;
read("d:/gem32_12.mpl"):
with(GeM): with(linalg): with(DEtools): with(PDEtools):
```
(ii) Declaration of variables:
```
gem_decl_vars(indeps=[...], deps=[...], freefunc=[...], freeconst=[...]);
```
(iii) Input of the PDE system:
```
gem_decl_eqs([...], solve_for=[...]);
```
(iv) Generation of determining equations:
```
det_eqs := gem_conslaw_det_eqs([...]);
```
(v) Selection of unknown multipliers:
```
CL_multipliers := gem_conslaw_multipliers();
```
(vi) Reduction of the over-determined system:
```
simplified_eqs := DEtools[rifsimp](det_eqs, CL_multipliers, mindim=1);
```
(vii) Solution of determining equations:
```
multipliers_sol := pdsolve(simplified_eqs[Solved]);
```
(viii) Computation of fluxes:
```
gem_get_CL_fluxes(multipliers_sol);
```

6.2 | Symmetries

A *symmetry group* of a differential equation maps each solution to another solution. Continuous (Lie) symmetries are therefore inherent to every non-trivial system. The foundational concepts were introduced by Sophus Lie in the late nineteenth century and have since evolved into a versatile tool for analysing ODEs and PDEs.

For an n-dimensional independent variable x and m-component dependent variable u, a one-parameter group of point transformations reads

$$(x')^i = f^i(x,u;\varepsilon), \qquad (u')^\nu = g^\nu(x,u;\varepsilon), \qquad i \in \{1,\dots,n\},\ \nu \in \{1,\dots,m\},$$

or, in infinitesimal form,

$$(x')^i = x^i + \varepsilon\,\xi^i(x,u) + O(\varepsilon^2), \qquad (u')^\nu = u^\nu + \varepsilon\,\eta^\nu(x,u) + O(\varepsilon^2).$$

The associated generator is

$$X = \xi^i(x,u)\,\frac{\partial}{\partial x^i} + \eta^\nu(x,u)\,\frac{\partial}{\partial u^\nu}.$$

Its K-th prolongation is obtained via the standard formulae involving total derivatives D_i; cf. (133). The group is a

symmetry of (130) iff

$$X^{(K)}\, L^{\sigma} = 0 \quad \text{whenever} \quad L^{\sigma} = 0, \qquad \sigma \in \{1, \dots, N\}.$$

The `GeM` workflow for symmetries.

(i) Initialisation.

(ii) Declaration of variables and parameters.

(iii) Input of the PDE system.

(iv) Generation of determining equations:

```
det_eqs := gem_symm_det_eqs([...]);
```

(v) Selection of symmetry components:

```
sym_components := gem_symm_components();
```

(vi) Reduction of the system:

```
simplified_eqs := DEtools[rifsimp](det_eqs, sym_components, mindim=1);
```

(vii) Solution of determining equations:

```
symm_sol := pdsolve(simplified_eqs[Solved]);
```

(viii) Output of symmetries:

```
gem_output_symm(symm_sol);
```

Detailed examples for both the Boussinesq and the full cylindrical blood-flow models are provided below, together with the resulting conservation laws, symmetry generators, and the corresponding one-parameter transformation groups.

Conservation laws and symmetries for the Boussinesq system.

For the cylindrical Boussinesq system (65), (66) with constant radius r_0, a direct multiplier search yields the local conservation law

$$\left[\bar{u} + \frac{1}{2}\tilde{\beta}\,\gamma\,\eta_x + \frac{2}{3}\tilde{\alpha}\,\eta_{xt} - \frac{1}{18}\,r_0^2\,\bar{u}_{xx}\right]_t + \left[\frac{1}{2}\,\bar{u}^2 + \tilde{\beta}\,\eta + \frac{1}{2}\tilde{\beta}\,\gamma\,\eta_t - \frac{1}{9}\,r_0^2\,\bar{u}_{tx} + \frac{1}{3}\,\tilde{\alpha}\,\eta_{tt}\right]_x = 0. \tag{136}$$

Here $\tilde{\alpha} = \rho^{w}\,\mathrm{h}/\rho$ and $\tilde{\beta}(x) = \mathrm{E}\,\mathrm{h}/(\rho\,r_0^2)$. The corresponding multipliers are

- $\lambda_1(t, x, \eta, \bar{u}, \dots) = 0$,
- $\lambda_2(t, x, \eta, \bar{u}, \dots) = 1$.

The infinitesimal symmetry generators are

$$X_1 = \partial_x, \qquad X_2 = \partial_t,$$

with associated point transformations

$$x' = x + \varepsilon_1, \quad t' = t, \quad \eta' = \eta, \quad \bar{u}' = \bar{u}; \qquad x' = x, \quad t' = t + \varepsilon_2, \quad \eta' = \eta, \quad \bar{u}' = \bar{u}.$$

These represent spatial and temporal translations.

Conservation laws and symmetries of the full cylindrical model (constant unperturbed radius).

For $r_0 = \text{const}$, the governing equations read

$$\frac{(r_0+\eta)^2}{2}\,\bar{u}_x - \frac{(r_0+\eta)^3}{12}\,\eta_x\,\bar{u}_{xx} - \frac{(r_0+\eta)^4}{48}\,\bar{u}_{xxx} + (r_0+\eta)\,\eta_t + (r_0+\eta)\,\eta_x\,\bar{u} \;=\; 0, \tag{137}$$

$$\begin{aligned}(r_0+\eta)\,\bar{u}_t + \frac{(r_0+\eta)^2}{6}\,\eta_t\,\bar{u}_{xx} + (r_0+\eta)\,\bar{u}\,\bar{u}_x + \frac{(r_0+\eta)^2}{6}\,\eta_x\,\bar{u}\,\bar{u}_{xx}\\ + \Big(\tilde{\alpha}\,\eta_{tt} + \tilde{\beta}\,\eta + \tilde{\beta}\,\gamma\,\eta_t\Big)_x\,(r_0+\eta) + \frac{(r_0+\eta)^3}{12}\,\bar{u}_x\,\bar{u}_{xx} - \frac{1}{6}\,\frac{\partial}{\partial x}\Big[(r_0+\eta)^3\big(\bar{u}_{xt} + \bar{u}\,\bar{u}_{xx} - \tfrac{1}{2}\,\bar{u}_x^2\big)\Big] \;=\; 0.\end{aligned} \tag{138}$$

In the multiplier ansatz adopted, *two* independent sets are obtained:

$$\big\{\lambda_1 = 1,\ \lambda_2 = 0\big\}, \qquad \big\{\lambda_3 = 0,\ \lambda_4 = \tfrac{1}{r_0+\eta}\big\}.$$

Each set generates a distinct local conservation law.

First conservation law.

With $\lambda_1 = 1$ the characteristic form yields

$$\Big[\eta\,r_0 + \tfrac{1}{2}\,\eta^2\Big]_t + \Big[-\tfrac{1}{48}\,\eta^4\,\bar{u}_{xx} - \tfrac{1}{12}\,r_0\,\eta^3\,\bar{u}_{xx} - \tfrac{1}{8}\,r_0^2\,\eta^2\,\bar{u}_{xx} - \tfrac{1}{12}\,r_0^3\,\eta\,\bar{u}_{xx} - \tfrac{1}{48}\,r_0^4\,\bar{u}_{xx} + \tfrac{1}{2}\,\eta^2\,\bar{u} + r_0\,\eta\,\bar{u} + \tfrac{1}{2}\,r_0^2\,\bar{u}\Big]_x = 0. \tag{139}$$

Second conservation law.

With $\lambda_4 = 1/(r_0+\eta)$ one obtains

$$\begin{aligned}&\Big[\bar{u} + \tfrac{1}{2}\,\tilde{\beta}\,\gamma\,\eta_x - \tfrac{1}{18}\,r_0^2\,\bar{u}_{xx} + \tfrac{2}{3}\,\tilde{\alpha}\,\eta_{xt} + \tfrac{5}{108}\,\bar{u}\,\eta_x^2 + \tfrac{1}{27}\,\bar{u}_{xx}\,\eta^2 + \tfrac{1}{36}\,r_0\,\bar{u}_{xx}\,\eta\\ &\quad - \tfrac{5}{108}\,\eta\,\eta_x\,\bar{u}_x - \tfrac{5}{72}\,r_0\,\eta_x\,\bar{u}_x + \tfrac{5}{108}\,\eta\,\eta_{xx}\,\bar{u} + \tfrac{5}{72}\,r_0\,\eta_{xx}\,\bar{u}\Big]_t + \Big[-\tfrac{1}{6}\,\bar{u}\,\bar{u}_{xx}\,\eta^2 - \tfrac{1}{3}\,r_0\,\bar{u}\,\bar{u}_{xx}\,\eta - \tfrac{1}{6}\,r_0^2\,\bar{u}\,\bar{u}_{xx}\\ &\quad + \tfrac{1}{8}\,\bar{u}_x^2\,\eta^2 + \tfrac{1}{4}\,r_0\,\bar{u}_x^2\,\eta + \tfrac{1}{8}\,r_0^2\,\bar{u}_x^2 - \tfrac{11}{54}\,\eta^2\,\bar{u}_{tx} - \tfrac{13}{36}\,r_0\,\eta\,\bar{u}_{tx} - \tfrac{1}{9}\,r_0^2\,\bar{u}_{tx}\\ &\quad + \eta\,\tilde{\beta} + \tfrac{1}{2}\,\tilde{\beta}\,\gamma\,\eta_t + \tfrac{1}{3}\,\tilde{\alpha}\,\eta_{tt} - \tfrac{5}{108}\,\bar{u}\,\eta\,\eta_{tx} - \tfrac{5}{72}\,r_0\,\bar{u}\,\eta_{tx} + \tfrac{5}{54}\,\bar{u}_x\,\eta\,\eta_t + \tfrac{5}{36}\,r_0\,\bar{u}_x\,\eta_t\\ &\quad - \tfrac{5}{108}\,\eta\,\eta_x\,\bar{u}_t - \tfrac{5}{72}\,r_0\,\eta_x\,\bar{u}_t + \tfrac{1}{2}\,\bar{u}^2\Big]_x = 0.\end{aligned} \tag{140}$$

Both conserved vectors (139), (140) are of third order in spatial derivatives and reduce, in the weakly nonlinear limit $\eta \ll r_0$, to the classical mass and momentum balances for long waves in an elastic vessel.

Symmetry generators.

For the constant-radius system the complete Lie algebra of point symmetries is spanned by

$$X_1 = \partial_x, \qquad X_2 = \partial_t,$$

corresponding to spatial and temporal translations. The induced one-parameter groups act by

$$(x,t,\eta,\bar{u}) \;\mapsto\; (x+\varepsilon_1,\,t,\,\eta,\,\bar{u}), \qquad (x,t,\eta,\bar{u}) \;\mapsto\; (x,\,t+\varepsilon_2,\,\eta,\,\bar{u}).$$

Conservation laws and symmetries of the full cylindrical model (variable unperturbed radius)

For $r_0 = r_0(x)$ and $r^w = r_0(x) + \eta(x,t)$ the governing equations assume the form (61), (62). Only a single non-trivial multiplier survives, $\lambda_1 = 1$, $\lambda_2 = 0$, giving the conservation law

$$\Big[\eta\, r_0 + \tfrac{1}{2}\,\eta^2\Big]_t + \Big[-\tfrac{1}{48}\,\eta^4\,\bar{u}_{xx} - \tfrac{1}{12}\,\eta^3\, r_0\,\bar{u}_{xx} - \tfrac{1}{8}\,\eta^2\, r_0^2\,\bar{u}_{xx} - \tfrac{1}{12}\,\eta\, r_0^3\,\bar{u}_{xx} - \tfrac{1}{48}\, r_0^4\,\bar{u}_{xx} + \tfrac{1}{2}\,\eta^2\,\bar{u} + r_0\,\eta\,\bar{u} + \tfrac{1}{2}\, r_0^2\,\bar{u}\Big]_x = 0\,, \quad (141)$$

which reduces to (139) when r_0 is constant. The Lie algebra of point symmetries now depends on $r_0(x)$ and the parameters α, β, γ. The seven representative cases obtained with `GeM` are listed below:

Case 1. Generic data (α, β, γ arbitrary; $r_0(x)$ arbitrary): $X_1 = \partial_t$.
Case 2. $r_0'' = 0$ ($r_0 = r_{00} + r_{01}x$): $X_1 = \partial_t$, $X_2 = \partial_\eta - \dfrac{1}{r_{01}}\partial_x$.
Case 3. $\beta = 0$: $X_1 = \partial_t$, $X_2 = \bar{u}\,\partial_{\bar{u}} - t\,\partial_t$.
Case 4. $\beta = 0$ and $r_0'' = 0$: $X_1 = \partial_t$, $X_2 = \partial_\eta - \dfrac{1}{r_{01}}\partial_x$, $X_3 = \bar{u}\,\partial_{\bar{u}} - t\,\partial_t$.
Case 5. $r_0' = 0$ ($r_0 = r_{00}$): $X_1 = \partial_x$, $X_2 = \partial_t$.
Case 6. $\alpha = \gamma = r_0' = 0$: $X_1 = \partial_x$, $X_2 = \partial_t$, $X_3 = t\,\partial_x + \partial_{\bar{u}}$.
Case 7. $\alpha = \beta = r_0' = 0$: $X_1 = \partial_x$, $X_2 = \partial_t$, $X_3 = t\,\partial_x + \partial_{\bar{u}}$, $X_4 = \bar{u}\,\partial_{\bar{u}} - t\,\partial_t$.

All multipliers, conserved vectors, and symmetry generators have been derived with the `GeM` package in Maple Cheviakov (2007). Complete worksheets and verification scripts are provided in accompanying codes.

7 | MODULATIONAL INSTABILITY ANALYSIS

The cubic Nonlinear Schrödinger (NLS) equation,

$$\mathrm{i}\,\psi_t + \psi_{xx} + |\psi|^2\psi = 0\,, \quad (142)$$

is the canonical envelope model for weakly non-linear, weakly dispersive wave packets Sulem and Sulem (1999); Zakharov and Shabat (1972). It emerges, *inter alia*, in non-linear optics, water-wave theory, Bose–Einstein condensates, and plasma physics, and admits both analytical solutions (in the integrable focusing case) and efficient numerical discretisations Agrawal (2013); Taha and Ablowitz (1984). The first systematic derivation of (142) as a modulation equation for narrow-band wave trains was given independently by Benney–Newell (1967) and Zakharov (1968). Subsequent refinements include rigorous error estimates for water waves (Sulem & Sulem 1992) and multi-scale expansions that connect the NLS to lower-order models such as the KdV and BBM equations; see the reviews by Peregrine (1983) and Hammack and Henderson (1993) for historical details.

7.1 | Plane waves and Modulational Instability (MI)

Equation (142) admits the spatially homogeneous solution

$$\psi_0(x,t) = A\,\exp(\mathrm{i}|A|^2 t), \qquad A \in \mathbb{C}\setminus\{0\}, \tag{143}$$

often called a *plane wave*. To test its spectral stability we set

$$\psi(x,t) = \left[A + \varepsilon\,\varphi(x,t)\right]\,\exp(\mathrm{i}|A|^2 t), \qquad 0 < \varepsilon \ll 1,$$

linearise in ε, and seek normal modes $\varphi \propto \exp(\sigma t + \mathrm{i}qx)$. A straightforward calculation gives the dispersion relation

$$\sigma^2 = q^2(2|A|^2 - q^2). \tag{144}$$

Thus long-wave perturbations with $0 < q^2 < 2|A|^2$ grow exponentially in time, a manifestation of the Benjamin–Feir (BF) or Modulational Instability (MI).

Theorem 4 (Benjamin–Feir criterion) *Let ψ_0 be the plane-wave solution (143) of the focusing NLS equation (142). Then ψ_0 is modulationally unstable: for every wavenumber q satisfying $0 < q^2 < 2|A|^2$, there exists a perturbation of the form $\varphi(x,t) = \left[\hat{a}\,\mathrm{e}^{\sigma t} + \hat{b}\,\mathrm{e}^{-\sigma t}\right]\mathrm{e}^{\mathrm{i}qx}$, with growth rate $\sigma(q) = q\sqrt{2|A|^2 - q^2} > 0$. Conversely, all perturbations with $q^2 \geq 2|A|^2$ remain neutral. Hence the homogeneous state (143) is unstable to side-band perturbations whose wavelengths exceed the critical value $\lambda_c = \pi/|A|$.*

Theorem 4 furnishes the standard Benjamin–Feir instability criterion and will serve as the reference point for the modulational stability of the KdV- and BBM-derived NLS envelopes obtained in the preceding sections.

7.2 | Modulational instability analysis in KdV wave packets

This section derives the cubic Nonlinear Schrödinger (NLS) equation from the Korteweg–de Vries–Burgers (KdVB) equation using a systematic multiple-scales expansion. The KdVB equation models wave propagation with dispersion, non-linearity, and dissipation, while the NLS equation governs the slow modulation of nearly monochromatic wave trains. The derivation clarifies the transformation process and the physical implications of each term. The KdVB equation is given by

$$\eta_t + \tilde{c}\eta_x + \frac{5\tilde{c}}{2r_0}\eta\eta_x + \frac{\tilde{c}(12\tilde{\alpha} + 3r_0)r_0}{48}\eta_{xxx} - \frac{r_0\tilde{\beta}\gamma}{4}\eta_{xx} = 0, \tag{145}$$

where $\eta(x,t)$ represents the wave amplitude, and $\tilde{c}$, r_0, $\tilde{\alpha}$, $\tilde{\beta}$, and γ are constants. For clarity, define the coefficients:

$$a = \tilde{c}, \qquad b = \frac{5\tilde{c}}{2r_0}, \qquad c = \frac{\tilde{c}(12\tilde{\alpha} + 3r_0)r_0}{48}, \qquad d = -\frac{r_0\tilde{\beta}\gamma}{4}. \tag{146}$$

Here, a relates to linear advection, b to non-linear steepening, c to dispersion, and d to dissipation.

| Multiple-Scales Expansion

To study the slowly varying dynamics of a wave train, we employ a multi-scale perturbation approach. We seek a solution of the form (*cf.* Dias and Bridges (2005)):

$$\eta(x,t) = \varepsilon\left(\eta_0 + \varepsilon\eta_1(x,X,t,T_1,T_2) + \varepsilon^2\eta_2(x,X,t,T_1,T_2) + \varepsilon^3\eta_3(x,X,t,T_1,T_2) + \dots\right), \tag{147}$$

where $\varepsilon \ll 1$ is a small parameter, and the slow scales are defined as:

$$X = \varepsilon x, \quad T_1 = \varepsilon t, \quad T_2 = \varepsilon^2 t.$$

Here, η_0 represents the leading-order wave train, and $\eta_1, \eta_2, \eta_3, \dots$ are higher-order corrections that depend on both fast scales (x, t) and slow scales (X, T_1, T_2). We assume the leading-order solution η_0 is a slowly modulated plane wave:

$$\eta_0 = A(X,T_1,T_2)\exp(i\theta(x,t)) + \text{c.c.}, \tag{148}$$

where $A(X, T_1, T_2)$ is the complex amplitude modulating on the slow scales, $\theta(x,t) = Kx - \omega t$ is the phase with wave number K and frequency ω, and "c.c." denotes the complex conjugate. This form captures a rapidly oscillating wave with slowly varying amplitude. To account for the multiple scales, we expand the partial derivatives as follows:

$$\partial_t \to \partial_t + \varepsilon\partial_{T_1} + \varepsilon^2\partial_{T_2}, \quad \partial_x \to \partial_x + \varepsilon\partial_X, \partial_x^3 \to \partial_x^3 + 3\varepsilon\partial_x^2\partial_X + 3\varepsilon^2\partial_x\partial_X^2 + \varepsilon^3\partial_X^3.$$

These expansions reflect the contributions of derivatives across both fast and slow scales, enabling us to separate the dynamics at different orders of ε.

7.2.1 | Multi-Scale Analysis with SNegligiblemall Dissipation

In this section, we continue the multi-scale analysis of the KdVB equation, focusing on the case where the dissipative term coefficient satisfies $d = O(\varepsilon^3)$. This assumption simplifies the perturbation analysis, allowing us to derive the Nonlinear Schrödinger (NLS) equation for the amplitude of the wave train.

Substituting the ansatz (147) into the KdVB equation (145) and collecting terms at $O(\varepsilon)$, we obtain:

$$\left(\partial_t + a\partial_x + c\partial_x^3\right)\eta_0 = 0, \tag{149}$$

where $a = \tilde{c}$, $c = \dfrac{\tilde{c}(12\tilde{\alpha} + 3r_0)r_0}{48}$, and $\eta_0 = A(X,T_1,T_2)\exp(\mathrm{i}\theta) + \text{c.c.}$, with $\theta = kx - \omega t$. This yields the dispersion relation:

$$\omega = ak - ck^3. \tag{150}$$

The phase velocity is:

$$s = \frac{\omega}{k} = a - ck^2,$$

indicating dispersion since s depends on the wave number k. The group velocity, which governs the propagation of the wave packet's envelope, is:

$$c_g = \frac{d\omega}{dk} = a - 3ck^2.$$

At $O(\varepsilon^2)$, the equation becomes:

$$\left(\partial_t + a\partial_x + c\partial_x^3\right)\eta_1 = -\left(\partial_{T_1} + a\partial_X - 3ck^2\partial_X\right)\eta_0 - b\partial_x\left(\frac{1}{2}\eta_0^2\right), \tag{151}$$

where $b = \frac{5}{2}\frac{1}{r_0}\tilde{c}$. The right-hand side includes terms proportional to $\exp(\pm i\theta)$ and $\exp(\pm 2i\theta)$. The resonant terms proportional to $\exp(\pm i\theta)$ would lead to secular growth in η_1 and must be eliminated by imposing:

$$\left(\partial_{T_1} + c_g\partial_X\right)\eta_0 = 0 \implies A(X, T_1, T_2) = A(X - c_g T_1, T_2). \tag{152}$$

This indicates that the amplitude A propagates at the group velocity c_g. The remaining non-resonant term is:

$$\partial_x\left(\frac{1}{2}\eta_0^2\right) = ikA^2\exp(2i\theta) + \text{c.c.}.$$

We assume a solution for η_1 of the form:

$$\eta_1 = B_0(X, T_1, T_2) + \left[B_1(X, T_1, T_2)e^{i\theta} + \text{c.c.}\right] + \left[B_2(X, T_1, T_2)e^{2i\theta} + \text{c.c.}\right]. \tag{153}$$

Substituting into (151) and matching terms proportional to $\exp(2i\theta)$, we find:

$$B_2 = \frac{b}{6ck^2}A^2, \tag{154}$$

while B_0 and B_1 remain undetermined at this order.

At $O(\varepsilon^3)$, the equation is:

$$\left(\partial_t + a\partial_x + c\partial_x^3\right)\eta_2 = -\left(\partial_{T_2} + 3c\partial_x\partial_X^2\right)\eta_0 - \left(\partial_{T_1} + a\partial_X + 3c\partial_x^2\partial_X\right)\eta_1 - b\partial_x(\eta_0\eta_1) - b\eta_0\partial_X\eta_0. \tag{155}$$

To prevent secular growth, we eliminate resonant terms independent of θ and proportional to $\exp(\pm i\theta)$. The θ-independent terms give:

$$\left(\partial_{T_1} + a\partial_X\right)B_0 + b\partial_X|A|^2 = 0, \tag{156}$$

yielding:

$$B_0 = \phi(X - aT_1) - \frac{b|A|^2(X - c_g T_1)}{3ck^2},$$

where ϕ is an arbitrary function. The terms proportional to $\exp(i\theta)$ give:

$$\mathrm{i}\partial_{T_2} A - 3k\,\partial_X^2 A + \left(\partial_{T_1} + (a - 3ck^2)\,\partial_X\right) B_1 + ikb\left(AB_0 + A^* B_2\right) = 0. \tag{157}$$

To ensure B_1 depends only on $X - c_g T_1$, we set:

$$\left(\partial_{T_1} + (a - 3ck^2)\,\partial_X\right) B_1 = 0,$$

since $a - 3ck^2 = c_g$. Substituting B_0 and B_2 into (157), we obtain:

$$\mathrm{i}\partial_{T_2} A - 3k\,\partial_X^2 A + \frac{b^2 k A|A|^2}{6ck^2} - \frac{kbA\phi}{3ck^2} = 0\,.$$

Assuming $\phi = 0$ (a common simplification for initial conditions), and defining $\zeta = X - c_g T_1$ and $\beta = \dfrac{b^2}{6ck}$, we rewrite the equation as the NLS equation:

$$\mathrm{i}\partial_{T_2} A - 3k\,\partial_\zeta^2 A + \beta A|A|^2 = 0. \tag{158}$$

7.2.2 | Multi-Scale Analysis with Significant Dissipation

In this section, we extend the multi-scale analysis of the KdVB equation to the case where the dissipative term coefficient satisfies $d = O(1)$. This introduces a significant dissipative effect, modifying the dispersion relation and resulting in a complex group velocity, ultimately leading to a modified Nonlinear Schrödinger (NLS) equation.

Substituting the ansatz (147) into the KdVB equation (145) and collecting terms at $O(\varepsilon)$, we obtain:

$$\left(\partial_t + a\,\partial_x + c\,\partial_x^3 + d\,\partial_x^2\right)\eta_0 = 0, \tag{159}$$

where $a = \tilde{c}$, $c = \frac{\tilde{c}(12\tilde{\alpha}+3r_0)r_0}{48}$, $d = -\frac{r_0}{4}\tilde{\beta}\gamma$, and $\eta_0 = A(X, T_1, T_2)\exp(i\theta) + \text{c.c.}$, with $\theta = kx - \omega t$. This yields the dispersion relation:

$$\omega = ak - ck^3 + \mathrm{i}dk^2. \tag{160}$$

The group velocity, accounting for dissipation, is:

$$c_g = \frac{d\omega}{dk} = a - 3ck^2 + 2\mathrm{i}dk. \tag{161}$$

The imaginary component in c_g reflects the dissipative effect on wave packet propagation.

At $O(\varepsilon^2)$, the equation is:

$$\left(\partial_t + a\,\partial_x + c\,\partial_x^3 + d\,\partial_x^2\right)\eta_1 = -\left(\partial_{T_1} + a\,\partial_X - 3ck^2\,\partial_X + 2\mathrm{i}dk\,\partial_X\right)\eta_0 - b\,\partial_x\left(\frac{1}{2}\eta_0^2\right), \tag{162}$$

where $b = \frac{5}{2}\frac{1}{r_0}\tilde{c}$. The right-hand side contains terms proportional to $\exp(\pm\mathrm{i}\theta)$ and $\exp(\pm 2\mathrm{i}\theta)$. To eliminate secular

growth in η_1, we remove resonant terms proportional to $\exp(\pm i\theta)$ by imposing:

$$\left(\partial_{T_1} + c_g \partial_X\right) \eta_0 = 0 \implies A(X, T_1, T_2) = A(X - c_g T_1, T_2). \tag{163}$$

This indicates that the amplitude A propagates at the complex group velocity c_g. The non-resonant term is:

$$\partial_x \left(\frac{1}{2}\eta_0^2\right) = \mathrm{i}k A^2 \exp(2\mathrm{i}\theta) + \text{c.c.}.$$

We assume a solution for η_1 as in (153):

$$\eta_1 = B_0(X, T_1, T_2) + \left[B_1(X, T_1, T_2)\mathrm{e}^{\mathrm{i}\theta} + \text{c.c.}\right] + \left[B_2(X, T_1, T_2)\mathrm{e}^{2\mathrm{i}\theta} + \text{c.c.}\right].$$

Substituting into (162) and matching terms proportional to $\exp(2i\theta)$, we find:

$$B_2 = \frac{b}{6ck^2 - 2\mathrm{i}dk} A^2, \tag{164}$$

while B_0 and B_1 remain undetermined at this order.

At $O(\varepsilon^3)$, the equation is:

$$\begin{aligned}\left(\partial_t + a\partial_x + c\partial_x^3 + d\partial_x^2\right)\eta_2 = &-\left(\partial_{T_2} + 3c\partial_x\partial_X^2 + d\partial_X^2\right)\eta_0 \\ &- \left(\partial_{T_1} + a\partial_X + 3c\partial_x^2\partial_X + 2d\partial_x\partial_X\right)\eta_1 - b\partial_x(\eta_0\eta_1) - b\eta_0\partial_X\eta_0.\end{aligned} \tag{165}$$

To prevent secular growth, we eliminate resonant terms independent of θ and proportional to $\exp(\pm i\theta)$. The θ-independent terms give:

$$\left(\partial_{T_1} + a\partial_X\right) B_0 + b\partial_X |A|^2 = 0, \tag{166}$$

yielding:

$$B_0 = \phi(X - aT_1) - \frac{b|A|^2(X - c_g T_1)}{3ck^2 - 2\mathrm{i}dk},$$

where ϕ is an arbitrary function. The terms proportional to $\exp(\mathrm{i}\theta)$ give:

$$\left(\partial_{T_2} + 3\mathrm{i}k\partial_X^2 + d\partial_X^2\right) A + \left(\partial_{T_1} + (a - 3ck^2)\partial_X\right) B_1 + \mathrm{i}kb\left(AB_0 + A^* B_2\right) = 0. \tag{167}$$

Assuming B_1 depends only on $X - c_g T_1$, we set:

$$\left(\partial_{T_1} + (a - 3ck^2)\partial_X\right) B_1 = 0,$$

since $a - 3ck^2 = \mathrm{Re}(c_g)$. Substituting B_0 and B_2 into (167), and assuming $\phi = 0$, we obtain:

$$\partial_{T_2} A + 3ik\,\partial_X^2 A + d\,\partial_X^2 A + ikb^2 \left(\frac{1}{6ck^2 - 2idk} - \frac{1}{3ck^2 - 2idk} \right) |A|^2 A = 0.$$

Defining $\zeta = X - c_g T_1$, $m = \frac{1}{6ck^2 - 2idk}$, and $n = \frac{1}{3ck^2 - 2idk}$, and rewriting in standard form, we obtain the modified NLS equation:

$$i\partial_{T_2} A - 3k\,\partial_\zeta^2 A + id\,\partial_\zeta^2 A + ikb^2 (m - n)|A|^2 A = 0. \tag{168}$$

7.2.3 | Multi-scale Analysis with Intermediate Dissipation

In this section, we perform a multi-scale analysis of the KdVB equation for the case where the dissipative term coefficient is $d = O(\varepsilon^2)$, *i.e.*, $d = \varepsilon^2 \tilde{d}$, with $\tilde{d}$ a constant. This intermediate dissipation strength affects the dynamics at higher orders, leading to a modified Nonlinear Schrödinger (NLS) equation.

Substituting the ansatz (147) into the KdVB equation (145), the equations at $O(\varepsilon)$ and $O(\varepsilon^2)$ are identical to those in the first case ($d = O(\varepsilon^3)$), as the dissipative term $d\,\partial_x^2 \eta$ only appears at $O(\varepsilon^3)$ or higher. Thus, we have:

- At $O(\varepsilon)$: The leading-order equation (149) and dispersion relation (150):

$$\left(\partial_t + a\,\partial_x + c\,\partial_x^3 \right) \eta_0 = 0, \quad \omega = ak - ck^3,$$

  with group velocity $c_g = a - 3ck^2$.
- At $O(\varepsilon^2)$: The second-order equation (151), secular condition (152), and solution for B_2 (154):

$$A(X, T_1, T_2) = A(X - c_g T_1, T_2), \quad B_2 = \frac{b}{6ck^2} A^2.$$

The coefficients are $a = \tilde{c}$, $b = \frac{5}{2} \frac{1}{r_0} \tilde{c}$, and $c = \frac{\tilde{c}(12\tilde{\alpha} + 3r_0) r_0}{48}$.

At $O(\varepsilon^3)$, the dissipative term introduces a difference. The equation is:

$$\left(\partial_t + a\,\partial_x + c\,\partial_x^3 \right) \eta_2 = - \left(\partial_{T_2} + 3c\,\partial_x\,\partial_X^2 + \tilde{d}\,\partial_x^2 \right) \eta_0 - \left(\partial_{T_1} + a\,\partial_X + 3c\,\partial_x^2\,\partial_X \right) \eta_1 - b\,\partial_x (\eta_0 \eta_1) - b\eta_0\,\partial_X \eta_0. \tag{169}$$

The θ-independent resonant terms yield the same equation as in the first case (156):

$$\left(\partial_{T_1} + a\,\partial_X \right) B_0 + b\,\partial_X |A|^2 = 0,$$

giving:

$$B_0 = \phi(X - aT_1) - \frac{b|A|^2 (X - c_g T_1)}{3ck^2},$$

where ϕ is an arbitrary function. For simplicity, we set $\phi = 0$. The terms proportional to $\exp(i\theta)$ give:

$$\partial_{T_2} A + 3ik\,\partial_X^2 A - k^2 \tilde{d} A + ikb \left(A B_0 + A^* B_2 \right) = 0. \tag{170}$$

Substituting B_0 and B_2, and defining $\zeta = X - c_g T_1$, we obtain:

$$\partial_{T_2} A + 3\mathrm{i}k\,\partial_\zeta^2 A - k^2 \tilde{d} A + \nu^\star A|A|^2 = 0,$$

where:

$$\nu^\star = \frac{-2\mathrm{i}kb^2 + \mathrm{i}kb}{ck^2} = \frac{\mathrm{i}kb(1-2b)}{ck^2}.$$

Rewriting in standard NLS form:

$$\mathrm{i}\partial_{T_2} A - 3k\,\partial_\zeta^2 A + \mathrm{i}k^2 \tilde{d} A - \mathrm{i}\nu^\star A|A|^2 = 0. \tag{171}$$

7.2.4 | Instability analysis

Modulational instability is a fundamental phenomenon observed in nonlinear dispersive systems, such as surface waves on deep water Benjamin and Feir (1967); Yuen and Lake (1975, 1980); Remoissenet (1996) and light waves in optical fibers Tai et al. (1986). It describes the growth of small perturbations to a plane wave, leading to complex nonlinear dynamics. In one-dimensional systems, numerical simulations of the focusing cubic Nonlinear Schrödinger (NLS) equation on periodic domains reveal recurrent behavior reminiscent of the Fermi–Pasta–Ulam (FPU) phenomenon Fermi et al. (1955); Yuen and Ferguson (1978); Hafizi (1981).

| Case 1: Negligible Dissipation ($d = O(\varepsilon^3)$)

For the Nonlinear Schrödinger (NLS) equation (158):

$$\mathrm{i}\partial_{T_2} A - 3k\,\partial_\zeta^2 A + \beta A|A|^2 = 0, \quad \beta = \frac{b^2}{6ck}, \quad \zeta = X - c_g T_1,$$

a plane wave solution is:

$$A_0(T_2) = a_0 \exp(\mathrm{i}\beta a_0^2 T_2), \tag{172}$$

where $a_0 \in \mathbb{R}^+$ is the amplitude. To study stability, we introduce a small perturbation:

$$A(\zeta, T_2) = A_0(T_2)[1 + a(\zeta, T_2)], \quad |a| \ll 1. \tag{173}$$

Substituting into (158) and linearizing, we obtain:

$$\mathrm{i}\partial_{T_2} a = 3k\,\partial_\zeta^2 a - \beta a_0^2 (a + a^*), \tag{174}$$

where a^* is the complex conjugate of a. Assuming $a = u(\zeta, T_2) + \mathrm{i}v(\zeta, T_2)$ with real u and v, we get:

$$\partial_{T_2} \begin{pmatrix} u \\ v \end{pmatrix} = \begin{pmatrix} 0 & 3k\,\partial_\zeta^2 \\ -3k\,\partial_\zeta^2 + 2\beta a_0^2 & 0 \end{pmatrix} \begin{pmatrix} u \\ v \end{pmatrix}. \tag{175}$$

Seeking solutions of the form $(u, v) \propto \exp(iq\zeta - i\lambda T_2)$, the dispersion relation is:

$$\lambda^2 = 9k^2q^4 + 6\beta k a_0^2 q^2. \tag{176}$$

If $\beta k > 0$, then for small $q^2 < -\frac{2\beta a_0^2}{3k}$, $\lambda^2 < 0$, indicating instability due to imaginary λ.

| Case 2: Significant Dissipation ($d = O(1)$)

For the modified NLS equation (168):

$$i\partial_{T_2} A - 3k\partial_\zeta^2 A + id\partial_\zeta^2 A + ikb^2(m-n)|A|^2 A = 0,$$

where $m = \frac{1}{6ck^2 - 2idk}$, $n = \frac{1}{3ck^2 - 2idk}$, a plane wave solution is:

$$A_0(T_2) = a_0 \exp(iRa_0^2 T_2), \tag{177}$$

where $a_0 \in \mathbb{R}^+$ and $R = kb^2(m-n) = kb^2\left(\frac{1}{6ck^2-2idk} - \frac{1}{3ck^2-2idk}\right)$. Perturbing as in (173), we obtain:

$$i\partial_{T_2} a = 3k\partial_\zeta^2 a - id\partial_\zeta^2 a - Ra_0^2(a + a^*). \tag{178}$$

Assuming $a = u + iv$, the system becomes:

$$\partial_{T_2}\begin{pmatrix} u \\ v \end{pmatrix} = \begin{pmatrix} -2Qa_0^2 - d\partial_\zeta^2 & 3k\partial_\zeta^2 \\ -3k\partial_\zeta^2 + 2Na_0^2 & -d\partial_\zeta^2 \end{pmatrix}\begin{pmatrix} u \\ v \end{pmatrix}, \tag{179}$$

where:

$$Q = \mathrm{Re}(R) = \frac{-2b^2k^2d(9c^2k^4 + 4d^2k^2) + 2b^2dk^2(36c^2k^4 + 4d^2k^2)}{(36c^2k^4 + 4d^2k^2)(9c^2k^4 + 4d^2k^2)},$$

$$N = \mathrm{Re}(R) = Q.$$

Seeking solutions $\propto \exp(iq\zeta - i\lambda T_2)$, the dispersion relation is:

$$\lambda^2 = (9k^2 + d^2)q^4 + (6Na_0^2 k - 2dQa_0^2)q^2. \tag{180}$$

The stability depends on the sign and magnitude of $6Nk - 2dQ$, with instability possible for certain q^2 when the coefficient of q^2 is negative.

| Summary of Multi-Scale Analysis and Modulational Instability

The multi-scale analysis of the KdV–Burgers equation (145) for a slowly modulated wave train $\eta_0 = A\exp(i\theta) +$ c.c. reveals how dissipation affects the governing Nonlinear Schrödinger (NLS) equations and the MI of plane wave

solutions. The results vary with the dissipation coefficient d:

Negligible Dissipation ($d = O(\varepsilon^3)$): The NLS equation (158) is purely dispersive with a cubic nonlinearity. The MI analysis (176) shows that plane waves are unstable for wave numbers $q^2 < -\frac{2\beta a_0^2}{3k}$ when $\beta k > 0$, driven by the interplay of dispersion and nonlinearity.

Significant Dissipation ($d = O(1)$): The modified NLS equation (168) includes a dissipative term $id\partial_\zeta^2 A$, altering the dynamics. The instability condition (180) depends on the coefficient $6Nk - 2dQ$, indicating that dissipation modifies the range of unstable wave numbers, potentially stabilizing or destabilizing the wave depending on system parameters.

Intermediate Dissipation ($d = O(\varepsilon^2)$, $d = \varepsilon^2\tilde{d}$): The NLS equation (171) introduces a linear dissipative term $ik^2\tilde{d}A$. While MI was not analyzed here, the presence of dissipation suggests a modified instability threshold, requiring further perturbation analysis.

These findings underscore the complex interplay between nonlinearity, dispersion, and dissipation in nonlinear wave dynamics. The derived NLS equations and instability conditions provide critical insights into the stability of wave trains in dispersive media, with applications to physical systems like water waves and optical fibers.

7.3 | Modulational instability analysis in BBM wave packets

The Benjamin–Bona–Mahony (BBM) equation models the unidirectional propagation of long waves in dispersive systems, offering an alternative to the Korteweg–de Vries (KdV) equation with improved high-frequency behavior. In normalized variables, the viscous BBM equation is:

$$\partial_t\eta + \tilde{c}\partial_x\eta + \frac{5}{2}\frac{1}{r_0}\tilde{c}\eta\partial_x\eta - \frac{(12\tilde{\alpha} + 3r_0)r_0}{48}\partial_x^2\partial_t\eta - \frac{r_0}{4}\gamma\tilde{\beta}\partial_x^2\eta = 0, \tag{181}$$

where $\eta(x,t)$ is the wave field, $\tilde{c}$ is a characteristic speed, r_0, $\tilde{\alpha}$, $\tilde{\beta}$, and γ are system parameters, and subscripts denote partial derivatives.

To study nonlinear wave packets, we assume a slowly modulated wave train solution of the form:

$$\eta(x,t) = \varepsilon A(\xi,\tau)\exp(i\theta) + \text{c.c.}, \tag{182}$$

where $A(\xi,\tau)$ is the complex amplitude, $\theta = kx - \omega t$ with wave number k and frequency ω, and "c.c." denotes the complex conjugate. The slow scales are:

$$\xi = \varepsilon(x - pt), \qquad \tau = \varepsilon^2 t, \tag{183}$$

where $\varepsilon \ll 1$ is a small parameter and p is the group velocity to be determined. We expand the solution as an asymptotic series:

$$\eta(x,t) = \varepsilon\eta_1 + \varepsilon^2\eta_2 + \varepsilon^3\eta_3 + \dots. \tag{184}$$

Substituting (184) into (181), applying the slow scales (183), and collecting terms at $O(\varepsilon)$, we obtain:

$$\left(\partial_t + a\partial_x - c\partial_t\partial_x^2 + d\partial_x^2\right)\eta_1 = 0, \tag{185}$$

where $a = \tilde{c}$, $b = \frac{5}{2}\frac{1}{r_0}\tilde{c}$, $c = \frac{(12\tilde{\alpha}+3r_0)r_0}{48}$, and $d = -\frac{r_0}{4}\gamma\tilde{\beta}$. For $\eta_1 = A(\xi,\tau)\exp(i\theta) + \text{c.c.}$, this yields the dispersion relation:

$$\omega = \frac{ak}{1+ck^2} + \mathrm{i}\frac{dk^2}{1+ck^2}. \tag{186}$$

The group velocity is:

$$p = \frac{d\omega}{dk} = \frac{a(1-ck^2)+2\mathrm{i}dk}{(1+ck^2)^2}.$$

At $O(\varepsilon^2)$, the equation is:

$$\left(\partial_t + a\partial_x - c\partial_t\partial_x^2 + d\partial_x^2\right)\eta_2 = \left(p\partial_\xi - a\partial_\xi + 2c\partial_t\partial_x\partial_\xi - cp\partial_x^2\partial_\xi - 2d\partial_x\partial_\xi\right)\eta_1 - b\partial_x(\eta_1\eta_1). \tag{187}$$

The right-hand side includes terms proportional to $\exp(\pm\mathrm{i}\theta)$ and $\exp(\pm 2\mathrm{i}\theta)$. To eliminate secular growth in η_2, resonant terms proportional to $\exp(\pm\mathrm{i}\theta)$ are set to zero, confirming the group velocity p above. The non-resonant terms give:

$$\left(\partial_t + a\partial_x - c\partial_t\partial_x^2 + d\partial_x^2\right)\eta_2 = -bikA^2\exp(2\mathrm{i}\theta) + \text{c.c.}. \tag{188}$$

Assuming a solution:

$$\eta_2 = B(\xi,\tau)\exp(2\mathrm{i}\theta) + \text{c.c.} + C(\xi,\tau), \tag{189}$$

we find:

$$B(\xi,\tau) = \sigma A^2, \quad \sigma = \frac{b(1+ck^2)}{6ack^2 + 4\mathrm{i}cdk^3 - 2\mathrm{i}dk}. \tag{190}$$

At $O(\varepsilon^3)$, the equation is:

$$\begin{aligned}\left(\partial_t + a\partial_x - c\partial_t\partial_x^2 + d\partial_x^2\right)\eta_3 = &-\left(\partial_\tau - c\partial_\tau\partial_\xi^2 + 2cp\partial_x\partial_\xi^2 - c\partial_x^2\partial_\tau + d\partial_\xi^2\right)\eta_1 \\ &-\left(-p\partial_\xi + a\partial_\xi - 2c\partial_t\partial_x\partial_\xi + cp\partial_x^2\partial_\xi + 2d\partial_x\partial_\xi\right)\eta_2 - b\partial_x(\eta_1\eta_2).\end{aligned} \tag{191}$$

Substituting (182) and (189), we eliminate resonant terms. The θ-independent terms give:

$$(p-a)\partial_\xi C + b\partial_\xi|A|^2 = 0, \tag{192}$$

yielding:

$$C(\xi,\tau) = \nu|A|^2, \qquad \nu = \frac{b}{p-a} = \frac{b(1+ck^2)^2}{-3ack^2+2idk-ac^2k^4}.$$

The $\exp(i\theta)$ resonant terms yield:

$$\left(-\partial_\tau - i\omega c\partial_\xi^2 - 2ikpc\partial_\xi^2 - cik^2\partial_\tau - d\partial_\xi^2\right)A - bik(AC + A^*B) = 0. \tag{193}$$

Substituting B and C, we obtain the NLS equation:

$$\partial_\tau A + iM\partial_\xi^2 A + iNA|A|^2 = 0, \tag{194}$$

where:

$$M = \frac{\omega c + 2kpc - id}{1+ck^2}, \qquad N = \frac{bk(\nu+\sigma)}{1+ck^2}.$$

The derivation of the NLS equation (194) from the viscous BBM equation provides a framework for understanding the modulation of wave packets in dispersive systems with viscosity. The coefficients M and N encapsulate the effects of dispersion, dissipation, and nonlinearity, offering insights into wave stability and dynamics in applications such as water waves.

7.3.1 | Instability Analysis

Modulational Instability (MI) is a key phenomenon in nonlinear wave systems, where small perturbations to a plane wave can grow exponentially, leading to complex dynamics. Here, we analyze the stability of plane wave solutions to the Nonlinear Schrödinger (NLS) equation (194) derived from the viscous Benjamin–Bona–Mahony (BBM) equation:

$$\partial_\tau A + iM\partial_\xi^2 A + iNA|A|^2 = 0,$$

where $M = \frac{\omega c + 2kpc - id}{1+ck^2}$, $N = \frac{bk(\nu+\sigma)}{1+ck^2}$, and the coefficients are defined as in the previous derivation. The NLS equation (194) admits a plane wave solution of the form:

$$A_0(\tau) = a_0\exp(-iNa_0^2\tau), \tag{195}$$

where $a_0 \in \mathbb{R}^+$ is the constant amplitude. To study its stability, we introduce a small perturbation:

$$A(\xi,\tau) = a_0 e^{-iNa_0^2\tau}[1 + a(\xi,\tau)], \qquad |a| \ll 1. \tag{196}$$

Substituting (196) into (194) and linearizing, we obtain:

$$i\partial_\tau a - M\partial_\xi^2 a - Na_0^2(a + a^*) = 0, \tag{197}$$

where a^* is the complex conjugate of a. Assuming $a = u(\xi,\tau) + \mathrm{i}v(\xi,\tau)$ with real u and v, we rewrite (197) as a system:

$$\partial_\tau \begin{pmatrix} u \\ v \end{pmatrix} = \begin{pmatrix} 0 & M\partial_\xi^2 \\ M\partial_\xi^2 - 2Na_0^2 & 0 \end{pmatrix} \begin{pmatrix} u \\ v \end{pmatrix}. \tag{198}$$

Seeking solutions of the form $(u, v) \propto \exp(iq\xi - i\lambda\tau)$, we substitute into (198) to obtain the dispersion relation:

$$\lambda^2 = M^2q^4 - 2NMa_0^2q^2. \tag{199}$$

The stability of the plane wave depends on the sign of λ^2:

- If $\lambda^2 > 0$, perturbations oscillate, indicating stability.
- If $\lambda^2 < 0$, perturbations grow exponentially, indicating MI.

Instability occurs when $MN > 0$ and $q^2 < \dfrac{2Na_0^2}{M}$, as the quadratic term dominates for small q. The interplay between M (dispersion/dissipation) and N (nonlinearity) governs the instability threshold.

The dispersion relation (199) highlights the role of dispersion, dissipation, and nonlinearity in the stability of wave packets in the viscous BBM system. The coefficients M and N, derived from the BBM parameters, determine the range of wave numbers q for which instability occurs. This analysis provides insights into the dynamics of long waves in dispersive media, with applications to water waves and other nonlinear systems.

8 | CONCLUSIONS AND DISCUSSION

In this work, we have conducted a comprehensive investigation of pulsatile flow within deformable vessels featuring viscoelastic walls. Grounded in the assumption of axisymmetric flow and considering an ideal fluid for simplicity, we have developed a coherent hierarchy of asymptotic models that capture the complex dynamics governing these intricate systems. Our analysis centered on implementing model order reduction under the long-wave assumption of axi-symmetric Euler equations, which led to the derivation of novel asymptotic model equations offering a detailed portrayal of long-crested pulse propagation in deformable tubes with cylindrical symmetry. This conceptual framework builds upon foundations introduced in Mitsotakis et al. (2018).

Acknowledging the impact of viscous stresses in bio-fluids, we extended our study to incorporate these effects, traditionally addressed through hyperbolic systems of equations. The constraints posed by cylindrical symmetry prompted us to propose various weakly dispersive extensions, enhancing the accuracy of fluid dynamics representation in deformable vessels. Our research began with an in-depth scrutiny of the fully nonlinear regime, resulting in the formulation of a Serre–Green–Naghdi (SGN) system in cylindrical geometry. This system generalises the planar SGN equations to realistic vascular settings and serves as the parent model from which all subsequent approximations descend.

To enhance tractability, we presented a derivation of the weakly nonlinear counterpart of our SGN system. Additionally, we introduced one-dimensional reductions exemplified by Korteweg–de Vries (KdV) and Benjamin–Bona–Mahony (BBM) type equations, further simplifying the system while preserving essential dynamics.

Our analytical exploration provided valuable insights into the fundamental characteristics of these newly formulated systems. We systematically examined symmetries, conservation laws, and Whitham solitons, offering a compre-

hensive perspective on their behavior. Linear properties, such as dispersion relations, were meticulously discussed in relation to the base model. Furthermore, through multi-scale analysis, we derived cubic Nonlinear Schrödinger (NLS) equations and investigated MI, shedding light on the emergence of Stokes waves from both KdV and BBM equations.

The methodologies and insights developed in this work contribute significantly to our understanding of pulsatile flow within deformable vessels and represent a valuable addition to the broader fields of fluid dynamics and mathematical modeling. As we conclude, we anticipate that our findings will stimulate further investigations and contribute to the ongoing dialogue in this dynamic field, positioning this research at the forefront of discussions on complex fluid systems.

9 | PERSPECTIVES

This work provides a foundational understanding of the mathematical and numerical modeling of nonlinear wave propagation in fluid systems. However, several aspects remain open to further exploration and offer opportunities for extending the research presented here. Building upon the results of this study, we identify multiple promising directions for future research that would expand the scope of our analysis.

A natural extension of this work involves the study of solitary wave solutions for the Serre–Green–Naghdi (SGN) system in cylindrical coordinates. A comprehensive numerical investigation of this system would provide valuable insights into the stability, shape, and velocity of such solitary waves. Moreover, understanding how these waves interact in cylindrical settings would significantly enhance our knowledge of wave dynamics in confined geometries.

The reduced 0D system derived in this article offers a simplified framework for analyzing complex fluid dynamics. A detailed numerical study of this system would enable validation of the theoretical results and exploration of its dynamical features. Such an analysis could uncover critical aspects of its solution space, including fixed points, oscillatory behavior, and transitions between regimes, helping identify practical scenarios where this reduced model can serve as a reliable approximation for more complex systems.

Further advancement in this field would benefit from deriving and studying the Nonlinear Schrödinger (NLS) equations for the SGN system in cylindrical coordinates and for the Boussinesq system. This investigation would include examining modulation instability phenomena in these systems, shedding light on the stability and evolution of wave trains in cylindrical geometries.

Additionally, finding and characterizing Stokes waves in the SGN and Boussinesq systems in cylindrical coordinates represents an essential step toward a complete understanding of these models. This analysis would complement the solitary wave solutions and provide further insights into the dynamics of nonlinear waves in such configurations.

These perspectives aim to extend the theoretical and numerical framework developed in this study, contributing to a deeper understanding of nonlinear wave propagation in fluid dynamics. The proposed extensions not only advance the theoretical and numerical understanding of the systems studied in this work but also hold significant implications for biomedical applications. The investigation of nonlinear wave phenomena in cylindrical geometries is particularly relevant for modeling blood flow in arteries, where such configurations naturally occur. By addressing these perspectives, future research can provide deeper insights into the mechanics of pulse propagation in blood vessels, bridging the gap between mathematical modeling and physiological applications, and offering new tools for understanding and predicting hemodynamic behaviors in real-world scenarios.

Code availability

The Maple (Maplesoft™) scripts developed and used in this work, along with the LaTeX source files of this article, are made openly available at the following URL:

https://github.com/dutykh/SerreCyl/

Acknowledgements

DD and REC would like to acknowledge the invaluable support of Prof. Stéphane Gerbi (University Savoie Mont Blanc, France), without whom this work would have appeared much later, or perhaps not at all.

Conflict of interest

The authors declare that there are no conflicts of interest regarding the publication of this article.

Supporting Information

Further details are available in the PhD manuscript of Rim El Cheikh, which serves as supplementary material to this article.

Data availability statement

No experimental data were used in the preparation of this study. However, any other data or materials related to this research are available from the corresponding author upon reasonable request by email.

Acronyms

BBM Benjamin–Bona–Mahony. 1–5, 23, 25, 26, 30, 34, 38, 39, 45, 46, 54, 56–58, 65, 66
BF Benjamin–Feir. 46

FPU Fermi–Pasta–Ulam. 52

IBVP Initial Boundary Value Problem. 8

KdV Korteweg–de Vries. 1–5, 23, 25, 26, 28, 30, 33–35, 37–39, 45, 46, 53, 54, 57, 58
KdVB Korteweg–de Vries–Burgers. 46, 47, 49, 51

MI Modulational Instability. 1, 3–5, 46, 53, 54, 56–58

NLS Nonlinear Schrödinger. 45–47, 49, 51–54, 56, 58

PDE Partial Differential Equation. 22

SGN Serre–Green–Naghdi. 1, 4, 19, 20, 22, 57, 58

References

Agrawal, G. (2013) *Nonlinear Fiber Optics*. Elsevier.

Agrawal, G. P. and Pattanayak, D. N. (1979) Gaussian beam propagation beyond the paraxial approximation. *Journal of the Optical Society of America*, **69**, 575.

Alastruey, J., Khir, A. W., Matthys, K. S., Segers, P., Sherwin, S. J., Verdonck, P. R., Parker, K. H. and Peiró, J. (2011) Pulse wave propagation in a model human arterial network: Assessment of 1-d visco-elastic simulations against in vitro measurements. *Journal of Biomechanics*, **44**, 2250–2258. URL: http://linkinghub.elsevier.com/retrieve/pii/S0021929011004386.

Alastruey, J., Parker, K. H. and Sherwin, S. J. (2008) Lumped parameter outflow models for 1-d blood flow simulations: effect on pulse waves and parameter estimation. *Comm. Comp. Phys.*, **4**, 317–336.

Arnold, V. I. (1997) *Mathematical Methods of Classical Mechanics*. Springer, 2nd edn.

Avolio, A. P. (1980) Multi-branched model of the human arterial system. *Medical & Biological Engineering & Computing*, **18**, 709–718.

Benjamin, T. B., Bona, J. L. and Mahony, J. J. (1972) Model equations for long waves in nonlinear dispersive systems. *Philos. Trans. Royal Soc. London Ser. A*, **272**, 47–78.

Benjamin, T. B. and Feir, J. E. (1967) The disintegration of wavetrains in deep water. part 1. *J. Fluid Mech.*, **27**.

Bluman, G. and Kumei, S. (1987) On invariance properties of the wave equation. *Journal of Mathematical Physics*, **28**, 307–318.

Bona, J. L., Chen, M. and Saut, J.-C. (2002) Boussinesq equations and other systems for small-amplitude long waves in nonlinear dispersive media. i: Derivation and linear theory. *J. Nonlinear Sci.*, **12**, 283–318.

Bona, J. L., Colin, T. and Lannes, D. (2005) Long wave approximations for water waves. *Arch. Rational Mech. Anal.*, **178**, 373–410.

Bona, J. L., Dougalis, V. A. and Mitsotakis, D. E. (2008) Numerical solution of boussinesq systems of kdv-kdv type ii. evolution of radiating solitary waves. *Nonlinearity*, **21**, 2825–2848.

Bona, J. L. and Smith, R. (1975) The initial-value problem for the korteweg-de vries equation. *Phil. Trans. R. Soc. A*, **278**, 555–601. URL: http://rsta.royalsocietypublishing.org/cgi/doi/10.1098/rsta.1975.0035.

Bourdarias, C., Ersoy, M. and Gerbi, S. (2012) A mathematical model for unsteady mixed flows in closed water pipes. *Science China Mathematics*, **55**, 221–244. URL: http://link.springer.com/10.1007/s11425-011-4353-z.

Bourdarias, C. and Gerbi, S. (2007) A finite volume scheme for a model coupling free surface and pressurised flows in pipes. *J. Comp. Appl. Math.*, **209**, 109–131.

— (2008) A conservative model for unsteady flows in deformable closed pipes and its implicit second-order finite volume discretisation. *Computers and Fluids*, **37**, 1225–1237. URL: http://linkinghub.elsevier.com/retrieve/pii/S0045793008000042.

Boussinesq, J. V. (1895) Lois de l'extinction de la houle en haute mer. *C. R. Acad. Sci. Paris*, **121**, 15–20.

Boyd, J. P. (2000) *Chebyshev and Fourier Spectral Methods*. Dover Publications, New York, 2nd edn.

Catanho, M., Sinha, M. and Vijayan, V. (2012) Model of aortic blood flow using the windkessel effect. *Tech. rep.*, BENG 221 Mathematical Methods in Bioengineering Report.

Chandran, K. B., Rittgers, S. E. and Yoganathan, A. P. (2012) *Biofluid Mechanics: The Human Circulation*. CRC Press, 2 edn.

Chen, H. and Bona, J. (2002) Solitary waves in nonlinear dispersive systems. *Discrete Contin. Dynam. Syst. Ser. B*, **2**, 313–378. URL: http://www.aimsciences.org/journals/displayArticles.jsp?paperID=475.

Cheviakov, A. F. (2007) Gem software package for computation of symmetries and conservation laws of differential equations. *Comp. Phys. Comm.*, **176**, 48–61. URL: http://linkinghub.elsevier.com/retrieve/pii/S001046550600316X.

— (2010) Symbolic computation of local symmetries of nonlinear and linear partial and ordinary differential equations. *Math. Comp. Sci.*, **4**, 203–222. URL: http://link.springer.com/10.1007/s11786-010-0051-4.

Clamond, D. and Dutykh, D. (2012) Practical use of variational principles for modeling water waves. *Phys. D*, **241**, 25–36. URL: https://hal.archives-ouvertes.fr/hal-00456891/.

Clamond, D., Dutykh, D. and Mitsotakis, D. (2017) Conservative modified serre–green–naghdi equations with improved dispersion characteristics. *Comm. Nonlin. Sci. Num. Sim.*, **45**, 245–257.

— (2019) Hamiltonian regularisation of shallow water equations with uneven bottom. *J. Phys. A: Math. Gen*, **52**, 42LT01. URL: http://iopscience.iop.org/article/10.1088/1751-8121/ab3eb2https://iopscience.iop.org/article/10.1088/1751-8121/ab3eb2.

— (2024) *A variational approach to water wave modelling*, vol. 3. International Association for Hydro-Environment Engineering and Research (IAHR). URL: https://www.iahr.org/library/infor?pid=29802.

Clebsch, A. (1859) Ueber die integration der hydrodynamischen gleichungen. *Journal für die reine und angewandte Mathematik*, **1859**, 1–10.

Delestre, O. and Lagrée, P. (2013) A 'well-balanced' finite volume scheme for blood flow simulation. *International Journal for Numerical Methods in Fluids*, **72**, 177–205.

Dias, F. and Bridges, T. (2005) *Weakly Nonlinear Wave Packets and the Nonlinear Schrödinger Equation*, 29–67. Springer Vienna.

Dougalis, V. A. and Mitsotakis, D. E. (2008) Theory and numerical analysis of boussinesq systems: A review. In *Effective Computational Methods in Wave Propagation* (eds. N. A. Kampanis, V. A. Dougalis and J. A. Ekaterinaris), 63–110. CRC Press.

Dougalis, V. A., Mitsotakis, D. E. and Saut, J.-C. (2007) On some boussinesq systems in two space dimensions: Theory and numerical analysis. *Math. Model. Num. Anal.*, **41**, 254–825.

Dutykh, D. (2009a) Group and phase velocities in the free-surface visco-potential flow: New kind of boundary layer induced instability. *Physics Letters, Section A: General, Atomic and Solid State Physics*, **373**, 3212–3216.

— (2009b) Visco-potential free-surface flows and long wave modelling. *Eur. J. Mech. B/Fluids*, **28**, 430–443.

Dutykh, D., Chhay, M. and Fedele, F. (2013a) Geometric numerical schemes for the kdv equation. *Comp. Math. Math. Phys.*, **53**, 221–236.

Dutykh, D. and Clamond, D. (2011) Shallow water equations for large bathymetry variations. *J. Phys. A: Math. Theor.*, **44**, 332001.

— (2016) Modified shallow water equations for significantly varying seabeds. *Appl. Math. Model.*, **40**, 9767–9787. URL: http://hal.archives-ouvertes.fr/hal-00675209/http://arxiv.org/abs/1202.6542http://linkinghub.elsevier.com/retrieve/pii/S0307904X16303444.

Dutykh, D., Clamond, D., Milewski, P. and Mitsotakis, D. (2013b) Finite volume and pseudo-spectral schemes for the fully nonlinear 1d serre equations. *Eur. J. Appl. Math.*, **24**, 761–787. URL: http://hal.archives-ouvertes.fr/hal-00587994/.

Dutykh, D., Clamond, D. and Mitsotakis, D. (2015) Adaptive modeling of shallow fully nonlinear gravity waves. *RIMS Kôkyûroku*, **1947**, 45–65.

Dutykh, D. and Dias, F. (2007a) Dissipative boussinesq equations. *Comptes Rendus Mécanique*, **335**, 559–583. URL: https://linkinghub.elsevier.com/retrieve/pii/S1631072107001362.

— (2007b) Viscous potential free-surface flows in a fluid layer of finite depth. *Comptes Rendus Mathematique*, **345**, 113–118. URL: https://linkinghub.elsevier.com/retrieve/pii/S1631073X07002415.

Dutykh, D. and Goubet, O. (2016) Derivation of dissipative boussinesq equations using the dirichlet-to-neumann operator approach. *Math. Comp. Simul.*, **127**, 80–93. URL: http://linkinghub.elsevier.com/retrieve/pii/S0378475414000706.

Dutykh, D. and Pelinovsky, E. (2014) Numerical simulation of a solitonic gas in kdv and kdv-bbm equations. *Phys. Lett. A*, **378**, 3102–3110. URL: http://linkinghub.elsevier.com/retrieve/pii/S0375960114008895.

Dutykh, D. and Tobisch, E. (2015) Direct dynamical energy cascade in the modified kdv equation. *Phys. D*, **297**, 76–87. URL: http://hal.archives-ouvertes.fr/hal-00990724/http://linkinghub.elsevier.com/retrieve/pii/S0167278915000032.

Evans, L. C. (2010) *Partial Differential Equations*. American Mathematical Society, 2 edn.

Fermi, E., Pasta, J. and Ulam, S. (1955) Studies of nonlinear problems. *Tech. rep.*, Los Alamos National Laboratory.

Formaggia, L., Lamponi, D. and Quarteroni, A. (2003) One-dimensional models for blood flow in arteries. *Journal of Engineering Mathematics*, **47**, 251–276. URL: http://link.springer.com/10.1023/B:ENGI.0000007980.01347.29.

Fung, Y.-C. (1993) *Biomechanics: Mechanical Properties of Living Tissues*. Springer New York. URL: http://link.springer.com/10.1007/978-1-4757-2257-4.

Fung, Y. C. (1997) *Biomechanics: circulation*. Springer New York. URL: http://link.springer.com/10.1007/978-1-4757-2696-1.

Goldstein, H., Poole, C. and Safko, J. (2001) *Classical Mechanics*. Addison-Wesley Pub. Co., 3 edn.

Hafizi, B. (1981) Nonlinear evolution equations, recurrence and stochasticity. *Physics of Fluids*, **24**, 1791–1798.

Hammack, J. L. and Henderson, D. M. (1993) Resonant interactions among surface water waves. *Annual Review of Fluid Mechanics*, **25**, 55–97.

Hargreaves, R. (1908) Xxxvii. a pressure-integral as kinetic potential. *The London, Edinburgh, and Dublin Philosophical Magazine and Journal of Science*, **16**, 436–444.

Ibragimov, N. H. (1995) *CRC Handbook of Lie Group Analysis of Differential Equations*, vol. III. CRC Press.

Khakimzyanov, G., Dutykh, D., Fedotova, Z. and Gusev, O. (2020) *Dispersive Shallow Water Waves*. Springer International Publishing. URL: http://link.springer.com/10.1007/978-3-030-46267-3.

Khakimzyanov, G. S., Dutykh, D., Fedotova, Z. I. and Mitsotakis, D. E. (2018) Dispersive shallow water wave modelling. part i: Model derivation on a globally flat space. *Commun. Comput. Phys.*, **23**, 1–29.

Knops, R. J. and Stuart, C. A. (1984) Quasiconvexity and uniqueness of equilibrium solutions in nonlinear elasticity. *Archive for Rational Mechanics and Analysis*, **86**, 233–249.

Korteweg, D. J. and de Vries, G. (1895) On the change of form of long waves advancing in a rectangular canal, and on a new type of long stationary waves. *Phil. Mag.*, **39**, 422–443.

Lagrée, P.-Y. (2000) An inverse technique to deduce the elasticity of a large artery. *The European Physical Journal Applied Physics*, **9**, 153–163.

Lamb, H. (1932) *Hydrodynamics*. Cambridge University Press.

Lambert, J. W. (1958) On the nonlinearities of fluid flow in nonrigid tubes. *Journal of the Franklin Institute*, **266**, 83–102.

Lanczos, C. (1970) *The Variational Principles of Mechanics*. New York: Dover Publications.

Landau, L. D. and Lifshitz, E. M. (1987) *Fluid Mechanics*. Pergamon Press, 2nd edn.

Lavrentiev, M. (1947) On the theory of long waves. *Akad. Nauk. Ukrain. R. S. R., Zbornik Prac. Inst. Mat.*, **8**, 13–69.

Lax, P. D. (1968) Integrals of nonlinear equations of evolution and solitary waves. *Commun. Pure Appl. Math.*, **21**, 467–490.

LeVeque, R. J. (2002) *Finite Volume Methods for Hyperbolic Problems*. Cambridge University Press.

Luke, J. C. (1967) A variational principle for a fluid with a free surface. *J. Fluid Mech.*, **27**, 375–397.

Milišić, V. and Quarteroni, A. (2004) Analysis of lumped parameter models for blood flow simulations and their relation with 1d models. *ESAIM: M2AN*, **38**, 613–632. URL: http://www.esaim-m2an.org/10.1051/m2an:2004036.

Mitsotakis, D., Dutykh, D. and Li, Q. (2018) Asymptotic nonlinear and dispersive pulsatile flow in elastic vessels with cylindrical symmetry. *Computers and Mathematics with Applications*, **75**, 4022–4047. URL: https://linkinghub.elsevier.com/retrieve/pii/S0898122118301408.

Mitsotakis, D., Dutykh, D., Li, Q. and Peach, E. (2019) On some model equations for pulsatile flow in viscoelastic vessels. *Wave Motion*, **90**, 139–151. URL: https://linkinghub.elsevier.com/retrieve/pii/S0165212518303159.

Newell, A. C. (1977) Finite amplitude instabilities of partial difference equations. *SIAM Journal of Applied Mathematics*, **33**, 133–160.

Nutku, Y. (1987) On a new class of completely integrable nonlinear wave equations. ii. multi-hamiltonian structure. *J. Math. Phys.*, **28**, 2579–2585. URL: http://aip.scitation.org/doi/10.1063/1.527749.

Olver, P. J. (1993) *Applications of Lie groups to differential equations*, vol. 107. Springer-Verlag, 2 edn.

Peregrine, D. H. (1983) Water waves, nonlinear schrödinger equations and their solutions. *J. Austral. Math. Soc. Ser. B*, **25**, 16–43.

Petrov, A. A. (1964) Variational statement of the problem of liquid motion in a container of finite dimensions. *Prikl. Math. Mekh.*, **28**, 917–922.

Quarteroni, A. and Formaggia, L. (2004) *Mathematical Modelling and Numerical Simulation of the Cardiovascular System*, 3–127. Elsevier B.V. URL: http://linkinghub.elsevier.com/retrieve/pii/S1570865903120017.

Radder, A. C. (1999) Hamiltonian dynamics of water waves. *Adv. Coastal Ocean Engng*, **4**, 21–59.

Remoissenet, M. (1996) Solitons and modulational instability. *Annales Des Télécommunications*, **51**, 297–303.

Roe, P. L. (2005) Computational fluid dynamics - retrospective and prospective. *International Journal of Computational Fluid Dynamics*, **19**, 581–594. URL: http://www.tandfonline.com/doi/abs/10.1080/10618560600585315.

Segers, P., Dubois, F., Wachter, D. D. and Verdonck, P. (1998) Role and relevancy of a cardiovascular simulator. *Cardiovascular Engineering*, **3**, 48–56.

Serre, F. (1956) Contribution à l'étude des ondes longues irrotationnelles. *La Houille Blanche*, 375–390. URL: http://www.shf-lhb.org/10.1051/lhb/1956033.

Sherwin, S. J., Franke, V., Peiró, J. and Parker, K. (2003) One-dimensional modelling of a vascular network in space-time variables. *Journal of Engineering Mathematics*, **47**, 217–250. URL: http://link.springer.com/10.1023/B:ENGI.0000007979.32871.e2.

Sjöberg, A. and Mahomed, F. M. (2004) Non-local symmetries and conservation laws for one-dimensional gas dynamics equations. *Applied Mathematics and Computation*, **150**, 379–397.

Sulem, C. and Sulem, P.-L. (1999) *The Nonlinear Schrödinger Equation. Self-Focusing and Wave Collapse*. Springer-Verlag, New York.

Taha, T. R. and Ablowitz, M. J. (1984) Analytical and numerical aspects of certain nonlinear evolution equations. iii. numerical, korteweg-de vries equation. *J. Comput. Phys*, **55**, 231–253. URL: http://linkinghub.elsevier.com/retrieve/pii/0021999184900044.

Tai, K., Tomita, A. and Hasegawa, A. (1986) Observation of modulational instability in single-mode fiber. In *Optical Fiber Communication*, WG1. OSA.

Tijsseling, A. and Anderson, A. (2012) *A. Isebree Moens and D.J. Korteweg: on the speed of propagation of waves in elastic tubes*, vol. 1242. Technische Universiteit Eindhoven, casa-report edn.

Trefethen, L. N. (2000) *Spectral methods in MatLab*. Society for Industrial and Applied Mathematics, Philadelphia, PA, USA. URL: http://web.comlab.ox.ac.uk/oucl/work/nick.trefethen/spectral.html.

van de Vosse, F. N. and Stergiopulos, N. (2011) Pulse wave propagation in the arterial tree. *Ann. Rev. Fluid Mech.*, **43**, 467–499. URL: http://www.annualreviews.org/doi/10.1146/annurev-fluid-122109-160730.

Whitham, G. B. (1999) *Linear and Nonlinear Waves*. John Wiley & Sons, Inc. URL: http://doi.wiley.com/10.1002/9781118032954.

Yuen, H. C. and Ferguson, W. E. (1978) Relationship between benjamin-feir instability and recurrence in the nonlinear schrödinger equation. *Physics of Fluids*, **21**, 1275–1278.

Yuen, H. C. and Lake, B. M. (1975) Nonlinear deep water waves: Theory and experiment. *Physics of Fluids*, **18**, 956–960.

— (1980) Instabilities of waves on deep water. *Annual Review of Fluid Mechanics*, **12**, 303–334.

Zabusky, N. J. and Galvin, C. C. J. (1971) Shallow water waves, the korteweg-de vries equation and solitons. *J. Fluid Mech.*, **47**, 811–824.

Zakharov, V. E. (1968) Stability of periodic waves of finite amplitude on the surface of a deep fluid. *J. Appl. Mech. Tech. Phys.*, **9**, 190–194.

Zakharov, V. E. and Kuznetsov, E. A. (1997) Hamiltonian formalism for nonlinear waves. *Usp. Fiz. Nauk*, **167**, 1137–1168.

Zakharov, V. E. and Shabat, A. B. (1972) Exact theory of two-dimensional self-focusing and one-dimensional self-modulation of waves in nonlinear media. *Soviet Physics-JETP*, **34**, 62–69.

A | A WINDKESSEL MODEL FOR PULSATILE FLOW IN VISCOELASTIC VESSELS BASED ON SERRE-TYPE APPROXIMATIONS

In the late nineteenth century, Otto Frank developed the *Windkessel* model, drawing an analogy between the cardiovascular system and a closed hydraulic circuit. In his description, the heart functions as a pump connected to a chamber that is almost entirely filled with water except for a small pocket of air; compression of the water forces air out of the chamber in a manner reminiscent of ventricular ejection. Windkessel representations are therefore routinely employed to quantify the load placed upon the heart during a cardiac cycle Catanho et al. (2012).

When modelling the cardiac cycle, the Windkessel approach accounts for *arterial compliance*, *peripheral resistance*, and *inertia*. For a hydraulic system, it may be regarded as the counterpart of Poiseuille's law, comparing blood motion through arteries to viscous flow in pipes.

Windkessel and other lumped-parameter models are often derived from electrical-circuit analogies in which current represents volumetric blood flow rate and voltage represents arterial pressure Avolio (1980); Segers et al. (1998); Milišić and Quarteroni (2004). In this picture, electrical resistances mimic viscous losses, capacitors represent vascular compliance (volume storage), and inductors reproduce the inertial effects of the blood column.

In the electrical analogy, pressure plays the role of voltage, whereas flow rate corresponds to current. A two-element Windkessel model incorporates arterial compliance and total peripheral resistance. Here the compliance of the systemic arteries is represented by a capacitor C $\left[\mathrm{cm}^3\,\mathrm{mmHg}^{-1}\right]$, and the peripheral vascular resistance is represented by a resistor R $\left[\mathrm{mmHg\,s\,cm}^{-3}\right]$. The inflow rate $Q(t)$ $[\mathrm{cm}^3\,\mathrm{s}^{-1}]$ corresponds to an electric current, whereas the outlet pressure $P(t)$ $[\mathrm{mmHg}]$ corresponds to a voltage source.

In what follows, we obtain a zero-dimensional (0D) ordinary differential system by spatially averaging the viscous BBM-type equation,

$$\eta_t + \tilde{c}\,\eta_x + \frac{5}{2}\,\frac{\tilde{c}}{r_0}\,\eta\,\eta_x - \frac{(12\tilde{\alpha} + 3r_0)\,r_0}{48}\,\eta_{xxt} - \frac{r_0}{4}\,\gamma\,\tilde{\beta}\,\eta_{xx} = 0. \tag{200}$$

Assuming $\eta_x = -\eta_t + O(\varepsilon, \delta^2)$ and substituting this relation into (200) we obtain

$$\eta_t + \tilde{c}\,\eta_x + \frac{5}{2}\,\frac{\tilde{c}}{r_0}\,\eta\,\eta_x + \frac{(12\tilde{\alpha} + 3r_0)\,r_0}{48}\,\eta_{xtt} - \frac{r_0}{4}\,\gamma\,\tilde{\beta}\,\eta_{tt} = 0. \tag{201}$$

Multiplication by 48 yields

$$48\,\eta_t + 48\,\tilde{c}\,\eta_x + \frac{120\,\tilde{c}}{r_0}\,\eta\,\eta_x + (12\tilde{\alpha} + 3r_0)\,r_0\,\eta_{xtt} - 12\,r_0\,\gamma\,\tilde{\beta}\,\eta_{tt} = 0. \tag{202}$$

Introducing

$$A' = 48, \qquad B' = (12\tilde{\alpha} + 3r_0)\,r_0, \qquad C' = -12\,r_0\,\gamma\,\tilde{\beta},$$

equation (202) becomes

$$A'\,\eta_t + 48\,\tilde{c}\,\eta_x + \frac{120\,\tilde{c}}{r_0}\,\eta\,\eta_x + B'\,\eta_{xtt} + C'\,\eta_{tt} = 0. \tag{203}$$

Integrating over $x \in [a, b]$ gives

$$A' \int_a^b \eta_t\,\mathrm{d}x + 48\,\tilde{c} \int_a^b \eta_x\,\mathrm{d}x + \frac{120\,\tilde{c}}{r_0} \int_a^b \eta\,\eta_x\,\mathrm{d}x + B' \int_a^b \eta_{xtt}\,\mathrm{d}x + C' \int_a^b \eta_{tt}\,\mathrm{d}x = 0. \tag{204}$$

Defining

$$\hat{\eta}(t) = \frac{1}{b-a} \int_a^b \eta(x,t)\,\mathrm{d}x, \qquad \eta_1(t) = \eta(a,t), \qquad \eta_2(t) = \eta(b,t),$$

and setting $A = A'(b-a)$, $B = B'(b-a)$ and $C = C'(b-a)$, we obtain the lumped relation

$$A\,\dot{\tilde{\eta}} + B\,\ddot{\eta}_2 - B\,\ddot{\eta}_1 + C\,\ddot{\tilde{\eta}} + \frac{120\,\tilde{c}}{r_0}\left(\eta_2^2 - \eta_1^2\right) + 48\,\tilde{c}\,(\eta_2 - \eta_1) - B\,\ddot{\eta}_1 + \frac{120\,\tilde{c}}{r_0}\left(\eta_2^2 - \eta_1^2\right) + 48\,\tilde{c}\,(\eta_2 - \eta_1) = 0. \tag{205}$$

By integrating the governing BBM-type equation over space, we have derived a consistent 0D system that provides a compact yet accurate description of the haemodynamics in a compliant arterial segment. Such lumped models, when embedded in larger cardiovascular networks, furnish an invaluable tool for predicting pressure-flow relations and assessing ventricular afterload in both physiological and pathological conditions.